

NOTE TO USERS

This reproduction is the best copy available.

UMI[®]

**Effect of frother on bubble coalescence, break-up, and
initial rise velocity**

Willy Andrés Kracht Gajardo

Department of Mining and Materials Engineering,
McGill University,
Montréal, Canada

A thesis submitted to McGill University in partial fulfillment of the
requirements of the degree of Doctor of Philosophy

© Willy A. Kracht G.

July 2008



Library and Archives
Canada

Published Heritage
Branch

395 Wellington Street
Ottawa ON K1A 0N4
Canada

Bibliothèque et
Archives Canada

Direction du
Patrimoine de l'édition

395, rue Wellington
Ottawa ON K1A 0N4
Canada

Your file *Votre référence*
ISBN: 978-0-494-66574-9
Our file *Notre référence*
ISBN: 978-0-494-66574-9

NOTICE:

The author has granted a non-exclusive license allowing Library and Archives Canada to reproduce, publish, archive, preserve, conserve, communicate to the public by telecommunication or on the Internet, loan, distribute and sell theses worldwide, for commercial or non-commercial purposes, in microform, paper, electronic and/or any other formats.

The author retains copyright ownership and moral rights in this thesis. Neither the thesis nor substantial extracts from it may be printed or otherwise reproduced without the author's permission.

AVIS:

L'auteur a accordé une licence non exclusive permettant à la Bibliothèque et Archives Canada de reproduire, publier, archiver, sauvegarder, conserver, transmettre au public par télécommunication ou par l'Internet, prêter, distribuer et vendre des thèses partout dans le monde, à des fins commerciales ou autres, sur support microforme, papier, électronique et/ou autres formats.

L'auteur conserve la propriété du droit d'auteur et des droits moraux qui protègent cette thèse. Ni la thèse ni des extraits substantiels de celle-ci ne doivent être imprimés ou autrement reproduits sans son autorisation.

In compliance with the Canadian Privacy Act some supporting forms may have been removed from this thesis.

While these forms may be included in the document page count, their removal does not represent any loss of content from the thesis.

Conformément à la loi canadienne sur la protection de la vie privée, quelques formulaires secondaires ont été enlevés de cette thèse.

Bien que ces formulaires aient inclus dans la pagination, il n'y aura aucun contenu manquant.


Canada

*Dedicated to my beloved
Gabriela and Beatriz*

Abstract

Frothers are used in flotation to aid generation of small bubbles, but little is known about the mechanisms that take place in the flotation machine to produce such an effect. Coalescence prevention is the common explanation, although the exact mechanism is obscure and almost no attention has been paid to a frother effect on bubble break-up, the other possible mechanism. This thesis presents a technique to study the effect of frothers on bubble coalescence at the generation stage (at a capillary tube) and a technique to study the effect of frothers on bubble coalescence and break-up in a turbulent field. The first technique is based on the sound bubbles emit when they form and coalesce. The sound signal was linked to bubble formation and coalescence events using high-speed cinematography. The technique has a resolution capable of detecting coalescence events that occur within 1-2 ms. The second technique allows discriminating between coalescence and break-up and is based on the exposure of a mono-size distribution of bubbles to a turbulent field generated by a three-bladed axial flow impeller. Analysis of bubble size distributions after contact with the turbulent field gives the coalescence and break-up fraction. The results show frothers reduce coalescence and alter the bubble size distribution of bubbles generated by break-up.

In the course of high-speed imaging an effect of frother on bubble shape and motion after formation was detected. Analysis of this forms the third major component of the work. A dependence of velocity on bubble aspect ratio is shown, which is in line with recent literature.

Résumé

En flottation, les moussants sont utilisés pour faciliter la génération de petites bulles, mais on sait peu de choses sur les mécanismes qui entourent cet effet dans les systèmes de flottation. Bien que son mécanisme reste encore obscur, une explication classique est l'inhibition de la coalescence, alors qu'un autre mécanisme possible, l'effet du moussant sur la taille d'une bulle a été très peu étudié. Cette thèse présente une technique d'étude de l'effet du moussant sur la coalescence d'une bulle à son stade de formation (à la sortie d'un tube capillaire) et une technique pour étudier l'effet des moussants sur la coalescence et la scission de bulles dans un champ de turbulence. La première technique est basée sur le son émis par les bulles qui se forment et coalescent. Le signal sonore fut relié aux événements de formation et de coalescence de bulles à l'aide de la cinématographie à haute vitesse. La technique permet de détecter un événement de coalescence avec une résolution temporelle de 1-2 ms. La seconde technique permet de discriminer entre la coalescence et la scission et consiste à exposer une population de bulles d'une seule taille à un champ de turbulence créé par une hélice d'agitation à trois pales axiales. L'analyse des distributions après contact avec le champ de turbulence donne la fraction de bulles qui coalescent et qui se scindent. Les résultats montrent que les moussants réduisent la coalescence et changent la distribution dans la taille des bulles générées par scission.

Au cours de l'analyse des séquences d'images à haute vitesse, un effet du moussant sur la forme et le mouvement des bulles a été détecté. L'analyse de ces formes constitue la troisième composante majeure du travail. Une dépendance de la vitesse sur la forme des bulles est montrée, en accord avec la littérature récente.

Resumen

Los espumantes tienen un importante efecto en la reducción del tamaño de burbujas en flotación, no obstante, es muy poco lo que se sabe acerca de los mecanismos que operan en la celda de flotación para producir tal efecto. La explicación más común atribuye el efecto a la prevención de coalescencia, pero el mecanismo exacto es desconocido y el efecto de los espumantes en la ruptura de burbujas no ha sido considerado. Esta tesis presenta una técnica para estudiar el efecto de los espumantes en la coalescencia de burbujas en su etapa de formación (en un tubo capilar) y una técnica para estudiar el efecto en la coalescencia y ruptura de burbujas sometidas a turbulencia. La primera técnica se basa en el sonido que emiten las burbujas cuando se forman y coalescen. La señal sonora fue asociada a la formación y coalescencia de burbujas usando una cámara de video de alta velocidad. La técnica tiene una resolución capaz de detectar coalescencia en tiempos tan cortos como 1-2 ms. La segunda técnica permite discriminar entre coalescencia y ruptura y se basa en la exposición de una distribución mono-tamaño de burbujas a la turbulencia generada por un impeler. El posterior análisis entrega la fracción de coalescencia y ruptura. Los resultados muestran que los espumantes reducen la coalescencia y alteran la distribución de tamaño de burbujas generadas por ruptura.

Al usar la cámara de alta velocidad se detectó que el espumante afecta la forma y movimiento de las burbujas después de que éstas se forman. El análisis de estas observaciones conforma el tercer componente de este trabajo. Se muestra cómo la velocidad depende de la razón de aspecto de las burbujas, lo que está de acuerdo con la literatura reciente.

Acknowledgements

I would like to express my gratitude to Professor James A. Finch for his guidance and constant support during my studies at McGill University.

This work was conducted under the Chair in Mineral Processing funded through an NSERC (Natural Sciences and Engineering Research Council of Canada) CRD (Collaborative Research and Development) grant now sponsored by Vale Inco, Xstrata Process Support, Teck Cominco, Agnico-Eagle, COREM, SGS Lakefield Research, Shell Canada and Flottec.

I would like to thank the Chilean Government for the Chilean National Scholarship (Beca Presidente de la República) and the University of Chile for granting a leave and for their financial support.

I want to thank my friends and colleagues at McGill University for their help, especially Dr. Cesar Gomez, Dr. Luis Calzado, Dr. Mustafa Tarkan, Dr. Stephanie Somot, and Ray Langlois.

Finally, I want to express my deep gratitude to my beloved wife and daughter, Gabriela and Beatriz, for their unconditional love and support, and to my parents, Willy and Angélica, and brothers, Juan and Erick, for their constant support and encouragement in all that I have done in my life.

Table of Contents

Abstract	i
Résumé	ii
Resumen	iii
Acknowledgements	iv
Table of Contents	v
Nomenclature	ix
List of figures	xi
List of tables	xv
Chapter 1 – Introduction	1
1.1 Introduction.....	1
1.2 Thesis objectives	4
1.3 Thesis structure	6
1.3 Contribution of authors	8
References.....	9
Chapter 2 – Literature review	13
2.1 Bubble coalescence	13
2.1.1 General Considerations	13
2.1.2 Film elasticity.....	15
2.1.3 Surface viscosity	16

2.1.4 Total stress	18
2.2 Break-up.....	19
2.3 Bubbles as a source of sound	22
2.4 Bubble shape and rise velocity	23
References.....	28

Chapter 3 - Coalescence inhibition at bubble generation stage.....34

3.1 Introduction.....	34
3.2 Bubble coalescence.....	34
3.2.1 General Considerations.....	34
3.2.2 Film elasticity.....	36
3.2.3 Surface viscosity	38
3.2.4 Total stress	40
3.2.5 Experimental requirements	41
3.3 Bubbles as a source of sound.....	41
3.4 Experimental	43
3.4.1 Apparatus	43
3.4.2 Reagents.....	44
3.4.3 Procedure	45
3.5 The technique.....	46
3.5.1 Validation.....	46
3.5.2 Signal recognition	47
3.6 Results and Discussion	54
3.6.1 Reliability.....	54
3.6.2 Concentration vs. gas flow rate.....	56
3.6.3 Salt vs. frother.....	62
3.7 Conclusions.....	65
References.....	67

Chapter 4 – Bubble break-up and the role of frother and salt.....73

4.1 Introduction.....	73
4.2 Coalescence.....	74
4.3 Break-up.....	75
4.4 Experimental.....	78
4.4.1 Apparatus.....	78
4.4.2 Procedure.....	80
4.4.3 Reagents.....	81
4.5 Results.....	83
4.5.1 Reliability.....	83
4.5.2 Effect of frother type and salt (NaCl) on bubble size distribution.....	84
4.5.3 Effect of frother concentration on bubble size distribution.....	91
4.5.4 Effect of impeller speed on bubble size distribution.....	92
4.6 Discussion.....	95
4.6.1 Qualitative Observations.....	95
4.6.2 Quantitative Examination.....	96
4.7 Conclusions.....	104
References.....	105

Chapter 5 – Bubble rise velocity and shape.....109

5.1 Introduction.....	109
5.2 Bubble shape and rise velocity.....	110
5.3 Experimental.....	115
5.3.1 Apparatus.....	115
5.3.2 Reagents.....	116
5.3.3 The Technique.....	117
5.4 Results.....	119
5.4.1 Effect of frother type and salt.....	119
5.4.2 Effect of frother concentration.....	127

5.4.3 Bubble rise velocity versus aspect ratio	129
5.5 Discussion	132
5.6 Conclusions	134
References	135
Chapter 6 – Unifying discussion	139
6.1 Introduction	139
6.2 Summary of frother effects	139
6.3 Commentary	140
References	144
Chapter 7 – Conclusions, contributions, and future work.....	145
7.1 Conclusions	145
7.2 Contributions to original knowledge	149
7.3 Suggestions for future work	150
References	152
Appendix.....	162
Appendix 1 – Reagent structure	162
Appendix 2 – High speed camera specifications	163
Appendix 3 – Experimental results of coalescence inhibition.....	164
Appendix 4 – Experimental results of bubble coalescence and break-up.....	170
Appendix 5 – Macro code for ImageJ.....	172

Nomenclature

A	cm^2	Bubble film area
A_c	cm^2	Cross-sectional area in the flotation machine
A_{cap}	cm^2	Area of spherical cap
A_R		Aspect ratio
b	L/mmol	Langmuir equilibrium constant
c	mmol/L	Concentration
CCC	mmol/L	Critical coalescence concentration
d	mm	Bubble diameter
d_{32}	mm	Sauter mean diameter
d_{eq}	mm	Equivalent bubble diameter
d_h	mm	Bubble diameter perpendicular to direction of movement
d_v	mm	Bubble diameter parallel to direction of movement
E	mN/m^2	Gibbs elasticity
f	$1/\text{s}$	Natural frequency of pulsation of bubbles
h	mm	Distance from edge of bubble to imaginary plane of break-up
J_g	cm/s	Superficial gas velocity
k		Polytropic index
k_y	$\text{mN}\cdot\text{m}/\text{mol}$	Change in surface tension with loading
P	Pa	Pressure inside bubble
P_0	Pa	Static pressure
Q_g	cm^3/s	Volumetric gas flow rate

r	mm	Bubble radius
S_b	1/s	Bubble surface area flux
v	cm/s	Bubble rise velocity
y	cm	Vertical position of bubble

Greek letters

Γ	mol/cm ²	Surface loading
Γ_m	mol/cm ²	Gibbs equilibrium loading
Γ_s	mol/cm ²	Saturation loading
ε	m	Local deformation
η_d	mN·s/m	Surface dilational viscosity
ρ_{air}	kg/m ³	Air density
ρ_l	kg/m ³	Liquid density
σ	mN/m	Surface tension
τ	mN	Total stress

List of figures

Figure 2.1. Film elasticity. (a) Film before stretching has uniform surface concentration of surfactant. (b) Stretching lowers local surface concentration of surfactant, and the local surface tension increases protecting the film.	16
Figure 2.2. Surface dilational viscosity.....	17
Figure 2.3. Sequence of images of bubble break-up by dumbbell stretching mechanism. (a) $t = 0$ ms, (b) $t = 8$ ms, (c) $t = 20$ ms, (d) $t = 22$ ms, and (e) $t = 25$ ms (Walter and Blanch, 1986. Reprinted with permission from Elsevier).....	20
Figure 2.4. Bubbles of equivalent volume rising in water. The size of each image is $0.32\text{ cm} \times 0.88\text{ cm}$. (Wu and Gharib, 2002. Reprinted with permission from the American Institute of Physics).....	27
Figure 3.1. Film elasticity. (a) Film before stretching has uniform surface concentration of surfactant. (b) Stretching lowers local surface concentration of surfactant, and the local surface tension increases protecting the film.	37
Figure 3.2. Surface dilational viscosity.....	39
Figure 3.3. Experimental set-up for measuring acoustic emissions of bubbles being formed and coalescing at a capillary tube.	44
Figure 3.4. Hydrophone Lab-40.....	44
Figure 3.5. Frequency analysis of sound produced by generation of two bubbles of 2.4 and 6 mm diameter.....	46
Figure 3.6. Sequence of images (1 ms apart) of bubble formation without coalescence. Dowfroth 250, 0.09 mmol/L, 10 sccm.....	48
Figure 3.7. Sound trace corresponding to image sequence in Figure 3.6.	48
Figure 3.8. Sequence of images (1 ms apart) of bubble formation and coalescence (frame 6). Dowfroth 250, 0.02 mmol/L, 16 sccm.....	50
Figure 3.9. Sound trace corresponding to image sequence in Figure 3.8.	50
Figure 3.10. Sequence of images (1 ms apart) of bubble formation and coalescence with two subsequent bubbles (frames 5 and 8 of sequence). Dowfroth 250, 0.04 mmol/L, 21 sccm.	52
Figure 3.11. Sound trace corresponding to image sequence in Figure 3.10.	52

Figure 3.12. Sound recording of bubble formation without coalescence. F-150, 0.024 mmol/L, 7.8 sccm.	53
Figure 3.13. Sound recording of bubble formation and coalescence with one subsequent bubble. F-150, 0.005 mmol/L, 7.8 sccm.	53
Figure 3.14. Repeat test for Pentanol.	55
Figure 3.15. Coalescence plot for frothers.	57
Figure 3.16. Surface tension data for Pentanol (Tuckermann, 2007); MIBC, Dowfroth 250, F-150 (Zhang, 2008).	57
Figure 3.17. Coalescence plot for <i>n</i> -alcohols (MIBC included).	58
Figure 3.18. Surface tension data for the homologous series of <i>n</i> -alcohols (Tuckermann, 2007).	59
Figure 3.19. Surface tension (after Tuckermann, 2007) vs. gas flow rate at the coalescence/non-coalescence boundary (Figure 3.17) for <i>n</i> -alcohols.	60
Figure 3.20. Schematic of frother action on coalescence prevention.	61
Figure 3.21. Coalescence plot for sodium chloride.	63
Figure 3.22. Sound recording of bubble formation showing partial coalescence prevention. NaCl 0.3 mol/L, 9.4 sccm.	63
Figure 3.23. Schematic of salt action on coalescence prevention.	64
Figure 4.1. Sequence of images of bubble break-up by dumbbell stretching mechanism. (a) $t = 0$ ms, (b) $t = 8$ ms, (c) $t = 20$ ms, (d) $t = 22$ ms, and (e) $t = 25$ ms (Walter and Blanch, 1986. Reprinted with permission from Elsevier).	76
Figure 4.2. Experimental set-up.	78
Figure 4.3. Impeller.	79
Figure 4.4. Capillary-sleeve system used to generate mono-size distribution of bubbles: (a) impeller off, (b) impeller on (420 RPM).	79
Figure 4.5. Repeat test for F-150: 0.012 mmol/L, 420 RPM.	83
Figure 4.6. Frother effect (Dowfroth 250) on bubble size distribution, 420 RPM.	85
Figure 4.7. Sequence of images (1 ms apart) of bubble coalescence. Water (no-frother), 420 RPM.	85
Figure 4.8. Sequence of images (2 ms apart) of bubble coalescence. Dowfroth 250, 0.038 mmol/L, 420 RPM.	86

Figure 4.9. Sequence of images (1 ms apart) of bubble break-up in water (no-frother) at 420 RPM showing a break-up event giving one large and one small bubble (frames 9-10).....	87
Figure 4.10. Sequence of images (1 ms apart) of bubble break-up in water (no-frother) at 420 RPM showing 3 daughter bubbles (frame 10) being produced from one mother bubble (frame 1).....	88
Figure 4.11. Sequence of images (1 ms apart) of bubble break-up. Dowfroth 250, 0.038 mmol/L, 420 RPM.	88
Figure 4.12. Sequence of images (1 ms apart) of bubble break-up in vicinity of blade. Dowfroth 250, 0.038 mmol/L at 420 RPM.....	88
Figure 4.13. Frother effect (Pentanol, MIBC, F-150) on bubble size distribution, 420 RPM.	89
Figure 4.14. Effect of salt (NaCl) on bubble size distribution, 420 RPM.	90
Figure 4.15. Effect of frother (Dowfroth 250) concentration on bubble size distribution, 420 RPM.	91
Figure 4.16. Effect of impeller speed on bubble size distributions. Water only.....	93
Figure 4.17. Effect of impeller speed on bubble size distributions. F-150, 0.012 mmol/L.....	94
Figure 4.18. Stretched bubble before break-up.....	97
Figure 4.19. Schematic of bubble break-up.	98
Figure 4.20. Difference between relative change in area for two daughter bubbles generated from a 2.5 mm diameter mother bubble. Bubble 2 is the larger of the two bubbles.	100
Figure 4.21. Evaluation of parenthesis in Equation 4.20.	103
Figure 5.1. Bubbles of equivalent volume rising in water. The size of each image is 0.32 cm × 0.88 cm. (Wu and Gharib, 2002. Reprinted with permission from the American Institute of Physics).....	113
Figure 5.2. Experimental set-up.....	115
Figure 5.3. Diameters d_h and d_v used to calculate the aspect ratio where dashed arrow indicates direction of movement.	118

Figure 5.4. Example of recorded images (taken from video each 30 ms). Tap water (no frother), Pentanol (0.40 mmol/L), and F-150 (0.012 mmol/L).....	120
Figure 5.5. Velocity and aspect ratio. Tap water. (Note symbols are used to identify the curves and have no other significance.).....	121
Figure 5.6. Sketch of high frequency oscillations of vertical diameter d_v	121
Figure 5.7. Velocity and aspect ratio. Dowfroth 250, 0.095 mmol/L.....	122
Figure 5.8. Velocity and aspect ratio. F-150, 0.012 mmol/L.....	123
Figure 5.9. Velocity and aspect ratio. Pentanol, 0.40 mmol/L.	124
Figure 5.10. Velocity and aspect ratio. MIBC, 0.098 mmol/L.	124
Figure 5.11. Velocity and aspect ratio. NaCl, 0.4 mol/L.	125
Figure 5.12. Velocity over first 20 ms. Tap water; Dowfroth 250, 0.095 mmol/L.....	126
Figure 5.13. Aspect ratio over first 20 ms. Tap water; Dowfroth 250, 0.095 mmol/L....	126
Figure 5.14. Images showing impact of frother concentration (taken from video each 25 ms). Dowfroth 250.	127
Figure 5.15. Velocity profile as a function of frother concentration. Dowfroth 250: 0.023, 0.038, and 0.095 mmol/L.....	128
Figure 5.16. Velocity profile as a function of frother concentration. F-150: 0.005, 0.012, and 0.024 mmol/L.....	128
Figure 5.17. Velocity profiles as a function of frother concentration. MIBC: 0.024, 0.049, and 0.098 mmol/L.....	129
Figure 5.18. Velocity vs. aspect ratio. Dowfroth 250: 0.011, 0.038, 0.057, and 0.095 mmol/L.....	130
Figure 5.19. Velocity vs. aspect ratio. MIBC: 0.024, 0.049, 0.098, 0.196 mmol/L.	131
Figure 5.20. Velocity vs. aspect ratio. F-150, 0.024 mmol/L; Dowfroth 250, 0.095 mmol/L; MIBC, 0.196 mmol/L; Pentanol, 0.567 mmol/L; sodium chloride 1.0 mol/L; and tap water.	132
Figure 6.1. Schematic of initial frother surface concentration at bubble surface. (a) before bubble starts growing (dashed circle shows region that will be occupied by bubble), (b) during bubble growth, (c) bubble immediately after detachment.	140
Figure A3.1. Gas flow meter calibration curve.....	164

List of tables

Table 3.1. Summary of reagents used.	45
Table 3.2. Concentration vs. gas flow rate: repeat test results for Pentanol.	55
Table 4.1. Summary of reagents used.	81
Table 4.2. Typical frother concentrations (mmol/L) used in flotation systems expressed on CCC scale (adapted from Nasset et al., 2007).	82
Table 4.3. Number frequency vs. bubble size: repeat test results for F-150, 0.012 mmol/L, 420 RPM.	84
Table 5.1. Summary of reagents used.	116
Table 5.2. Typical frother concentrations (mmol/L) used in flotation systems expressed on CCC scale (adapted from Nasset et al., 2007).	117
Table A2.1. Recording rate (fps) and image size configurations.	163
Table A3.1. Gas flow meter calibration.	164
Table A3.2. Boundary between coalescence and no-coalescence region for 1-butanol. .	165
Table A3.3. Boundary between coalescence and no-coalescence region for	165
Table A3.4. Boundary between coalescence and no-coalescence region for	166
Table A3.5. Boundary between coalescence and no-coalescence region for	166
Table A3.6. Boundary between coalescence and no-coalescence region for 1-hexanol. .	167
Table A3.7. Boundary between coalescence and no-coalescence region for 1-heptanol. .	167
Table A3.8. Boundary between coalescence and no-coalescence region for 1-octanol. .	168
Table A3.9. Boundary between coalescence and no-coalescence region for F-150.	168
Table A3.10. Boundary between coalescence and no-coalescence region for MIBC.	169
Table A3.11. Boundary between coalescence and no-coalescence region for	169
Table A4.1. Bubble size distribution. Water: 380, 420, and 500 RPM.	170
Table A4.2. Bubble size distribution. F-150: 380, 420, and 500 RPM.	170
Table A4.3. Bubble size distribution. Dowfroth 250.	171
Table A4.4. Bubble size distribution. Pentanol, MIBC, F-150, NaCl.	171

Chapter 1 – Introduction

1.1 Introduction

Flotation is a widely used process to separate particles according to their hydrophobicity. Separation is achieved by dispersing air into bubbles that collide with and attach to hydrophobic particles. In this context, gas dispersion is defined as the dispersion of air into bubbles. It is well documented that the gas dispersion properties (e.g. bubble size distribution) in the flotation process have a direct influence on flotation performance (Schwarz and Alexander, 2006). This is understandable as the amount of gas-liquid interfacial (i.e., bubble surface) area available affects particle collection kinetics.

Gas dispersion is today commonly characterized in flotation systems by the measured variables superficial gas velocity (J_g), gas holdup and bubble size distribution, and the derived variable, bubble surface area flux (S_b) (Gomez and Finch, 2002, 2007). The superficial gas velocity and bubble surface area flux are defined as (Finch and Dobby, 1990):

$$J_g = \frac{Q_g}{A_c} \quad (\text{Eq. 1.1})$$

$$S_b = \frac{6J_g}{d_{32}} \quad (\text{Eq. 1.2})$$

where Q_g is the volumetric gas flow rate flowing through cross-sectional area A_c in the flotation machine, and d_{32} is the Sauter mean diameter.

The S_b represents the interfacial area or flux of bubble surface area per cross-sectional area in the cell and is often taken as the ‘machine’ variable to relate to flotation rate (Gorain et al., 1997; Gorain et al., 1998; Hernandez et al., 2003). The bubble size not only affects S_b , but influences the particle collision and attachment processes (Dai et al., 2000; Tao, 2004); hence, understanding the phenomena that affect bubble size is crucial to understanding the flotation process.

The bubble size distribution results from the interaction of the air delivery system (e.g., through the impeller in a mechanical flotation machine) and, in most cases, a surfactant known as a frother. Even though bubble size distribution drives flotation performance, little is known about how frothers act in this regard. Analysis of froth formation and stability emphasizes mechanisms that retard coalescence (Harris, 1982; Pugh, 1996). This coalescence prevention explanation has been extended to bubble generation (Metso Minerals CBT, 2002). This in turn has led to apparent quantification by introducing the critical coalescence concentration (CCC), which is the frother concentration producing the minimum bubble size in a swarm (Cho and Laskowski, 2002; Grau and Laskowski, 2006). Nettet et al. (2007) substitute CCC_{95} , i.e., concentration achieving 95% of bubble size reduction compared to water alone, as the basis of more systematic measurement. The name infers that the function of the frother is to preserve the size of bubble produced (by whatever mechanism) by preventing coalescence. Others have made the same claim (Gomez et al., 2000) and the reference to non-coalescing systems (e.g. Parthasarathy et al., 1991) may also imply this mechanism. Laskowski (2003) states that at frother concentrations lower than CCC , the bubble size is determined by coalescence; while at concentrations higher than CCC the bubble size is determined by

the generation device and hydrodynamic conditions. He proposed the critical coalescence concentration concept, together with foaming properties, as a way of characterizing flotation frothers.

Studying bubble swarms, as in determining *CCC*, does not permit coalescence prevention to be separated from the other possibility, that frothers may act on break-up, a mechanism that has not received much attention (Finch et al., 2006; Acuna et al., 2007).

Frothers not only affect bubble size and froth stability, but also how bubbles move in a liquid (Frumkin and Levich, 1947; Dukhin et al., 1998). Clift et al. (2005), summarizing data spanning 70 years, show a decrease in terminal rise velocity of single air bubbles in water over the size range ca. 1 to 10 mm in the presence of so-called ‘surface-active contaminants’. Other authors have found that bubbles move at different terminal velocities depending on frother type (Zhou et al., 1992; Sam et al., 1996; Zhang et al., 1996). Azgomi et al. (2007) found that, for a given gas rate, different frothers may generate the same gas holdup but with different bubble sizes, which suggests that bubble swarm velocity is affected by the presence of frothers. Acuna and Finch (2008) generating a 2D swarm confirmed this frother type effect. The time history or local velocity profiles and bubble shape also depend on frother type and concentration (Sam et al., 1996; Krzan et al., 2004).

This thesis studies the effect that common frothers (Pentanol, MIBC (methyl isobutyl carbinol), Dowfroth 250 (polyglycol ether), F-150 (polyglycol)) and salt (sodium chloride) have on bubble coalescence, bubble break-up, and bubble shape and rise

velocity (close to the generation point). Sodium chloride is included in the list of tested reagents because of its ability to reduce bubble size in flotation systems (Quinn et al., 2007).

1.2 Thesis objectives

The general objective is to study the action of frother in the generation of small bubbles in flotation systems. To accomplish the general objective, the following sub-objectives are set:

1. To examine bubble coalescence at bubble generation stage in the presence of frothers and salt. This requires:
 - a. Development and validation of a technique able to probe coalescence events in a time range of a few milliseconds.
 - b. An experimental study to reveal the action of frothers (and salt) on coalescence prevention at bubble generation stage.
 - c. A theoretical evaluation of the experimental results.

2. To examine bubble coalescence/break-up events in the presence of frothers (and salt) in a turbulent field. This requires:
 - a. Development of a set-up and procedure that allows discrimination between bubble coalescence and bubble break-up in a turbulent field.
 - b. Establishment of the role of frothers (and salt) on bubble coalescence and break-up in a turbulent field.
 - c. A theoretical analysis of the observed action.

3. To examine the effect of frothers (and salt) on bubble shape stabilization and rise velocity close to generation point. This requires:
 - a. An image analysis technique to determine bubble shape (aspect ratio) and rise velocity of newly formed bubbles.
 - b. An experimental study of the effect frother (and salt) has on these two parameters.
 - c. Investigation of link between bubble shape and velocity.

1.3 Thesis structure

The thesis is written as a ‘manuscript-based thesis’. It is organized in seven chapters, three of which (Chapters 3, 4, and 5) stand by themselves. These Chapters will be presented for publication. A chapter is included (Chapter 6) that provides a unifying discussion of the findings presented in Chapters 3, 4, and 5. The thesis also includes a general introduction (Chapter 1), a literature review (Chapter 2), and a conclusion covering all the findings (Chapter 7). The structure of the thesis may be summarized as follows:

Chapter 1 – Introduction: The importance of frothers and their role in flotation are introduced. The thesis objectives and structure are presented.

Chapter 2 – Literature review: This covers bubble coalescence, break-up, bubble shape, and rise velocity. The data on frothers are emphasized.

Chapter 3 – Coalescence inhibition at generation stage: Description, development, and validation of a method to study bubble coalescence at the generation stage at a capillary are presented. Experimental results for different frothers and salt (NaCl) are presented together with a theoretical analysis.

Chapter 4 – Bubble break-up and the role of frother and salt: A set-up especially designed to discriminate between bubble coalescence and break-up events is introduced.

The effect of frothers (and salt) on bubble break-up is presented together with a theoretical analysis.

Chapter 5 – Bubble rise velocity and shape: The effect of frothers and salt on bubble rise velocity and shape stabilization over short times after bubble detachment from a capillary tube (ca. 40 ms) is evaluated. An analysis is presented showing a link between shape and velocity.

Chapter 6 – Unifying discussion: By cross-referencing the previous chapters, common features are identified and apparent conflicts resolved.

Chapter 7 – Conclusions, contributions, and future work: Conclusions and claims of original research are presented. Suggestions for future research are also outlined.

Following Chapter 7, a complete listing of references and five appendixes providing supporting material are included. Because of the thesis structure, some repetition is expected, especially in the introductory sections of the Chapters. The author apologizes for that. If the reader is inclined, s/he may either read the literature review in Chapter 2 then skip the literature review section in Chapters 3, 4, and 5 or skip Chapter 2 and read the literature review in those Chapters. As required, connecting texts that provide logical bridges between Chapters 3, 4, and 5 (manuscripts) are included (before the introduction in Chapters 4 and 5). These connecting texts are meant to ensure that the thesis has continuity.

1.3 Contribution of authors

All the manuscripts are co-authored by Prof. James A. Finch in his capacity as research supervisor. The candidate designed and conducted all the experiments. He wrote the first draft of every Chapter (manuscript) and considered the comments of the co-author in the generation of the final versions.

References

- Acuna, C. Nasset, J. E., Finch J.A. 2007. Impact of Frother on Bubble Production and Behaviour in the Pulp Zone. In Proceedings of the Sixth International Copper-Cobre Conference, Aug. 25-30, Toronto, Ont. Canada, Volume II Mineral Processing (Eds. R del Villar, J. E. Nasset, C. O. Gomez and A. W. Stradling) MetSoc CIM. 197-210.
- Acuna, C., Finch, J.A., 2008. Motion of individual bubbles rising in a swarm. Submitted to IMPC 2008, Beijing, China.
- Azgomi, F., Gomez, C.O., Finch, J.A., 2007. Characterizing frothers using gas hold-up. Canadian Metallurgical Quarterly 46 (3). 237-242.
- Cho, Y.S., Laskowski, J.S., 2002. Effect of flotation frothers on bubble size and foam stability. International Journal of Mineral Processing 64. 69-80.
- Clift, R., Grace, J.R., Weber, M.E., 2005. Bubbles, Drops, and Particles. Academic Press, New York, 2nd edition.
- Dai, Z., Fornasiero, D, Ralston, J., 2000. Particle-bubble collision models – a review. Advances in Colloid and Interface Science 85. 231-256.
- Dukhin, S.S., Miller, R., Loglio, G., 1998. Physico-chemical hydrodynamics of rising bubble. Studies in Interface Science Vol. 6: Drops and Bubbles in Interfacial Research. D. Möbius and R. Miller Editors, Elsevier Science.
- Finch, J.A., Doby, G.S., 1990. Column flotation. Pergamon Press: Elmsford, New York.
- Finch, J.A., Gélinas, S., Moyo, P., 2006. Frother-related research at McGill University. Minerals Engineering 19. 726-733.
- Frumkin, A., Levich, V.G., 1947. On surfactants and interfacial motion. Zh. Fizicheskoi Khimii 21. 1183-1204.

- Gomez, C.O., Escudero, R., Finch, J.A., 2000. Determining equivalent pore diameter for rigid porous spargers. *Canadian Journal of Chemical Engineering* 78. 785-792.
- Gomez, C.O., Finch, J.A., 2002. Gas dispersion measurements in flotation machines. *CIM Bulletin* 95 (1066). 73-78.
- Gomez, C.O., Finch, J.A., 2007. Gas dispersion measurements in flotation cells. *International Journal of Mineral Processing* 84 (1-4). 51-58.
- Gorain, B.K., Franzidis, J.P, Manlapig, E.V., 1997. Studies on impeller type, impeller speed and air flow rate in an industrial scale flotation cell, Part 4: Effect of bubble surface area flux on flotation performance. *Minerals Engineering* 10 (4). 367-379.
- Gorain, B.K., Napier-Munn, T.J., Franzidis, J.P, Manlapig, E.V., 1998. Studies on impeller type, impeller speed and air flow rate in an industrial scale flotation cell, Part 5: Validation of k-Sb relationship and effect of froth depth. *Minerals Engineering* 11 (7). 615-626.
- Grau, R.A., Laskowski, J.S., 2006. Role of frothers in bubble generation and coalescence in a mechanical flotation cell. *The Canadian Journal of Chemical Engineering* 84. 170-182.
- Harris, P.J., 1982. Principles of flotation. Chapter 13: Frothing phenomena and frothers. King, R.P., ed. *South African Institute of Mining and Metallurgy Monograph Series* No. 3.
- Hernandez, H., Gomez, C.O., Finch, J.A., 2003. Gas dispersion and de-inking in a flotation column. *Mineral Engineering* 16 (6). 739-744.
- Krzan, M., Lunkenheimer, K., Malysa, K., 2004. On the influence of the surfactant's polar group on the local and terminal velocities of bubbles. *Colloids and Surfaces A: Physicochemical and Engineering Aspects* 250. 431-441.

- Laskowski, J.S., 2003. Fundamental properties of flotation frothers. Proceedings of the 22nd International Mineral Processing Congress. Cape Town, South Africa. 788-797.
- Metso Minerals CBT (Computer Based Training), 2002. Mill Operator Training Package. Flotation Module. Formerly Brenda Process Technology CBT (Computer Based Training) (1996). Mill Operator Training Package. Flotation Module.
- Nesset, J.E., Finch, J.A., Gomez, C.O., 2007. Operating variables affecting the bubble size in forced-air mechanical flotation machines. In proceedings of Ninth Mill Operators' Conference, Fremantle, WA, Australia. 55-65.
- Parthasarathy, R., Jameson, G.J., Ahmed, N., 1991. Bubble breakup in stirred vessels. Predicting the Sauter mean diameter. Chemical Engineering Research and Design 69. 295-301.
- Pugh, R.J., 1996. Foaming, foam films, antifoaming and defoaming. Advances in Colloid and Interface Science 64. 67-102.
- Quinn, J.J., Kracht, W., Gomez, C.O., Gagnon, C., Finch, J.A., 2007. Comparing the effect of salts and frother (MIBC) on gas dispersion and froth properties. Minerals Engineering 20. 1296-1302.
- Sam, A., Gomez, C.O., Finch, J.A., 1996. Axial velocity profiles of single bubbles in water/frother solutions. International Journal of Mineral Processing 47. 177-196.
- Schwarz, S., Alexander, D., 2006. Gas dispersion measurements in industrial flotation cells. Minerals Engineering 19 (6-8). 554-560.
- Tao, D., 2004. Role of bubble size in flotation of coarse and fine particles – A review. Separation Science and Technology 39 (4). 741-760.

- Zhang, Y., Gomez, C.O., Finch, J.A., 1996. Terminal velocity of bubbles: approach and preliminary investigations. In Proceedings of the International Symposium of Column Flotation, COLUMN'96, Aug. 26-28, Montréal, Québec, Canada. Eds. C.O. Gomez, J.A. Finch. 63-69.
- Zhou, Z.A., Egiebor, N.O., Plitt, L.R., 1992. Frother effect on single bubble motion in a water column. Canadian Metallurgical Quarterly 31 (1). 11-16.

Chapter 2 – Literature review

This review examines phenomena pertinent to the thesis contents, namely: bubble coalescence and break-up, bubbles and sound, and bubble shape and motion.

2.1 Bubble coalescence

2.1.1 General Considerations

Water is not an easy media in which to generate small bubbles. This is why it is necessary to add reagents called frothers in most flotation systems. Frothers are surface-active agents (surfactants), i.e., they reduce surface tension. They are used in flotation to aid generation of small bubbles.

Most theories of frother action are associated with froth/foam formation and stability. They emphasize mechanisms that retard coalescence (Harris, 1982; Pugh, 1996). This same coalescence prevention is usually extended to explain formation of small bubbles (Metso Minerals CBT, 2002).

Coalescence is the process by which two or more bubbles come together to generate a new bubble. The most likely coalescence act is between two bubbles, known as binary coalescence. Coalescence occurs in three steps: collision, film thinning, and film rupture (Oolman and Blanch, 1986; Prince and Blanch, 1990; Machon et al., 1997; Tse et al., 1998). In collision, bubbles contact one other within a liquid. This step is controlled

by the hydrodynamics of the bulk liquid phase. Contact is characterized by a flattening of the facing bubble surfaces, leaving a thin film separating them. The initial thickness of this film is typically 10^{-3} to 10^{-4} cm. The film must thin to approximately 10^{-6} cm for rupture. The contact time has to be longer than the time required for the film to thin to rupture, otherwise coalescence does not occur. This step is controlled by the hydrodynamics of the liquid film and forces associated with surface tension gradients or surface visco-elastic effects if surfactants are present (Fruhner et al., 1999). Once sufficiently thin (ca. 10^{-6} cm), the film ruptures due to instability mechanisms, resulting in bubble coalescence. This last step is very fast compared to the other two.

In a global approach, coalescence prevention has apparently been quantified by the critical coalescence concentration (*CCC*), which is the frother concentration producing the minimum bubble size in a swarm (Cho and Laskowski, 2002; Grau and Laskowski, 2006). Nasset et al. (2007) substitute *CCC95*, i.e., concentration achieving 95% of bubble size reduction as the basis of more systematic measurement. The name obviously infers that the function of the frother is to preserve the size of bubble produced (by whatever mechanism) by preventing coalescence. Others have made the same claim (Gomez et al., 2000; Metso Minerals CBT, 2002). Laskowski (2003) states that at frother concentrations lower than *CCC* the bubble size is determined by coalescence, while at concentrations higher than *CCC* the bubble size is determined by the generation device and hydrodynamic conditions. He proposed the critical coalescence concentration concept, together with foaming properties, as a way of characterizing flotation frothers.

2.1.2 Film elasticity

A characteristic of surfactants is their ability to impart elasticity to liquid films, which is related to the increase in tension during stretching. The elasticity is called Gibbs elasticity if the mechanism of increasing tension involves redistribution of components in the film as in the case of surfactants (Rusanov and Krotov, 2003). The Gibbs elasticity may be expressed as follows (Hofmeier et al., 1995):

$$E = 2 \frac{d\sigma}{d \ln A} = 2A \frac{d\sigma}{dc} \frac{dc}{dA} \quad (\text{Eq. 2.1})$$

where σ is the surface tension, A the film area, c the concentration, and the factor 2 accounts for the fact that the film trapped between the bubbles has two liquid-air interfaces. (In the case of a bubble being deformed, e.g. by the action of turbulence, there is only one liquid-air surface and the factor in Equation 2.1 reduces to one.)

Gibbs elasticity may be seen as a measure of the ability of a liquid film to adjust its surface tension under the action of an external force. If the liquid film is stretched, the local surface concentration of surfactant decreases; as a consequence the local surface tension increases creating a restoring force that protects the film against rupture (Adamson, 1990). The surface tension gradients are counterbalanced by a shearing stress that generates a liquid counter flow along the surface into the film, the Marangoni effect (Hofmeier et al., 1995). Even though stretching may be minor when two bubbles collide, surface tension gradient-driven phenomena affect the coalescence process (Marucci, 1969). Figure 2.1 depicts the process: depletion of surface concentration of surfactant due to film stretching, resulting in an opposing surface tension gradient-generated force.

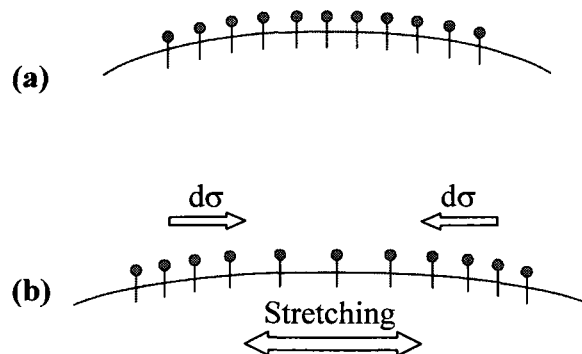


Figure 2.1. Film elasticity. (a) Film before stretching has uniform surface concentration of surfactant. (b) Stretching lowers local surface concentration of surfactant, and the local surface tension increases protecting the film.

2.1.3 Surface viscosity

Surface tension gradients generated during film stretching may be reduced by diffusion and adsorption of surfactant from the adjacent liquid. When such a relaxation process occurs, the surface has visco-elastic properties (Lucassen and Van Den Tempel, 1972).

When the rate of deformation is high, the system has no time to respond (diffusion-adsorption limited) and the effect is purely elastic. For slower rates of deformation diffusion-adsorption take place, which reduces surface tension gradients when compared to the purely elastic case, and visco-elastic properties appear. In the extreme case of very slow deformation, the surface maintains equilibrium and the surface tension gradient becomes zero (Monroy et al., 1998). The relationship between surface

tension gradient and deformation rate is characteristic of an intrinsic viscosity (Frunher and Wantke, 1996) and the ratio between them allows the calculation of the surface dilational viscosity, defined as (Dickinson, 1999):

$$\eta_d = \frac{d\sigma}{d \ln A / dt} \quad (\text{Eq. 2.2})$$

Figure 2.2 shows the process, diffusion-adsorption of surfactant molecules to the stretched film, resulting in the generation of surface dilational viscosity.

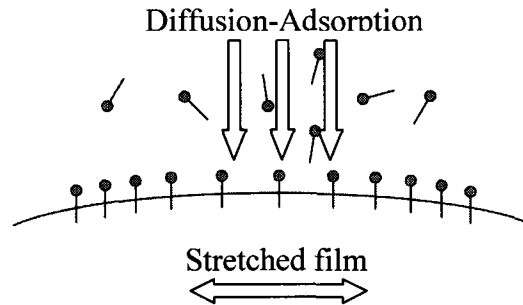


Figure 2.2. Surface dilational viscosity.

A contribution to the surface viscosity may come from the property of the adsorbed surfactant molecules to H-bond with neighboring water molecules via their polar groups (Schott, 1995) generating a local region of ‘organized’ water on the bubble (film) surface (Finch et al., 2006). Wang and Yoon (2006) introduce the notion that the bubble becomes less hydrophobic on addition of frother, which is again related to the H-bonding capability, i.e., it is a similar argument.

Studies of surfactant action on froth formation suggest that elasticity is not enough to explain froth stability and that surface dilational viscosity must be taken into account

(Fruhner et al., 1999). The same is expected in coalescence prevention during bubble formation.

2.1.4 Total stress

When a film is deformed, some internal forces appear as a reaction to the external force. Those forces are known as ‘stress’ and may be seen as the resistance of the film to deformation. According to the previous discussion, elasticity and surface viscosity appear as a reaction to deformation, so they have to be present in the definition of total stress.

The total stress τ , for a local deformation ε , may be defined as the sum of elastic and viscous components (Horozov, 1997):

$$\tau = E \cdot \varepsilon + \eta_d \cdot \dot{\varepsilon} \quad (\text{Eq. 2.3})$$

When two bubbles collide in presence of surfactant the ‘organized’ water may offer some resistance to flow. Together with the elasticity (E) this adds to film stability. The diffusion-adsorption of fresh surfactant molecules from internal layers in the film at the stretched surface restores the strength of the ‘organized’ region of water, protecting the film against rupture, and allowing for longer contact times between bubbles without coalescence (i.e., viscous component η_d of the total stress).

The total stress is zero for clean systems, i.e., water, because both elasticity and surface viscosity equal zero. Stress appears in the presence of surfactants and is expected to be a key component in coalescence prevention. This thesis (Chapter 3) explores

qualitatively the influence of the total stress in coalescence prevention for different frother types and concentrations.

Chapter 3 examines coalescence events using bubble generation at a capillary as a model system.

2.2 Break-up

Break-up (breakage) refers to bubbles (or an air stream) breaking into smaller bubbles. The break-up mechanism is modeled considering either collision of bubbles with turbulent eddies or bubbles interacting with wakes in a swarm. The studies that assume collision with turbulent eddies are based on the work of Hinze (1955). The eddies considered responsible for break-up are those of comparable size to the bubble. Larger eddies transport groups of bubbles, while eddies much smaller than the bubble do not have enough energy to cause break-up. The studies based on wake interactions are from experimental observations (Stewart, 1995) that suggest the wake environment provides the driving force in bubble-bubble interactions, including coalescence and break-up.

Walter and Blanch (1986) observed with high-speed photography that break-up occurred by a dumbbell stretching mechanism, with break-up time of the order of 25 ms. Figure 2.3 is taken from that work identifying one dumbbell dividing (and also showing the difficulty in imaging the event in bubble swarms).

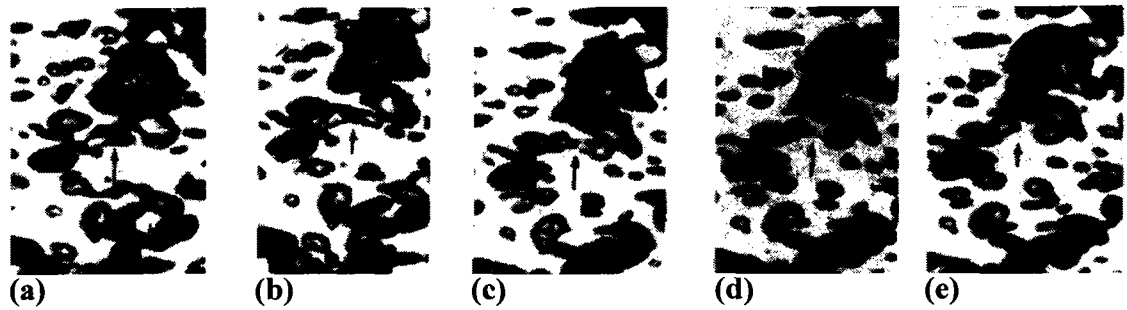


Figure 2.3. Sequence of images of bubble break-up by dumbbell stretching mechanism. (a) $t = 0$ ms, (b) $t = 8$ ms, (c) $t = 20$ ms, (d) $t = 22$ ms, and (e) $t = 25$ ms (Walter and Blanch, 1986. Reprinted with permission from Elsevier).

In the presence of frother, the dumbbell stretching mechanism will cause uneven frother distribution, which generates surface instabilities that may promote or retard break-up (Miller and Neogi, 1985; Dukhin et al., 1998; Finch et al., 2008). The same general argument applies to salts, in this case with water molecules substituting for the frother in terms of surface activity (Finch et al., 2008). This chapter explores frother effects on bubble break-up.

A break-up model must include not only the break-up rate but also the daughter size distribution (Wang et al., 2003). Wang et al. list four characteristics of the daughter bubble size distribution:

1. A local minimum should exist at equal (50:50) break-up fraction because the surface area and therefore surface energy increase is the highest of all possible break-up fractions. (The break-up fraction refers to the volume fraction of the mother bubble that becomes the daughter bubbles.) This local minimum should be

greater than zero because the probability of equal-size break-up, while small, is not zero.

2. The generation of small bubbles requires high energy because of the high capillary (internal) pressure. Therefore, the daughter bubble size distribution should vanish before the break-up fraction approaches zero.
3. The daughter bubble size distribution depends on the mother bubble size and the energy dissipation rate. Because of the restriction in generating small bubbles (high capillary pressures), the equal-size break-up probability increases with decreasing mother bubble size. In the case of energy dissipation rate, the higher the rate the higher the probability of unequal-size break-up.
4. The daughter bubble size distribution should not have any singularity point, i.e., the frequency vs. size plot should be smooth and well defined.

The daughter bubble size distribution is determined by the break-up fraction, so modeling this function is required for the correct representation of the physics of the process. Luo and Svendsen (1996), for instance, generated a break-up model without considering the capillary pressure restriction; consequently, their daughter bubble size distributions do not vanish for break-up fractions approaching zero.

Chapter 4 explores both qualitatively and quantitatively the effect of frothers on bubble break-up.

2.3 Bubbles as a source of sound

Acoustic emissions present a way of monitoring gas-liquid dispersions, solid systems and chemical reactions (Boyd and Varley, 2001). Sound emanating as a bubble forms has been widely studied in oceanography to identify sources of ambient sound in the oceans (e.g., Ye and Feuillade, 1997; Leighton 2004). The application in this thesis represents a novel approach to the fundamental study of bubble coalescence.

A bubble surface oscillates (pulsates) when a bubble is formed; these surface oscillations (pulsations) convey perturbations to the surrounding medium, water in this case, and a sound wave will move through the water in all directions (Dawson, 2002). The newly formed bubbles are considered freely oscillating (pulsating) bubbles, and the sound produced was first studied by Minnaert (1933). In recognition of this, bubble surface oscillations are also known as Minnaert pulsations. He showed that the natural frequency of pulsation of bubbles f under a static pressure P_0 in a liquid of density ρ_l relates to the bubble diameter d as follows:

$$f = \frac{1}{\pi d} \left(\frac{3kP_0}{\rho_l} \right)^{1/2} \quad (\text{Eq. 2.4})$$

where k is the so-called polytropic index, which takes different values depending on whether the process is isothermal (unhindered heat flow) or adiabatic (no heat flow). In the case of air it takes values between 1 (isothermal) and 1.4 (adiabatic) (Leighton and Walton, 1987).

To oscillate, an object must at some time receive an exciting force (Leighton, 1994). In this case the exciting force is the initial impulse received by the bubble at the moment of detachment from the capillary. For a freely rising bubble at all other times the force is zero and there is no sound emanated. There is another exciting force generated when bubbles burst (Vandewalle et al., 2001); and as will be shown, another exciting force is generated when bubbles coalesce.

A newly generated bubble behaves like a lightly damped simple harmonic oscillator (Leighton and Walton, 1987). The acoustic signal recorded for each bubble is sinusoidal with an exponential decay. When bubbles coalesce or break-up they also emit a decaying sinusoidal pulse of sound (Strasberg, 1956). Identification of sound with coalescence events, and its use to study coalescence prevention form part of the contribution of this thesis (Chapter 3).

2.4 Bubble shape and rise velocity

The presence of frother not only promotes the generation of small bubbles, but also affects how bubbles move. Bubble motion may be classified into three regimes depending on rise velocity (Kulkarni and Joshi, 2000). The bubble Reynolds (Re) and Eötvös (EO) numbers are used in the characterization, calculated from (Clift et al., 2005):

$$EO = \frac{g(\rho_l - \rho_{air})d_{eq}^2}{\sigma} \quad (\text{Eq. 2.5})$$

$$Re = \frac{\rho_l d_{eq} v}{\mu} \quad (\text{Eq. 2.6})$$

where g is the acceleration of gravity, ρ_l and ρ_{air} are the liquid and air density respectively, d_{eq} is the bubble equivalent spherical diameter, σ the surface tension, μ the liquid viscosity, and v the bubble rise velocity. The range of Eötvös number for bubbles in this study is $0.78 < Eo < 0.87$, and the range in Reynolds number is $210 < Re < 900$.

Tomiyama et al. (2002) summarize the role of surfactants on bubble dynamics in the three regimes as follows:

1. Viscous force dominant regime (small spherical bubble, $Eo < 0.25$): Accumulation of surfactants on bubble surface, together with the bubble motion, induces surface tension gradients and the Marangoni effect that makes the surface immobile and the bubble rise as a rigid sphere. The surface goes from free-slip to no-slip condition, resulting in an increase in viscous drag and decrease in terminal velocity.
2. Surface tension force dominant regime (intermediate size bubble, $0.25 < Eo < 40$): Surfactants reduce shape variation, making bubbles more spherical. The terminal velocity becomes close to that of bubbles in clean systems with small initial shape deformation. Terminal velocity gradually decreases with increasing bubble size in this regime (the authors give a range of bubble sizes (1.3 mm – 6 mm) based on a previous study (Peebles and Garber, 1953)). Most bubbles in flotation practice fall into categories 1 and 2.

3. Inertial force dominant regime (large bubble, $Eo > 40$): High inertia reduces the impact of surfactant in bubble motion and shape. The drag due to inertia is much higher than the viscous drag due to the Marangoni effect.

At Reynolds numbers higher than 200 ($Re > 200$), bubble buoyancy is complicated by bubble shape variation and bubble path instability (Dukhin et al., 1998). In a qualitative approach, it is suggested (Dukhin et al., 1998; Linton and Sutherland, 1957; Frumkin and Levich, 1947) that surfactants are swept to the rear of a rising bubble, generating a region of low surface concentration at the leading surface of the bubble and a region of large concentration at the rear pole of the bubble. The low concentration (leading) region remains mobile, whereas the high concentration (rear) region is characterized by retarded surface mobility (rear stagnant cap).

Acuna (2007) studied the effect of surfactants (frothers) on single bubbles of ca. 3.5 mm diameter generated at a capillary tip over the first 50 ms or so. He found that the effect of surfactant is not instantaneous, it taking time to diffuse/adsorb at the bubble surface and affect the properties. Bubbles blown in tap water and in surfactant solution (0.1 mmol/L polyglycol, F-150) behaved identically in terms of aspect ratio and local velocity over the first 10 ms following bubble detachment. After this the bubble in surfactant solution became more spherical than its water only cousin and slowed down significantly. Although over much shorter time periods, this work is in agreement with others (Sam et al., 1996; Zhang et al., 2001; Krzan et al., 2004, 2007).

Krzan et al. (2004, 2007) studied local (instantaneous) velocities and shape variations of bubbles rising in presence of surfactants. They confirmed the previous findings of Sam et al. (1996) and Zhang et al. (2001, 2003) that after initial acceleration, bubbles either attained a constant velocity (terminal velocity) at high concentrations of surfactant, or passed through a maximum in the local velocity followed by a deceleration prior to reaching terminal velocity for low concentrations of surfactant. The maximum in local velocity indicates that the dynamic steady state structure of the adsorption layer on the rising bubble is not yet established. Bubble shape also stabilized once terminal velocity was reached.

Differences in local rise velocity are not restricted to surfactant systems. Wu and Gharib (2002) produced spherical and ellipsoidal bubbles of equivalent volume in purified water and found that the spherical bubbles moved significantly slower than their ellipsoidal counterparts.

Figure 2.4 is taken from Wu and Gharib (2002), and shows the correlation that exists between bubble rise velocity and bubble shape: spherical bubbles rose more slowly than ellipsoidal bubbles (note the latter reaches the top of the frame sooner than the spherical bubble).

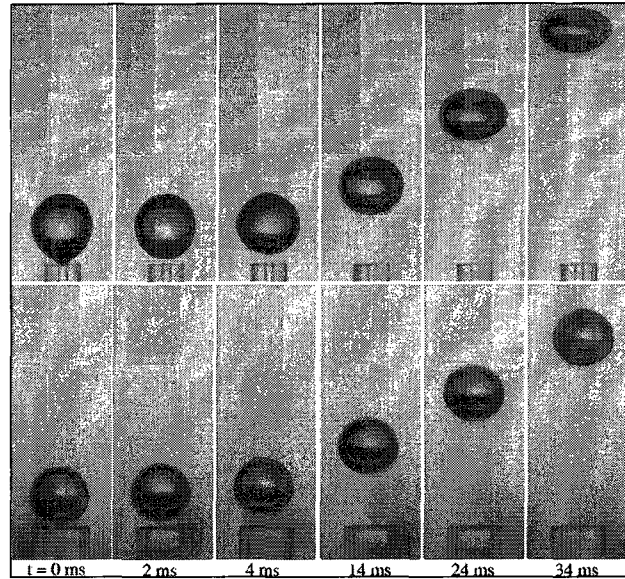


Figure 2.4. Bubbles of equivalent volume rising in water. The size of each image is $0.32 \text{ cm} \times 0.88 \text{ cm}$. (Wu and Gharib, 2002. Reprinted with permission from the American Institute of Physics).

De Vries et al. (2002) studied the influence of bubble shape oscillations on local velocities of bubbles in the absence of surfactants. They found that shape oscillations correlated with an oscillating bubble rise velocity and deduced that the oscillations in velocity were caused by variations in the added-mass term, which corresponds to an inertia effect originating as the rising bubble has to push water out of the way. The virtual or added-mass term is taken into account to calculate the exact rate of exchange of momentum of objects (bubbles) accelerating, rotating or oscillating in fluids, which depends on the shape of the bubbles (Kendoush, 2007).

From numerical analysis, Dijkhuizen et al. (2005) predicted oscillations in both shape and velocity of bubbles of 3 mm and larger in initially quiescent pure water. They considered the drag and virtual mass forces in their calculations.

The works of Wu and Gharib (2002), De Vries et al. (2002), and Dijkhuizen et al. (2005) therefore suggest it is bubble shape that controls velocity. The action of surfactant is then seen as one of modulating shape, making a bubble more spherical (due to surface tension gradient effects) that cause the bubble to slow down as opposed to the more direct effect of increasing drag due to surface tension gradient effects. Chapter 5 explores the validity of this suggestion for bubbles rising in surfactant solutions.

References

- Acuna, C., 2007. Measurement techniques to characterize bubble motion in swarms. McGill University, Montréal, QC, Canada. PhD Thesis.
- Adamson, A.W., 1990. Physical chemistry of surfaces, 5th Edition. John Wiley & Sons, Inc. New York.
- Boyd, J.W.R., Varley, J., 2001. The uses of passive measurement of acoustic emissions from chemical engineering processes. *Chemical Engineering Science* 56. 1749-1767.
- Cho, Y.S., Laskowski, J.S., 2002. Effect of flotation frothers on bubble size and foam stability. *International Journal of Mineral Processing* 64. 69-80.
- Clift, R., Grace, J.R., Weber, M.E., 2005. Bubbles, Drops, and Particles. Academic Press, New York, 2nd edition.
- Dawson, P., 2002. The physics of the oscillating bubble made simple. *European Journal of Radiology* 41. 176-178.
- De Vries, J., Luther, S., Lohse, D., 2002. Induced bubble shape oscillations and their impact on the rise velocity. *The European Physical Journal B* 29. 503-509.

- Dickinson, E., 1999. Adsorbed protein layers at fluid interfaces: interactions, structure and surface rheology. *Colloids and Surfaces B: Biointerfaces* 15. 161-176.
- Dijkhuizen, W., van den Hengel, E.I.V., Deen, N.G., van Sint Annaland, M., Kuipers, J.A.M., 2005. Numerical investigation of closures for interface forces acting on single air-bubbles in water using Volume of Fluid and Front Tracking models. *Chemical Engineering Science* 60. 6169-6175.
- Dukhin, S.S., Miller, R., Loglio, G., 1998. Physico-chemical hydrodynamics of rising bubble. *Studies in Interface Science Vol. 6: Drops and Bubbles in Interfacial Research*. D. Möbius and R. Miller Editors, Elsevier Science.
- Finch, J.A., Gélinas, S., Moyo, P., 2006. Frother-related research at McGill University. *Minerals Engineering* 19. 726-733.
- Finch, J.A., Nasset, J.E., Acuña, C., 2008. Role of frother on bubble production and behaviour in flotation. *Minerals Engineering*. Article in Press.
- Fruhner, H., Wantke, K.-D., 1996. A new oscillating bubble technique for measuring surface dilational properties. *Colloids and Surfaces A: Physicochemical and Engineering Aspects* 114. 53-59.
- Fruhner, H., Wantke, K.-D., Lunkenheimer, K., 1999. Relationship between surface dilational properties and foam stability. *Colloids and Surfaces A: Physicochemical and Engineering Aspects* 162. 193-202.
- Frumkin, A., Levich, V.G., 1947. On surfactants and interfacial motion. *Zh. Fizicheskoi Khimii* 21. 1183-1204.
- Gomez, C.O., Escudero, R., Finch, J.A., 2000. Determining equivalent pore diameter for rigid porous spargers. *Canadian Journal of Chemical Engineering* 78. 785-792.

- Grau, R.A., Laskowski, J.S., 2006. Role of frothers in bubble generation and coalescence in a mechanical flotation cell. *The Canadian Journal of Chemical Engineering* 84. 170-182.
- Harris, P.J., 1982. Principles of flotation. Chapter 13: Frothing phenomena and frothers. King, R.P., ed. *South African Institute of Mining and Metallurgy Monograph Series No. 3*.
- Hinze, J.O., 1955. Fundamentals of the hydrodynamic mechanism of splitting in dispersion processes. *AIChE Journal*. 1 (3). 289-295.
- Hofmeier, U., Yaminsky, V.V., Christenson, H.K., 1995. Observations of solute effects on bubble formation. *Journal of Colloid and Interface Science* 174. 199-210.
- Horozov, T.S., Kralchevsky, P.A., Danov, K.D., Ivanov, I.B., 1997. Interfacial rheology and kinetics of adsorption from surfactant solution. *Journal of Dispersion Science and Technology* 18 (6-7), 593-607.
- Kendoush, A.A., 2007. The virtual mass of an oblate-ellipsoidal bubble. *Physics Letters A* 366. 253-255.
- Krzan, M., Lunkenheimer, K., Malysa, K., 2004. On the influence of the surfactant's polar group on the local and terminal velocities of bubbles. *Colloids and Surfaces A: Physicochemical and Engineering Aspects* 250. 431-441.
- Krzan, M., Zawala, J., Malysa, K., 2007. Development of steady state adsorption distribution over interface of a bubble risitn in solutions of *n*-alkanols (C₅, C₈) and *n*-alkyltrimethylammonium bromides (C₈, C₁₂, C₁₆). *Colloids and Surfaces A: Physicochemical and Engineering Aspects* 298. 42-51.
- Kulkarni, A.A., Joshi, J.B., 2005. Bubble formation and bubble rise velocity in gas-liquid systems: a review. *Industrial & Chemical Engineering Research* 44. 5873-5931.

- Laskowski, J.S., 2003. Fundamental properties of flotation frothers. Proceedings of the 22nd International Mineral Processing Congress. Cape Town, South Africa. 788-797.
- Leighton, T.G., Walton, A., 1987. An experimental study of the sound emitted from gas bubbles in a liquid. *Eur. J. Phys.* 8. 98-104.
- Leighton, T.G., 1994. *The acoustic bubble*. New York: Academic Press.
- Leighton, T.G., 2004. From seas to surgeries, from babbling brooks to baby scans: the acoustics of gas bubbles in liquids. *International Journal of Modern Physics B* 18 (25). 3267-3314.
- Linton, M., Sutherland, K.L. 1957. Dynamic surface forces, drop circulation and liquid-liquid mass transfer. *Second International Congress on Surface Activity*, 1. Butterworth, London. 494-501.
- Lucassen, J., Van Den Tempel, M. 1972. Dynamic measurements of dilational properties of a liquid interface. *Chemical Engineering Science* 27. 1283-1291.
- Luo, H., Svendsen H.F., 1996. Theoretical model for drop and bubble breakup in turbulent dispersions. *AIChE Journal* 42 (5). 1225-1233.
- Machon, V., Pacek, A.W., Nienow A.W., 1997. Bubble sizes in electrolyte and alcohol solutions in a turbulent stirred vessel. *Trans IChemE* 75 (A). 339-348.
- Marrucci, G., 1969. A theory of coalescence. *Chemical Engineering Science* 24, 975-985.
- Metso Minerals CBT (Computer Based Training), 2002. Mill Operator Training Package. Flotation Module. Formerly Brenda Process Technology CBT (Computer Based Training) (1996). Mill Operator Training Package. Flotation Module.
- Miller, C.A., Neogi, P., 1985. Interfacial phenomena: equilibrium and dynamic effects. In: *Surfactant Science Series*, vol. 17, Chapter VI: Transport Effects on Interfacial Phenomena. 240-298.

- Minnaert, M., 1933. On musical air-bubbles and the sounds of running water. *Philosophical Magazine* 16, 235-248.
- Monroy, F., Giermanska Kahn, J., Langevin, D., 1998. Dilational viscoelasticity of surfactant monolayers. *Colloids and Surfaces A: Physicochemical and Engineering Aspects* 143, 251-260.
- Nesset, J.E., Finch, J.A., Gomez, C.O., 2007. Operating variables affecting the bubble size in forced-air mechanical flotation machines. In proceedings of Ninth Mill Operators' Conference, Freemantle, WA, Australia. 55-65.
- Oolman, T.O., Blanch, H.W., 1986. Bubble coalescence in stagnant liquids. *Chemical Engineering Communications* 43. 237-261.
- Peebles, F.N., Garber, H.J., 1953. Studies on the motion of gas bubbles in liquids. *Chemical Engineering Progress* 49 (2). 88-97.
- Prince, M.J., Blanch, H.W., 1990. Bubble coalescence and break-up in air-sparged bubble columns. *AIChE Journal* 36 (10). 1485-1499.
- Rusanov, A.I., Krotov, V.V., 2003. Gibbs elasticity of free thin liquid films. *Doklady Physical Chemistry* 393 (4-6). 350-352.
- Sam, A., Gomez, C.O., Finch, J.A., 1996. Axial velocity profiles of single bubbles in water/frother solutions. *International Journal of Mineral Processing* 47. 177-196.
- Schott, H. 1995. Hydrophilic-lipophilic balance, solubility parameter, and oil-water partition coefficient as universal parameters of nonionic surfactants. *Journal of Pharmaceutical Sciences* 84 (10). 1215-1222.
- Stewart C.W., 1995. Bubble interaction in low-viscosity liquids. *Int. J. Multiphase Flow* 21, No. 6, 1037-1046.

- Strasberg, 1956. Gas bubbles as sources of sound in liquids. *The Journal of the Acoustical Society of America* 28 (1). 20-26.
- Tomiyama, A. Celata G.P., Hosokawa, S., Yoshida, S., 2002. Terminal velocity of single bubbles in surface tension force dominant regime. *International Journal of Multiphase Flow* 28. 1497-1519.
- Vandevalle, N., Lentz, J.F., Dorbolo, S., Brisbois, F., 2001. Avalanches of popping bubbles in collapsing foams. *Physical Review Letters* 86 (1). 179-182.
- Walter J.F., Blanch H.W., 1986. Bubble break-up in gas-liquid bioreactors: break-up in turbulent flows. *The Chemical Engineering Journal* 32. B7-B17.
- Wang, L., Yoon, R-H., 2006. Role of hydrophobic force in the thinning of foam films containing a nonionic surfactant. *Colloids and Surfaces A: Physicochemical and Engineering Aspects* 282-283. 84-91.
- Wang, T., Wang, J., Jin, J., 2003. A novel theoretical breakup kernel function of bubble/droplet in a turbulent flow. *Chemical Engineering Science* 58. 4629-4637.
- Wu, M., Gharib, M., 2002. Experimental studies on the shape and path of small air bubbles rising in clean water. *Physics of Fluids* 14 (7). L49-L52.
- Ye, Z., Feuillede, C., 1997. Sound scattering by an air bubble near a plane sea surface. *The Journal of the Acoustical Society of America* 102 (2). 798-805.
- Zhang, Y., McLaughlin, J.B., Finch, J.A., 2001. Bubble velocity profile and model of surfactant mass transfer to bubble surface. *Chemical Engineering Science* 56. 6605-6616.
- Zhang, Y., Sam, A., Finch, J.A., 2003. Temperature effect on single bubble velocity profile in water and surfactant solution. *Colloids and Surfaces A: Physicochemical and Engineering Aspects* 223. 45-54.

Chapter 3 - Coalescence inhibition at bubble generation stage

3.1 Introduction

It is well documented that the gas dispersion properties in the flotation process have a direct influence on flotation performance (Schwarz and Alexander, 2006). Gas dispersion is today commonly characterized in flotation systems by the measured variables superficial gas velocity (J_g), gas holdup and bubble size distribution, and the derived variable, bubble surface area flux ($S_b = 6J_g/d$, where d is usually the Sauter mean bubble diameter, d_{32}) (Gomez and Finch, 2007). The S_b represents the interfacial area or flux of bubble surface area per cross-sectional area in the cell and is often taken as the ‘machine’ variable to relate to flotation rate (Gorain et al., 1997; Gorain et al., 1998; Hernandez et al., 2003). The bubble size not only affects S_b , but influences the particle collision and attachment processes (Dai et al., 2000; Tao, 2004); hence, understanding the phenomena that affect bubble size is crucial to understanding the flotation process.

3.2 Bubble coalescence

3.2.1 General Considerations

Water is not an easy media in which to generate small bubbles. This is why it is necessary to add reagents called frothers in most flotation systems. Frothers are surface-active agents (surfactants), i.e., they reduce surface tension. They are used in flotation to aid generation of small bubbles.

Most theories of frother action are associated with froth/foam formation and stability. They emphasize mechanisms that retard coalescence (Harris, 1982; Pugh, 1996). This same coalescence prevention is usually extended to explain formation of small bubbles (Metso Minerals CBT, 2002).

Coalescence is the process by which two or more bubbles come together to generate a new bubble. The most likely coalescence act is between two bubbles: this is known as binary coalescence. Coalescence occurs in three steps: collision, film thinning, and film rupture (Oolman and Blanch, 1986; Prince and Blanch, 1990; Machon et al., 1997; Tse et al., 1998). In collision, bubbles contact one other within a liquid. This step is controlled by the hydrodynamics of the bulk liquid phase. Contact is characterized by a flattening of the facing bubble surfaces, leaving a thin film separating them. The initial thickness of this film is typically 10^{-3} to 10^{-4} cm. The film must thin to approximately 10^{-6} cm in thickness for rupture. The contact time has to be longer than the time required for the film to thin to rupture, otherwise coalescence does not occur. This step is controlled by the hydrodynamics of the liquid film and forces associated with surface tension gradients or surface visco-elastic effects if surfactants are present (Fruhner et al., 1999). Once sufficiently thin (ca. 10^{-6} cm), the film ruptures due to instability mechanisms, resulting in bubble coalescence. This last step is very fast compared to the other two.

In a global approach, coalescence prevention has apparently been quantified by the critical coalescence concentration (*CCC*), which is the frother concentration producing the minimum bubble size in a swarm (Cho and Laskowski, 2002; Grau and Laskowski, 2006). Nettet et al. (2007) substitute *CCC95*, i.e., concentration achieving

95% of bubble size reduction as the basis of more systematic measurement. The name obviously infers that the function of the frother is to preserve the size of bubble produced (by whatever mechanism) by preventing coalescence. Others have made the same claim (Gomez et al., 2000; Metso Minerals CBT, 2002). Laskowski (2003) states that at frother concentrations lower than *CCC* the bubble size is determined by coalescence, while at concentrations higher than *CCC* the bubble size is determined by the generation device and hydrodynamic conditions. He proposed the critical coalescence concentration concept, together with foaming properties, as a way of characterizing flotation frothers.

3.2.2 Film elasticity

A characteristic of surfactants is their ability to impart elasticity to liquid films, which is related to the increase in tension during stretching. The elasticity is called Gibbs elasticity if the mechanism of increasing tension involves redistribution of components in the film as in the case of surfactants (Rusanov and Krotov, 2003). The Gibbs elasticity may be expressed as follows (Hofmeier et al., 1995):

$$E = 2 \frac{d\sigma}{d \ln A} = 2A \frac{d\sigma}{dc} \frac{dc}{dA} \quad (\text{Eq. 3.1})$$

where σ is the surface tension, A the film area, c the concentration, and the factor 2 accounts for the fact that the film trapped between the bubbles has two liquid-air interfaces. (In the case of a bubble being deformed, e.g. by the action of turbulence, there is only one liquid-air surface and the factor in Equation 3.1 reduces to one.)

Gibbs elasticity may be seen as a measure of the ability of a liquid film to adjust its surface tension under the action of an external force. If the liquid film is stretched, the local surface concentration of surfactant decreases; as a consequence the local surface tension increases creating a restoring force that protects the film against rupture (Adamson, 1990). The surface tension gradients are counterbalanced by a shearing stress that generates a liquid counter flow along the surface into the film, the Marangoni effect (Hofmeier et al., 1995). Even though stretching may be minor when two bubbles collide, surface tension gradient-driven phenomena affect the coalescence process (Marucci, 1969). Figure 3.1 depicts the process: depletion of surface concentration of surfactant due to film stretching, resulting in an opposing surface tension gradient-generated force.

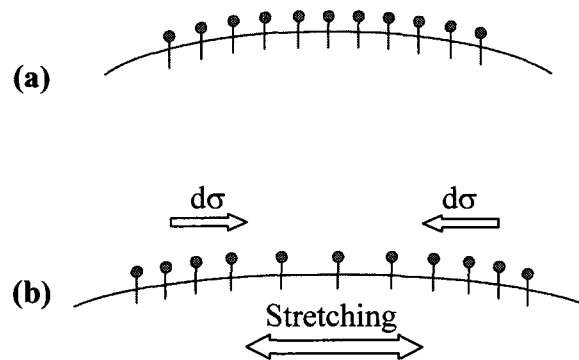


Figure 3.1. Film elasticity. (a) Film before stretching has uniform surface concentration of surfactant. (b) Stretching lowers local surface concentration of surfactant, and the local surface tension increases protecting the film.

3.2.3 Surface viscosity

Surface tension gradients generated during film stretching may be reduced by diffusion and adsorption of surfactant from the adjacent liquid. When such relaxation occurs, the surface has visco-elastic properties (Lucassen and Van Den Tempel, 1972).

When the rate of deformation is high, the system has no time to respond (diffusion-adsorption limited) and the effect is purely elastic. For slower rates of deformation diffusion-adsorption take place, which reduces surface tension gradients when compared to the purely elastic case, and visco-elastic properties appear. In the extreme case of very slow deformation, the surface may maintain equilibrium and the surface tension gradient becomes zero (Monroy et al., 1998). The relationship between surface tension gradient and deformation rate is characteristic of an intrinsic viscosity (Frunher and Wantke, 1996) and the ratio between them allows the calculation of the surface dilational viscosity, defined as (Dickinson, 1999):

$$\eta_a = \frac{d\sigma}{d \ln A / dt} \quad (\text{Eq. 3.2})$$

Figure 2.2 shows the process, diffusion-adsorption of surfactant molecules to the stretched film, resulting in the generation of surface dilational viscosity.

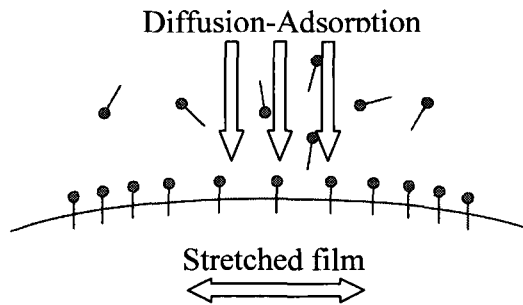


Figure 3.2. Surface dilational viscosity.

A contribution to the surface viscosity may come from the property of the adsorbed surfactant molecules to H-bond with neighboring water molecules via their polar groups (Schott, 1995) generating a local region of ‘organized’ water on the bubble (film) surface (Finch et al., 2006). Wang and Yoon (2006) introduce the notion that the bubble becomes less hydrophobic on addition of frother, which is again related to the H-bonding capability, i.e., it is a similar argument.

Studies of surfactant action on froth formation suggest that elasticity is not enough to explain froth stability and that surface dilational viscosity must be taken into account (Fruhner et al., 1999). The same is expected in coalescence prevention during bubble formation.

3.2.4 Total stress

When a film is deformed, some internal forces appear as a reaction to the external force. Those forces are known as ‘stress’ and may be seen as the resistance of the film to deformation. According to the previous discussion, elasticity and surface viscosity appear as a reaction to deformation, so they have to be present in the definition of total stress.

The total stress τ , for a local deformation ε , may be defined as the sum of elastic and viscous components (Horozov, 1997):

$$\tau = E \cdot \varepsilon + \eta_d \cdot \dot{\varepsilon} \quad (\text{Eq. 3.3})$$

When two bubbles collide in presence of surfactant the ‘organized’ water may offer some resistance to flow. Together with the elasticity (E) this adds to film stability. The diffusion-adsorption of fresh surfactant molecules from internal layers in the film at the stretched surface restores the strength of the ‘organized’ region of water, protecting the film against rupture, and allowing for longer contact times between bubbles without coalescence (i.e., viscous component η_d of the total stress).

The total stress is zero for clean systems, i.e., water, because both elasticity and surface viscosity equal zero. Stress appears in the presence of surfactants and is expected to be a key component in coalescence prevention. At the instant of bubble detachment, the surfactant concentration can be well below the equilibrium value, but it is not zero (this point is re-visited in Chapter 6). This chapter explores qualitatively the influence of the total stress in coalescence prevention for different frother types and concentrations.

3.2.5 Experimental requirements

To understand the effect that frothers have on coalescence it is necessary to conduct a study in which coalescence events are detected. The *CCC* approach using bubble swarms is not suited as coalescence and break-up events cannot be distinguished (Finch et al., 2006). Also, since coalescence events occur over a time frame of milliseconds, a technique able to probe this time interval is required. Many coalescence studies are based on bubble pairs formed at adjacent capillary tubes (Drogaris and Weiland, 1983; Kim and Lee, 1988; Ata and Jameson, 2007). These studies involve longer time frames than are realistic in bubble production (more akin to bubble-bubble interaction in the pulp or froth phase).

The chapter introduces the use of sound signals to study coalescence at the moment bubbles are generated at a capillary tube. The technique presented is based on the sound bubbles produce when newly formed.

3.3 Bubbles as a source of sound

Acoustic emissions present a way of monitoring gas-liquid dispersions, solid systems and chemical reactions (Boyd and Varley, 2001). Sound emanating as a bubble forms has been widely studied in oceanography to identify sources of ambient sound in the oceans (e.g., Ye and Feuillade, 1997; Leighton 2004). The application here represents a novel approach to the fundamental study of bubble coalescence.

A bubble surface oscillates (pulsates) when a bubble is formed; these surface oscillations (pulsations) convey perturbations to the surrounding medium, water in this case, and a sound wave will move through the water in all directions (Dawson, 2002). The newly formed bubbles are considered freely oscillating (pulsating) bubbles, and the sound produced was first studied by Minnaert (1933). In recognition of this, bubble surface oscillations are also known as Minnaert pulsations. He showed that the natural frequency of pulsation of bubbles f under a static pressure P_0 in a liquid of density ρ_l relates to the bubble diameter d as follows:

$$f = \frac{1}{\pi d} \left(\frac{3kP_0}{\rho_l} \right)^{1/2} \quad (\text{Eq. 3.4})$$

where k is the so-called polytropic index, which takes different values depending on whether the process is isothermal (unhindered heat flow) or adiabatic (no heat flow). In the case of air it takes values between 1 (isothermal) and 1.4 (adiabatic) (Leighton and Walton, 1987).

Considering the newly generated bubble as a freely oscillating bubble may initially appear erroneous because to oscillate, an object must at some time receive an exciting force (Leighton, 1994). In this case the exciting force is the initial impulse received by the bubble at the moment of detachment from the capillary. For a freely rising bubble at all other times the force is zero and there is no sound emanated. There is another exciting force generated when bubbles burst (Vandewalle et al., 2001); and as will be shown, another exciting force is generated when bubbles coalesce.

A newly generated bubble behaves like a lightly damped simple harmonic oscillator (Leighton and Walton, 1987). The acoustic signal recorded for each bubble is sinusoidal with an exponential decay. When bubbles coalesce or break-up they also emit a decaying sinusoidal pulse of sound (Strasberg, 1956). Identification of sound with coalescence events forms part of the contribution of this chapter.

3.4 Experimental

3.4.1 Apparatus

The experimental set-up (Figure 3.3) comprises a 30L acrylic tank where air bubbles are injected through a glass capillary tube. Gas flow rate is measured and regulated with a mass flow meter controller (Sierra, model 840DL1V1). The acoustic emissions are measured with a hydrophone Lab-40 (Figure 3.4), which has a wide frequency range, 5 to 85,000 Hz. The signal passes from the hydrophone to an amplifier before being transferred to a computer. The acoustic emissions were recorded with the freeware audio software Audacity. For the bulk of the work the capillary orifice was 0.2 mm diameter generating bubbles of about 2.4 mm diameter, depending on air flow rate (given in standard cubic centimeters per minute, sccm^{*})

^{*} Standard conditions: 1 atmosphere and 273.15 K.

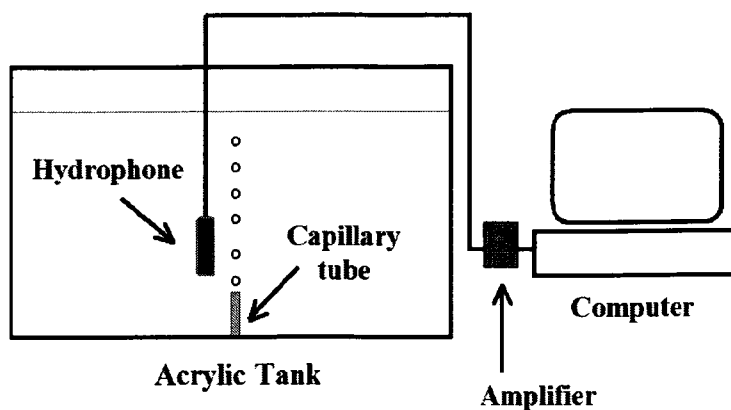


Figure 3.3. Experimental set-up for measuring acoustic emissions of bubbles being formed and coalescing at a capillary tube.

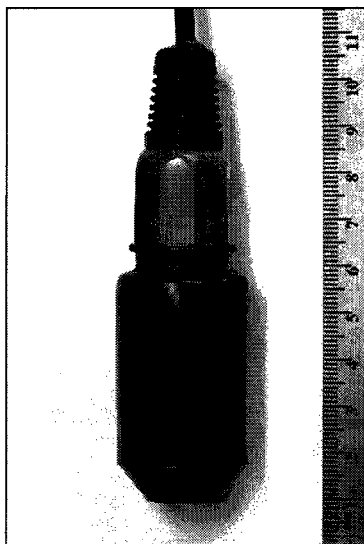


Figure 3.4. Hydrophone Lab-40.

3.4.2 Reagents

Table 3.1 summarizes the reagents used. These correspond to the homologous series of *n*-alcohols from Butanol to Octanol; and some typical surfactants used as frothers in flotation: MIBC (methyl isobutyl carbinol), Dowfroth 250 (polyglycol ether),

F-150 (polyglycol); and salt (sodium chloride). HLB numbers (hydrophile-lipophile balance) are included as a scale of surfactant solubility in water (Rao, 2004), the higher the HLB number the more water-soluble the reagent.

Table 3.1. Summary of reagents used.

Reagent	Formula	Molecular weight (g/gmol)	HLB number	Supplier
Butanol	CH ₃ (CH ₂) ₃ OH	74.12	7.0	Sigma Aldrich
Pentanol	CH ₃ (CH ₂) ₄ OH	88.15	6.5	Fisher
Hexanol	CH ₃ (CH ₂) ₅ OH	102.18	6.0	Acros
Heptanol	CH ₃ (CH ₂) ₆ OH	116.20	5.6	American Chemicals
Octanol	CH ₃ (CH ₂) ₇ OH	130.22	5.1	Fisher
MIBC	(CH ₃) ₂ CHCH ₂ CH(OH)CH ₃	102.18	6.1	Dow
Dowfroth 250 ¹	CH ₃ (PO) ₄ OH	264.35	7.8	Dow
F-150 ¹	H(PO) ₇ OH	425	8.5	Flottec
Sodium Chloride	NaCl	58.44	--	Fisher

¹ PO is propylene oxide (propoxy) [-O-CH₂-CH₂-CH₂-]

Solutions were made using Montréal tap water and the temperature was set at 20 degree Celsius (by combining warm and cold water). Between tests, the acrylic tank was emptied and carefully cleaned.

3.4.3 Procedure

For each condition, the acoustic signal was generated for a given bubbling frequency, i.e., gas flow rate. For a given frother concentration the gas flow rate was increased to

provoke coalescence and the gas rate at the onset of a coalescence event was recorded. The result is a plot of concentration vs. gas flow rate, which is analogous to a CCC vs. gas flow rate plot for the specific frother in this set-up.

3.5 The technique

3.5.1 Validation

The method selected to validate the technique was to test the Minnaert equation (Eq. 3.4). Bubbles of two diameters were generated in water, namely 2.4 and 6.0 mm. The signals were recorded and processed by Fourier analysis to determine the peak frequency corresponding to each bubble size (Minnaert frequency). Figure 3.5 shows the results.

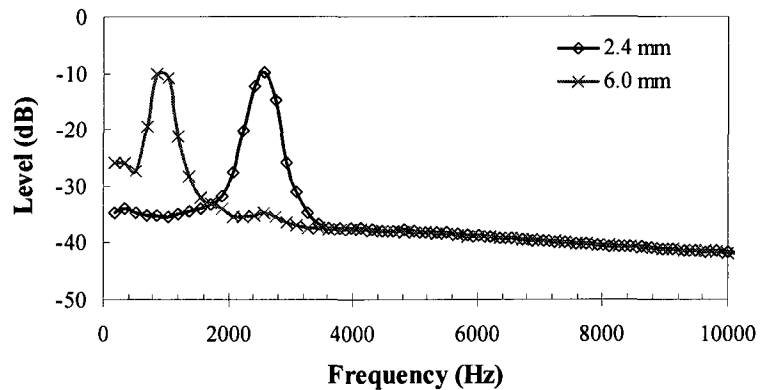


Figure 3.5. Frequency analysis of sound produced by generation of two bubbles of 2.4 and 6 mm diameter.

The peak frequencies were 2583 Hz for 2.4 mm bubbles and 1033 Hz for 6.0 mm bubbles. Given that both bubble sizes were generated under the same conditions, equation 3.2 reduces to saying that frequency and diameter are inversely proportional. This is verified here by noting that the same product of frequency and diameter is found (6,199 mm/s vs. 6,198 mm/s). This means signals are properly recorded and correspond to Minnaert pulsations.

3.5.2 Signal recognition

The next step was to identify sound traces with actual events. For this, a high-speed camera (TroubleShooter HR) was used. Figure 3.6 shows a sequence of images, 1 ms apart, of bubble formation: in frame 3 the first bubble detaches from the capillary tube, in frame 4 the subsequent bubble starts growing, contacting the first one for the next 7 ms (frames 5 to 11) with no coalescence. At the moment of detachment (frame 3) the bubble surface starts pulsating generating the pressure perturbations that propagate through the surrounding water. These pressure perturbations recorded with the hydrophone give the sound trace in Figure 3.7.

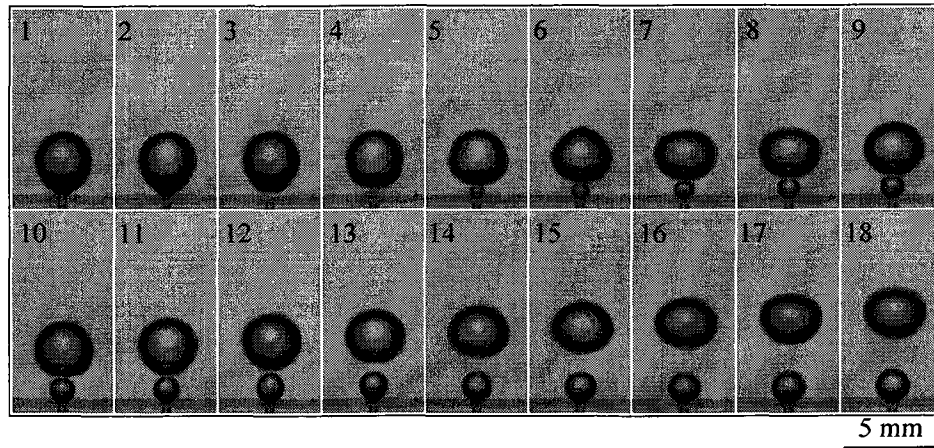


Figure 3.6. Sequence of images (1 ms apart) of bubble formation without coalescence.
Dowfroth 250, 0.09 mmol/L, 10 sccm.

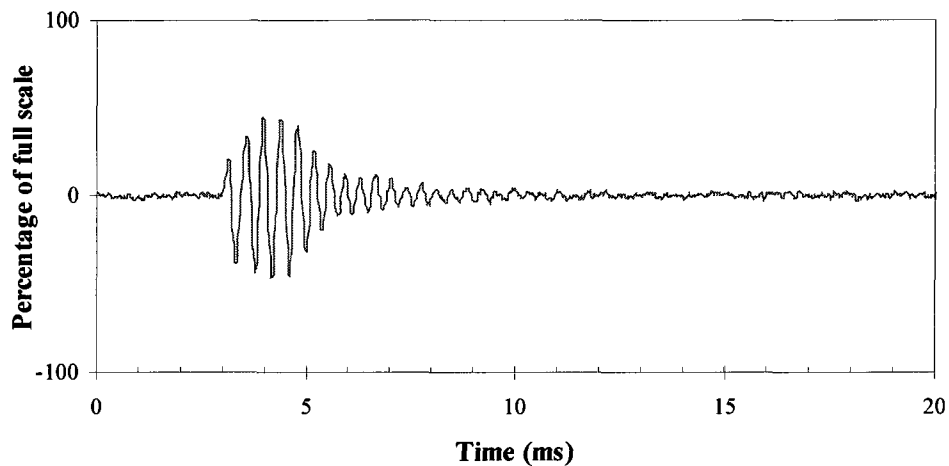


Figure 3.7. Sound trace corresponding to image sequence in Figure 3.6.

The surface pulsations have amplitudes much smaller than the bubble diameter. Leighton and Walton (1987) estimate, for a 2 mm air bubble in water, an initial pulsation amplitude of order of magnitude 10^{-8} m (10^{-5} mm). The amplitude of pulsation, together with the frequency, which for a 2.4 mm bubble is about 2.5 kHz (Figure 3.5), and the fact that the bubble is moving, make it extremely difficult to record these surface pulsations (Minnaert pulsations) responsible for the sound emissions even with high-speed

cinematography. The high-speed imaging did show surface oscillations on bubbles having amplitudes of an order of magnitude of 10^{-4} m (10^{-1} mm). These surface oscillations were not detected in the sound recordings because they involve only local liquid movement while the Minnaert pulsations lead to long-range liquid movement (Leighton and Walton, 1987) (the detectable surface oscillations are covered in Chapter 5).

Figure 3.8 shows a sequence of images (1 ms apart) of bubble formation with a coalescence event: in frame 3 the first bubble detaches from the capillary tube, in frame 4 the subsequent bubble starts growing, contacting the first bubble (frames 4 and 5), and coalescing with it in frame 6. That is, coalescence occurs within 1-2 ms. The characteristic sound trace for this sequence of bubble formation and coalescence is shown in Figure 3.9.

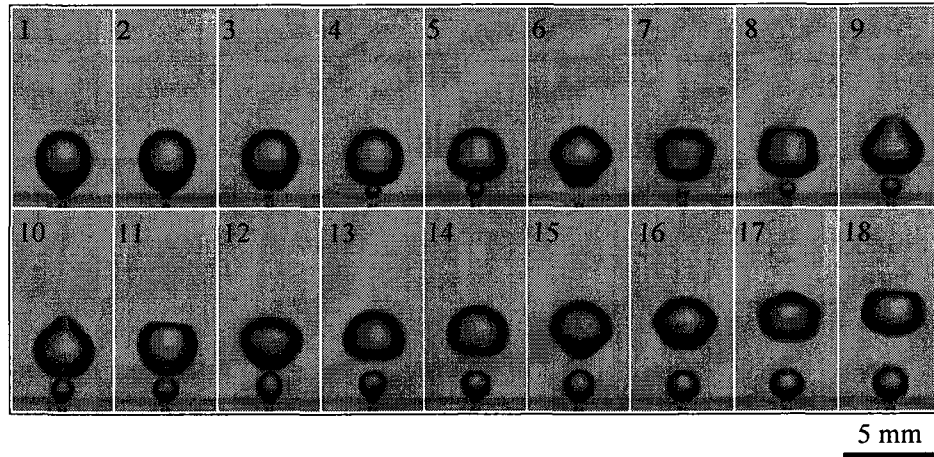


Figure 3.8. Sequence of images (1 ms apart) of bubble formation and coalescence (frame 6). Dowfroth 250, 0.02 mmol/L, 16 sccm.

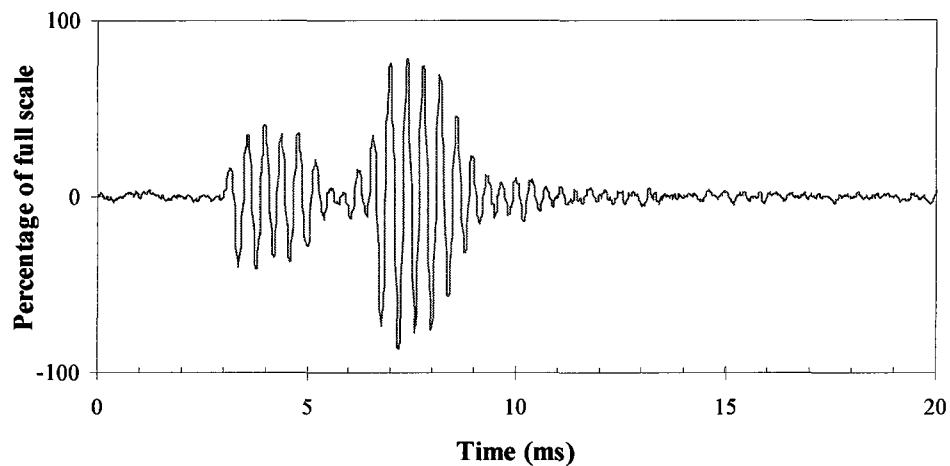


Figure 3.9. Sound trace corresponding to image sequence in Figure 3.8.

In Figure 3.9 the sound trace corresponds to release of the first bubble (frame 3 in Figure 3.8), whose amplitude of oscillation is similar to that in Figure 3.7 (i.e., it is the same event), followed by the second bubble coalescing with the first (frame 6 in Figure 3.8). Coalescence occurs while the second bubble is still attached to the capillary tip and is followed by immediate detachment. The combination of coalescence and detachment give the coalescence-formed bubble an initial impulse higher than the one received by the

first bubble, indicated by the higher oscillation amplitude. The technique is clearly capable of detecting the coalescence event within the 1-2 ms time frame.

Figure 3.10 shows a sequence of images (1 ms apart) of bubble formation with two coalescence events. In frame 3 the first bubble detaches from the capillary tube, in frame 4 the second bubble starts growing and coalescence occurs between frames 4 and 5. In frame 6, a third bubble emerges and also coalesces with the predecessor bubble (frame 8). Figure 3.11 shows the characteristic sound trace for this sequence of events. The coalescence events occur before the pulsations of the preceding bubble fully decay, this makes the system resonate, which combined with the higher initial impulse due to coalescence gives the third bubble an oscillation amplitude even higher than the second one.

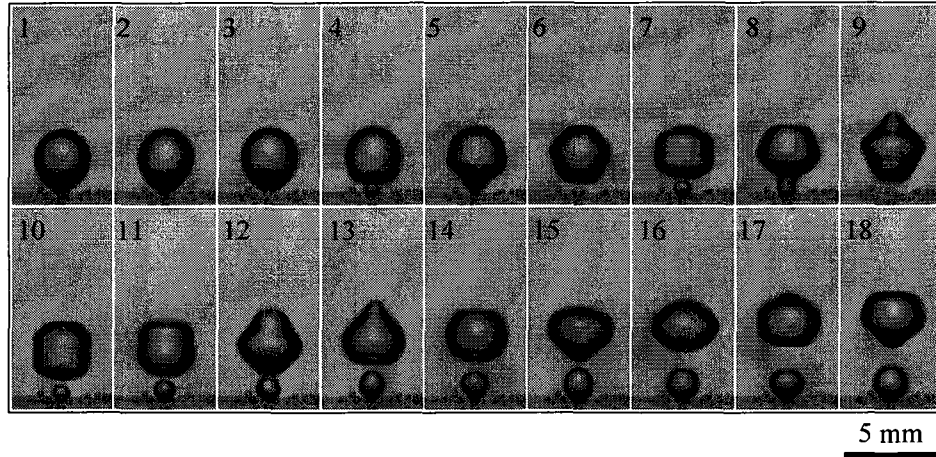


Figure 3.10. Sequence of images (1 ms apart) of bubble formation and coalescence with two subsequent bubbles (frames 5 and 8 of sequence). Dowfroth 250, 0.04 mmol/L, 21 sccm.

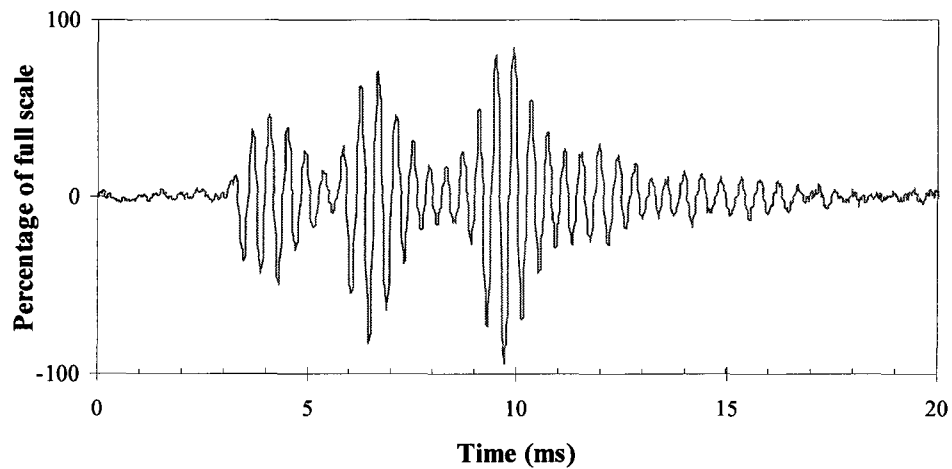


Figure 3.11. Sound trace corresponding to image sequence in Figure 3.10.

A sequence of bubble production at the capillary tube generates sound recordings like those shown in Figures 3.12 and 3.13. In the first, the figure depicts a series of 5 bubbles being formed without coalescence. Zooming in on one bubble formation event, Figure 3.12 would give a sound trace like that in Figure 3.7.

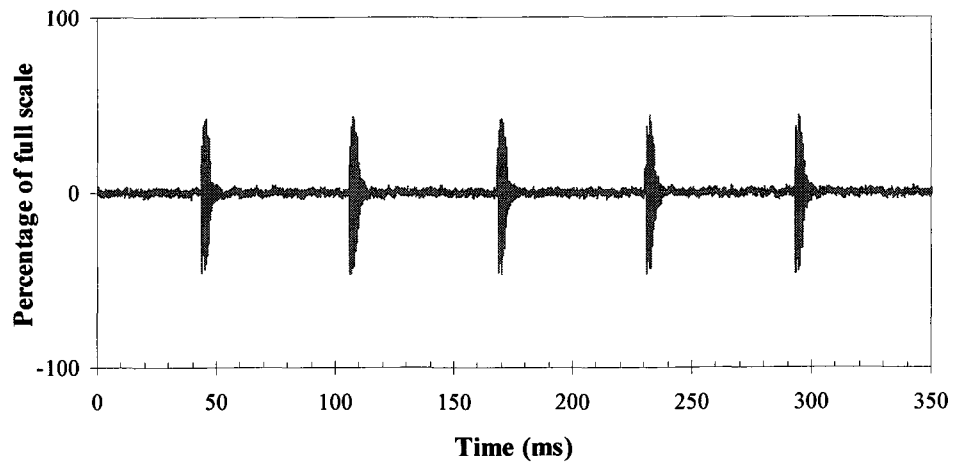


Figure 3.12. Sound recording of bubble formation without coalescence. F-150, 0.024 mmol/L, 7.8 sccm.

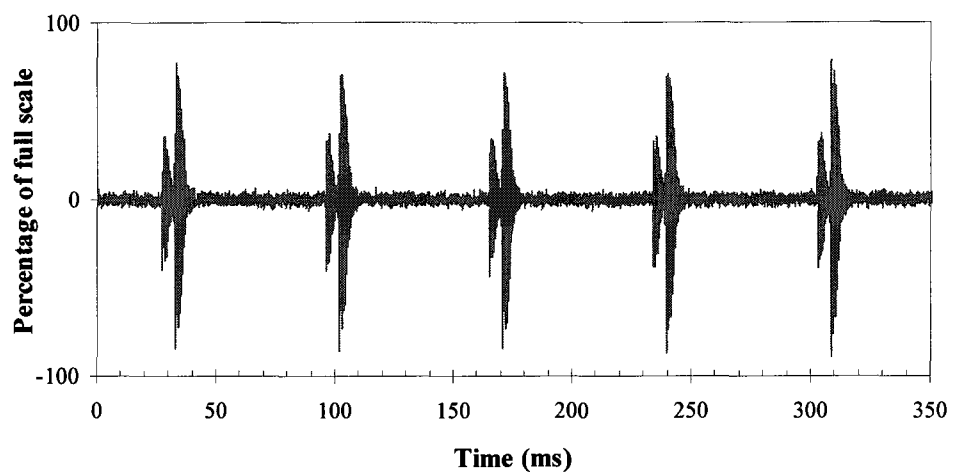


Figure 3.13. Sound recording of bubble formation and coalescence with one subsequent bubble. F-150, 0.005 mmol/L, 7.8 sccm.

The trace in Figure 3.13 shows 5 single coalescence events. Expanding, this figure would give a sound trace like the one in Figure 3.9. Note that the sound recordings also allow determination of the bubbling frequency, which given the gas flow rate is known, gives a check on the size of bubble. For example, for a gas flow rate of 9.4 sccm, a bubble

is produced each ca. 46 ms, which gives a bubble size of 2.4 mm, which was the same size determined by image analysis.

The visual confirmation of what the acoustic signals reveal means they can be used to study coalescence. This has some advantages over using high-speed imaging: sound recordings require little disk space (for instance, the sound recording of 1 minute of bubble generation at 128 kbps requires ca. 1 MB, whereas 1 minute of high-speed imaging requires ca. 13.6 GB (13,600 MB) at a resolution of 640 x 480); off-line analysis of the image sequence to identify coalescence events is tedious compared to the simple signal form of the sound recording; and high-speed imaging equipment is expensive compared to a hydrophone (the hydrophone used in this work cost less than 5% of the high-speed camera).

3.6 Results and Discussion

3.6.1 Reliability

Full repeat tests were conducted for Pentanol to establish the precision of the technique (Table 3.2). Figure 3.14 shows the results, including error bars representing the standard deviation. The line represents the boundary between coalescence events that occur above the line with the non-coalescence region below the line.

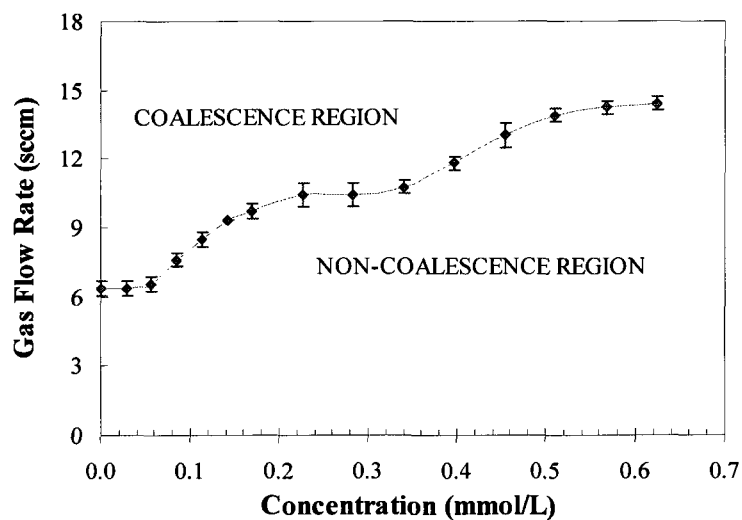


Figure 3.14. Repeat test for Pentanol.

Table 3.2. Concentration vs. gas flow rate: repeat test results for Pentanol.

Concentration (mmol/L)	Run 1 Gas flow rate (sccm)	Run 2 Gas flow rate (sccm)	Run 3 Gas flow rate (sccm)
0.00	6.2	6.7	6.2
0.03	6.2	6.7	6.2
0.06	6.2	6.7	6.8
0.09	7.8	7.8	7.3
0.11	8.3	8.3	8.8
0.14	9.4	9.4	9.4
0.17	9.9	9.9	9.4
0.23	10.4	10.9	9.9
0.28	10.4	10.9	9.9
0.34	10.4	10.9	10.9
0.40	11.5	12.0	12.0
0.45	12.5	13.0	13.6
0.51	13.6	14.1	14.1
0.57	14.1	14.6	14.1
0.62	14.6	14.6	14.1

3.6.2 Concentration vs. gas flow rate

Figure 3.15 presents the results for Pentanol and for three common frothers in flotation (MIBC, Dowfroth 250 and F-150). In the figure, the larger the area below the curve, the larger the non-coalescence region. In other words, the larger the area associated with a reagent the more effective is that reagent in preventing coalescence in the present set-up (i.e., between subsequent bubbles at a capillary tip). For the frothers tested, the ability to prevent coalescence increases with chain length, so they can be ordered as follows: Pentanol, MIBC, Dowfroth 250, and F-150. Previous findings (Nesset et al., 2007) show the same order in coalescence prevention using the *CCC95* concept for these reagents. Other authors (Moyo et al., 2007; Azgomi et al., 2007) who ranked these frothers according to water carrying rate and gas holdup, respectively, also found the same order. This order is also found in equilibrium surface tension reduction (Figure 3.16). The results suggest that coalescence prevention increases with increasing surface activity.

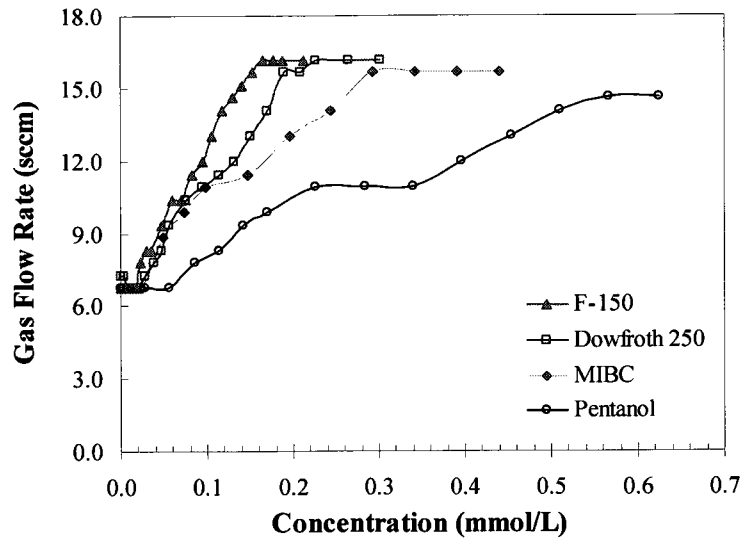


Figure 3.15. Coalescence plot for frothers.

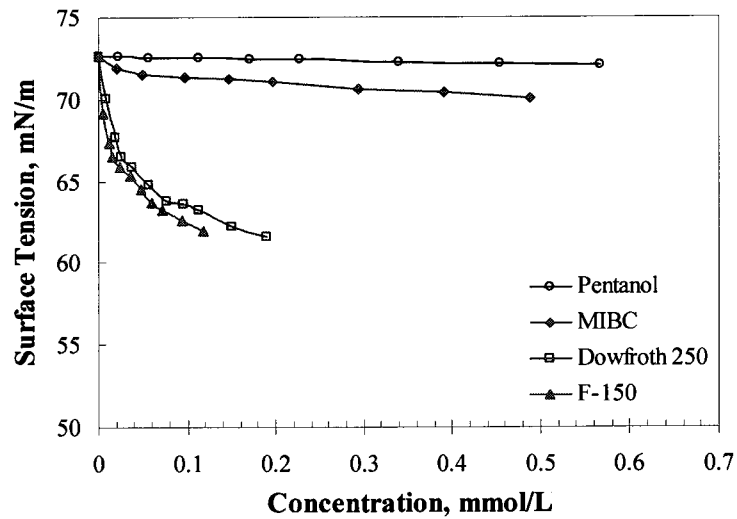


Figure 3.16. Surface tension data for Pentanol (Tuckermann, 2007); MIBC, Dowfroth 250, F-150 (Zhang, 2008).

The results of coalescence prevention for the *n*-alcohols are shown in Figure 3.17. MIBC, an isomer of Hexanol, is also included. Coalescence prevention increases with the number of carbons in the molecule (chain length) up to Heptanol (C_7), which gives a result similar to Octanol (C_8). The same behavior was found by Keitel and Onken (1982) studying the inhibition of bubble coalescence by various solutes in a bubble column. They found that for *n*-alcohols (C_1 - C_8) the limiting concentration, identified as that producing a decrease in Sauter mean diameter, decreases for increasing number of carbons, but appears to approach a limiting value for molecules with more than 6 carbons. Drogaris and Weiland (1983) studied coalescence (visually) between bubble pairs generated at two adjacent capillary orifices in stagnant liquid and also found that coalescence inhibition improves with increasing chain length for *n*-alcohols.

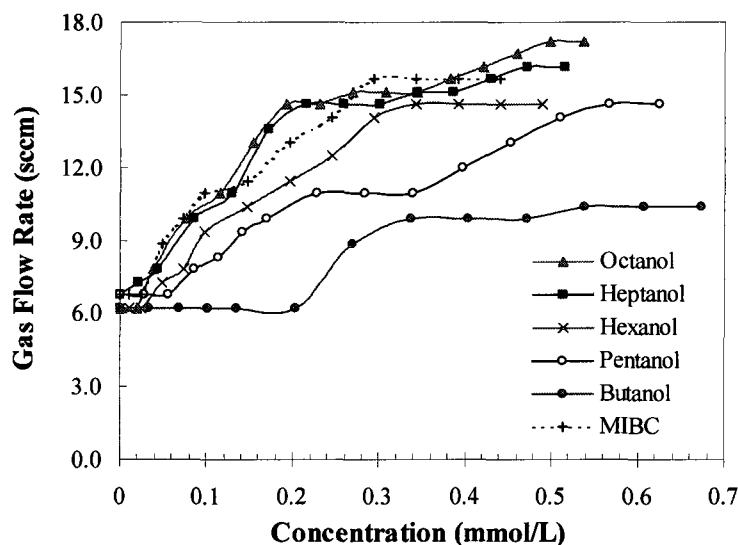


Figure 3.17. Coalescence plot for *n*-alcohols (MIBC included).

Figure 3.17 shows that the two 6-C alcohols, MIBC and Hexanol, have somewhat different trends, MIBC being more effective in preventing coalescence at lower

concentration than Hexanol (comparable to Octanol). This may be attributed to the branched structure of MIBC. Comley et al. (2002) postulate that because of the different structure, fewer molecules of MIBC are needed per unit area to cover a bubble, compared to Hexanol. Assuming monolayer coverage they calculate the area per frother molecule to be 0.33 nm^2 for MIBC and 0.22 nm^2 for Hexanol. This may explain why coalescence is prevented at a lower concentration of MIBC than Hexanol. A difference between MIBC and Hexanol was not seen in the more macroscopic measurements of gas hold-up (Azgomi et al., 2007) and water overflow rate from a column (Moyo et al., 2007).

Figure 3.18 shows the equilibrium surface tension data for the *n*-alcohols (Tuckermann, 2007). Note that *n*-alcohols reduce equilibrium surface tension in the same order that they retard coalescence. Hence, as the results for the common frothers also suggested, coalescence prevention increases with increasing reagent surface activity.

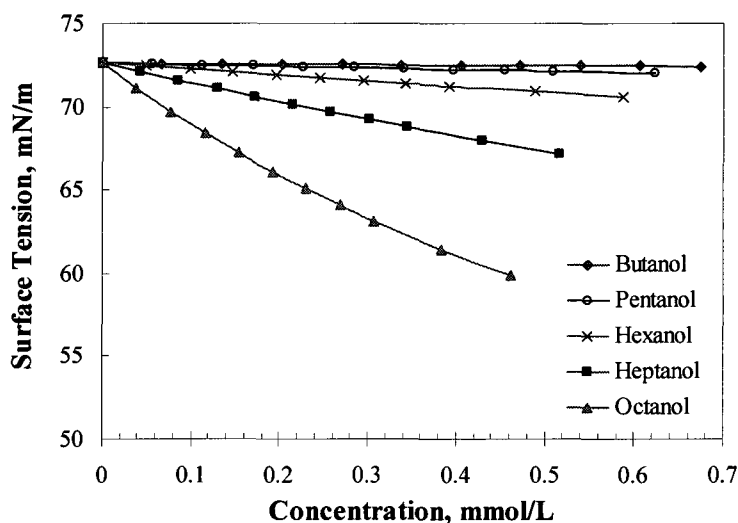


Figure 3.18. Surface tension data for the homologous series of *n*-alcohols (Tuckermann, 2007).

The correspondence with surface tension is only qualitative, however. For example, note that Heptanol and Octanol show a large difference in equilibrium surface tension (Figure 3.18) but their ability to prevent coalescence is comparable (Figure 3.17). Figure 3.19 shows the equilibrium surface tension versus gas flow rate at the coalescence/non-coalescence boundary for the *n*-alcohols, which further suggests that reduction in surface tension alone does not explain the effect on coalescence prevention. Previous works (Machon et al., 1997; Sweet et al., 1997; Grau et al., 2005) have also shown that coalescence prevention is not related to surface tension alone.

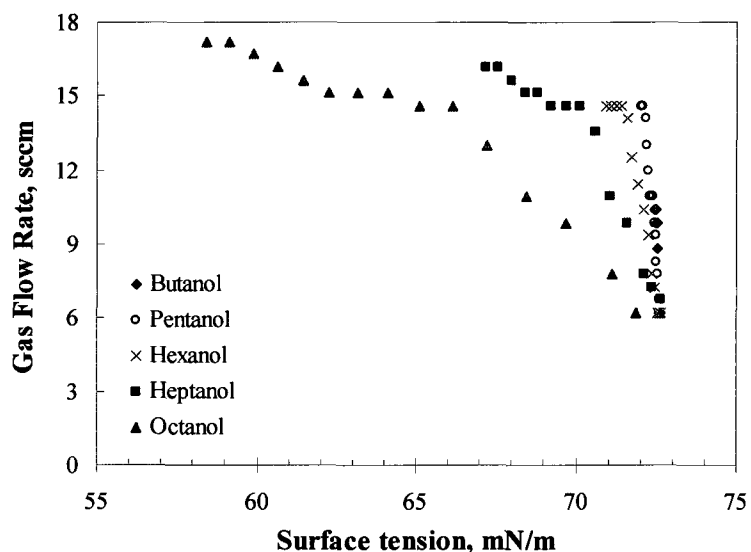


Figure 3.19. Surface tension (after Tuckermann, 2007) vs. gas flow rate at the coalescence/non-coalescence boundary (Figure 3.17) for *n*-alcohols.

The total stress, with its elastic and viscous components, offers a way to explain coalescence prevention in presence of surfactants. Contacting bubbles (e.g., frame 5, Figure 3.8) have a liquid film between them. This liquid film has two liquid-air interfaces – corresponding to the bubble surfaces – with some surfactant adsorbed on them and an

internal region that may be assumed to have the bulk liquid surfactant concentration. Figure 3.20 shows a schematic of the liquid film and the frother action. As a consequence of the collision the film is stretched, the local concentration of surfactant decreases and elasticity arises because of the surface tension gradients generated (elastic component of the total stress). For bubbles at the moment of creation the surface concentration of frother will probably be well below the equilibrium value but it is not zero and there will be some frother molecules there to initiate the action described.

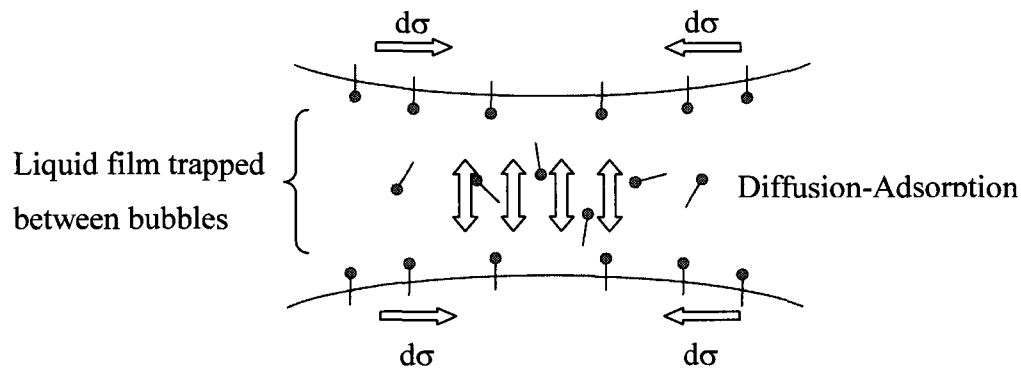


Figure 3.20. Schematic of frother action on coalescence prevention.

The link to surface tension may be that the more surface active the surfactant the higher the surface tension gradient that is likely generated. In other words, the elasticity component of the total stress is expected to increase in value for increasing surface activity, which generally means increasing surfactant chain length. On the other hand, increasing chain length is accompanied by a reduction in diffusion-adsorption rate: large surfactant molecules take longer to diffuse-adsorb onto the film surfaces, and the process of strengthening the 'organized' region of water is retarded. Hence, the viscous component of the total stress is expected to decrease in value for increasing chain length.

Therefore, the order found for the common flotation frothers and the *n*-alcohols in coalescence prevention may be explained by a combination of elastic and viscous component of the total stress theory (Eq. 3.3). To illustrate, the close results of coalescence prevention for Heptanol and Octanol suggest the contributions of the elastic and viscous components are offset, i.e., the increase in elasticity due to the higher surface activity of Octanol is counterbalanced by the reduction in diffusion-adsorption rate (viscous component) due to the larger size of the molecule.

3.6.3 Salt vs. frother

Electrolytes, in sufficient concentration, are also known to reduce bubble size (Keitel and Onken, 1982). For example, Quinn et al. (2007) found that 0.4 mol/L NaCl was equivalent to ca. 8-10 ppm MIBC (0.08-0.10 mmol/L). In order to elucidate whether electrolytes have the same effect as surfactants on coalescence inhibition in the present set-up, sodium chloride was tested. The coalescence plot for sodium chloride is presented in Figure 3.21.

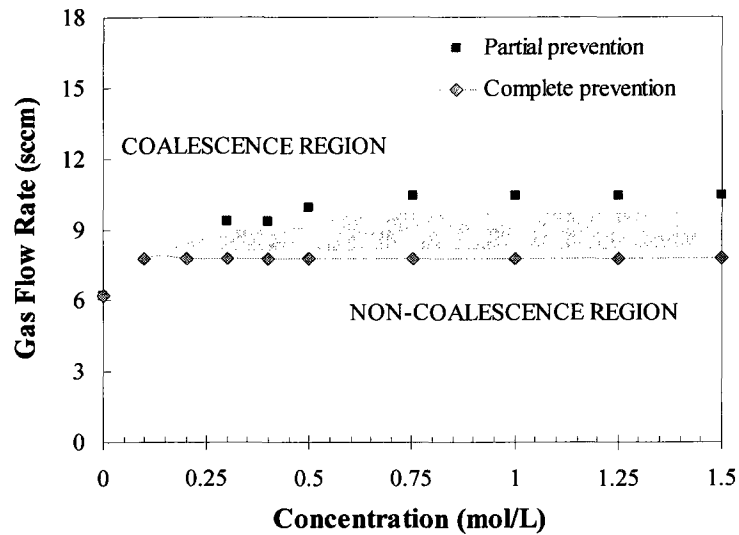


Figure 3.21. Coalescence plot for sodium chloride.

Unlike the frothers tested, sodium chloride does not show a sharp transition between non-coalescence and coalescence but rather a partial-coalescence region giving a signal like that in Figure 3.22, which shows three coalescence events and four non-coalescence events.

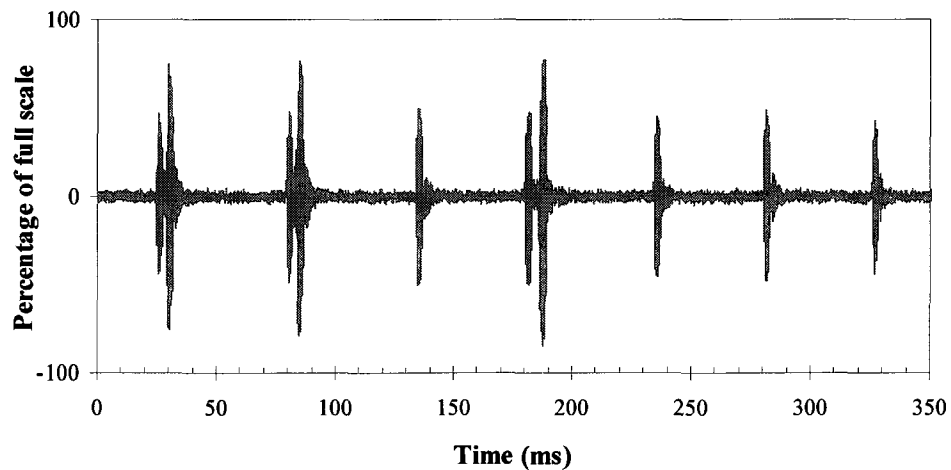


Figure 3.22. Sound recording of bubble formation showing partial coalescence prevention. NaCl 0.3 mol/L, 9.4 sccm.

This result suggests that sodium chloride is less effective than frothers in preventing coalescence. The total stress theory helps provide an explanation.

According to Weissenborn and Pugh (1996), surface tension gradients generated in presence of electrolytes are significantly smaller than those generated in presence surfactants. This would make the elastic component of the total stress less important for electrolytes (NaCl) than it is for frothers. The viscous component requires special attention: sodium chloride, unlike surfactants, does not adsorb on the liquid-air interface, the surface having a lower concentration of salt than the bulk (referred to as ‘negative adsorption’) and the surface tension increases. The film trapped between contacting bubbles should have a region with the composition of the bulk (internal region of the film) and two external regions with a lower salt concentration (liquid-air interfaces). Figure 3.23 shows a schematic of the liquid film between two colliding bubbles in presence of salt.

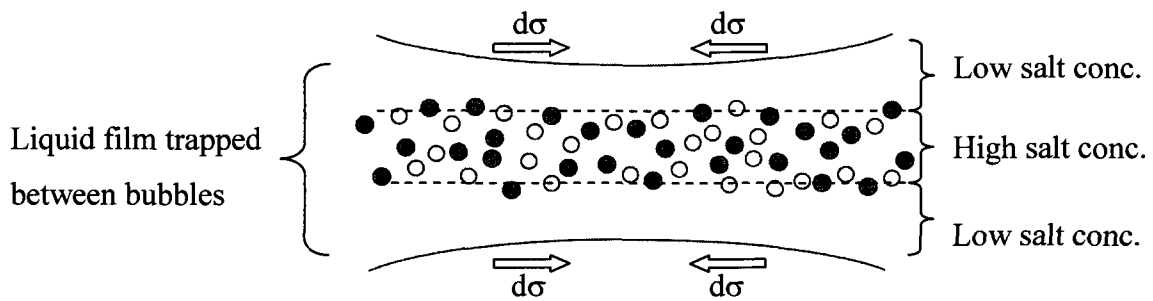


Figure 3.23. Schematic of salt action on coalescence prevention.

In this case the water molecules may be pictured, by analogy, to be assuming the role of surfactant, i.e., they will diffuse from the internal region of the film towards the surfaces to restore equilibrium surface tension, further increasing the salt concentration in the inner layers of the film and so increasing the film viscosity, which in turn increases the time needed to drain and rupture the film. This mechanism is countered by the osmotic pressure that opposes the diffusion of water to the external layers.

The total stress generated in presence of salt, therefore, should be lower than in the case of surfactants since the elastic component is less significant because of the small surface tension gradients generated, and the viscous component is not as effective because of the different nature of the electrolyte molecules. This may account for the results of coalescence prevention showing sodium chloride is less effective than the frothers.

Nevertheless, in actual flotation conditions salt (NaCl, 0.4 mol/L) is equally effective as MIBC (0.10 mmol/L) in reducing bubble size (Quinn et al., 2007). Under those conditions bubbles continue to interact away from the generation point, coalescing and breaking, and this may contribute to the difference from the idealized condition here.

3.7 Conclusions

The characteristic sound trace found when bubbles coalesce at a capillary tip allowed development of a novel technique to study bubble coalescence without incurring the high costs and disk space requirements of high-speed imaging. The technique uses a

hydrophone to record sounds, which are shown to be related to coalescence events. Signal recognition is straightforward and the technique has a resolution high enough to discriminate events that occur within 1 to 2 milliseconds.

The gas flow rate marking the boundary between coalescence and non-coalescence was determined as a function of reagent concentration. The results show that for common flotation frothers and *n*-alcohols (C₄-C₈) coalescence prevention increases with increasing concentration and chain length.

The total stress model, which considers elastic and viscous components and represents the internal forces that appear as a reaction to film stretching, is used to describe the process. The elastic component of the total stress increases in magnitude with increasing surfactant surface activity, which generally correlates with increasing chain length. On the other hand, the viscous component becomes less important for increasing chain length because of the lower diffusion-adsorption rates. The relative importance of both effects appears evident in the similar results of coalescence prevention for Heptanol and Octanol, where it can be argued the increase in elasticity due to the higher surface activity of Octanol is counterbalanced by the reduction in its diffusion-adsorption rate (viscous component) due to the larger size of the Octanol molecule.

Results for sodium chloride do not show such a well-defined boundary between coalescence and non-coalescence as the surfactants. The total stress generated in presence of sodium chloride is expected to be lower than with surfactants; the elastic component is insignificant because of the small surface gradients generated, and the viscous component

is not as effective because of the different nature of the electrolyte molecules compared to frothers.

References

- Adamson, A.W., 1990. Physical chemistry of surfaces, 5th Edition. John Wiley & Sons, Inc. New York.
- Ata, S., Jameson, G.J., 2007. Behaviour of particles during coalescence of bubbles. In proceedings of Flotation 07. Cape Town, South Africa, November 6-9. MEI Conferences. CD ROM.
- Azgomi, F., Gomez, C.O., Finch, J.A., 2007. Characterizing frothers using gas hold-up. Canadian Metallurgical Quarterly 46. 237-242.
- Boyd, J.W.R., Varley, J., 2001. The uses of passive measurement of acoustic emissions from chemical engineering processes. Chemical Engineering Science 56. 1749-1767.
- Cho, Y.S., Laskowski, J.S., 2002. Effect of flotation frothers on bubble size and foam stability. International Journal of Mineral Processing 64. 69-80.
- Comley, B.A., Harris, P.J., Bradshaw, D.J., Harris, M.C., 2002. Frother characterisation using dynamic surface tension measurements. International Journal of Mineral Processing 64. 81-100.
- Dai, Z., Fornasiero, D, Ralston, J., 2000. Particle-bubble collision models – a review. Advances in Colloid and Interface Science 85. 231-256.
- Dawson, P., 2002. The physics of the oscillating bubble made simple. European Journal of Radiology 41. 176-178.

- Dickinson, E., 1999. Adsorbed protein layers at fluid interfaces: interactions, structure and surface rheology. *Colloids and Surfaces B: Biointerfaces* 15. 161-176.
- Drogaris, G., Weiland, P., 1983. Coalescence behaviour of gas bubbles in aqueous solutions of *n*-alcohols and fatty acids. *Chemical Engineering Science* 38 (9). 1501-1506.
- Finch, J.A., Gélinas, S., Moyo, P., 2006. Frother-related research at McGill University. *Minerals Engineering* 19. 726-633.
- Fruhner, H., Wantke, K.-D., 1996. A new oscillating bubble technique for measuring surface dilational properties. *Colloids and Surfaces A: Physicochemical and Engineering Aspects* 114. 53-59.
- Fruhner, H., Wantke, K.-D., Lunkenheimer, K., 1999. Relationship between surface dilational properties and foam stability. *Colloids and Surfaces A: Physicochemical and Engineering Aspects* 162. 193-202.
- Gomez, C.O., Escudero, R., Finch, J.A., 2000. Determining equivalent pore diameter for rigid porous spargers. *Canadian Journal of Chemical Engineering* 78. 785-792.
- Gomez, C.O., Finch, J.A., 2007. Gas dispersion measurements in flotation cells. *International Journal of Mineral Processing* 84 (1-4). 51-58.
- Gorain, B.K., Franzidis, J.P., Manlapig, E.V., 1997. Studies on impeller type, impeller speed and air flow rate in an industrial scale flotation cell, Part 4: Effect of bubble surface area flux on flotation performance. *Minerals Engineering* 10 (4). 367-379.
- Gorain, B.K., Napier-Munn, T.J., Franzidis, J.P., Manlapig, E.V., 1998. Studies on impeller type, impeller speed and air flow rate in an industrial scale flotation cell, Part 5: Validation of $k-S_b$ relationship and effect of froth depth. *Minerals Engineering* 11 (7). 615-626.

- Grau, R.A., Laskowski, J.S., Heiskanen, K., 2005. Effect of frothers on bubble size. *International Journal of Mineral Processing* 76. 225-233.
- Grau, R.A., Laskowski, J.S., 2006. Role of frothers in bubble generation and coalescence in a mechanical flotation cell. *The Canadian Journal of Chemical Engineering* 84. 170-182.
- Harris, P.J., 1982. Principles of flotation. Chapter 13: Frothing phenomena and frothers. King, R.P., ed. *South African Institute of Mining and Metallurgy Monograph Series* No. 3.
- Hernandez, H., Gomez, C.O., Finch, J.A., 2003. Gas dispersion and de-inking in a flotation column. *Mineral Engineering* 16 (6). 739-744.
- Hofmeier, U., Yaminsky, V.V., Christenson, H.K., 1995. Observations of solute effects on bubble formation. *Journal of Colloid and Interface Science* 174. 199-210.
- Horozov, T.S., Kralchevsky, P.A., Danov, K.D., Ivanov, I.B., 1997. Interfacial rheology and kinetics of adsorption from surfactant solution. *Journal of Dispersion Science and Technology* 18 (6-7), 593-607.
- Keitel, G., Onken, U., 1982. Inhibition of bubble coalescence by solutes in air/water dispersions. *Chemical Engineering Science* 37 (11). 1635-1638.
- Kim, J.W., Lee, W.K., 1988. Coalescence behavior of two bubbles growing side-by-side. *Journal of Colloid and Interface Science* 123 (1), 303-305.
- Laskowski, J.S., 2003. Fundamental properties of flotation frothers. Proceedings of the 22nd International Mineral Processing Congress. Cape Town, South Africa. 788-797.
- Leighton, T.G., Walton, A., 1987. An experimental study of the sound emitted from gas bubbles in a liquid. *Eur. J. Phys.* 8. 98-104.
- Leighton, T.G., 1994. *The acoustic bubble*. New York: Academic Press.

- Leighton, T.G., 2004. From seas to surgeries, from babbling brooks to baby scans: the acoustics of gas bubbles in liquids. *International Journal of Modern Physics B* 18 (25). 3267-3314.
- Lucassen, J., Van Den Tempel, M. 1972. Dynamic measurements of dilational properties of a liquid interface. *Chemical Engineering Science* 27. 1283-1291.
- Machon, V., Pacek, A.W., Nienow A.W., 1997. Bubble sizes in electrolyte and alcohol solutions in a turbulent stirred vessel. *Trans IChemE* 75 (A). 339-348.
- Marrucci, G., 1969. A theory of coalescence. *Chemical Engineering Science* 24, 975-985.
- Metso Minerals CBT (Computer Based Training), 2002. Mill Operator Training Package. Flotation Module. Formerly Brenda Process Technology CBT (Computer Based Training) (1996). Mill Operator Training Package. Flotation Module.
- Minnaert, M., 1933. On musical air-bubbles and the sounds of running water. *Philosophical Magazine* 16, 235-248.
- Monroy, F., Giermanska Kahn, J., Langevin, D., 1998. Dilational viscoelasticity of surfactant monolayers. *Colloids and Surfaces A: Physicochemical and Engineering Aspects* 143, 251-260.
- Moyo, P., Gomez, C.O., Finch, J.A., 2007. Characterizing frothers using water carrying rate. *Canadian Metallurgical Quarterly* 46. 215-220.
- Nesset, J.E., Finch, J.A., Gomez, C.O., 2007. Operating variables affecting the bubble size in forced-air mechanical flotation machines. In proceedings of Ninth Mill Operators' Conference, Freemantle, WA, Australia. 55-65.
- Oolman, T.O., Blanch, H.W., 1986. Bubble coalescence in stagnant liquids. *Chemical Engineering Communications* 43. 237-261.

- Prince, M.J., Blanch, H.W., 1990. Bubble coalescence and break-up in air-sparged bubble columns. *AIChE Journal* 36 (10). 1485-1499.
- Pugh, R.J., 1996. Foaming, foam films, antifoaming and defoaming. *Advances in Colloid and Interface Science* 64. 67-102.
- Quinn, J.J., Kracht, W., Gomez, C.O., Gagnon, C., Finch, J.A., 2007. Comparing the effect of salts and frother (MIBC) on gas dispersion and froth properties. *Minerals Engineering* 20. 1296-1302.
- Rao, S.R., 2004. *Surface Chemistry of Froth Flotation, Second Edition, Vol 2. Reagents and Mechanisms. Revised Edition. First Edition by Jan Leja.* Kluwer Academic/Plenum Publishers.
- Rusanov, A.I., Krotov, V.V., 2003. Gibbs elasticity of free thin liquid films. *Doklady Physical Chemistry* 393 (4-6). 350-352.
- Schott, H. 1995. Hydrophilic-lipophilic balance, solubility parameter, and oil-water partition coefficient as universal parameters of nonionic surfactants. *Journal of Pharmaceutical Sciences* 84 (10). 1215-1222.
- Schwarz, S., Alexander, D., 2006. Gas dispersion measurements in industrial flotation cells. *Minerals Engineering* 19 (6-8). 554-560.
- Strasberg, 1956. Gas bubbles as sources of sound in liquids. *The Journal of the Acoustical Society of America* 28 (1). 20-26.
- Sweet, C., Van Hoogstraten, J., Harris, M., Laskowski, J.S., 1997. The effect of frothers on bubble size and frothability of aqueous solutions. In proceedings of Second UBC-McGill Bi-annual International Symposium of Fundamentals of Mineral Processing. Finch, J.A., Rao, S.R., Holubec, I., eds. Sudbury, Ontario. 235-245.

- Tao, D., 2004. Role of bubble size in flotation of coarse and fine particles – A review. *Separation Science and Technology* 39 (4). 741-760.
- Tse, K.L., Martin, T., McFarlane, C.M., Nienow, A.W., 1998. Visualisation of bubble coalescence in a coalescence cell, a stirred tank and a bubble column. *Chemical Engineering Science* 53 (23). 4031-4036.
- Tuckermann, R., 2007. Surface tension of aqueous solutions of water-soluble organic and inorganic compounds. *Atmospheric Environment* 41. 6265-6275.
- Vandevallé, N., Lentz, J.F., Dorbolo, S., Brisbois, F., 2001. Avalanches of popping bubbles in collapsing foams. *Physical Review Letters* 86 (1). 179-182.
- Wang, L., Yoon, R-H., 2006. Role of hydrophobic force in the thinning of foam films containing a nonionic surfactant. *Colloids and Surfaces A: Physicochemical and Engineering Aspects* 282-283. 84-91.
- Weissenborn, P.K., Pugh, R.J., 1996. Surface tension of aqueous solutions of electrolytes: relationship with ion hydration, oxygen solubility, and bubble coalescence. *Journal of colloid and interface science* 184. 550-563.
- Ye, Z., Feuillade, C., 1997. Sound scattering by an air bubble near a plane sea surface. *The Journal of the Acoustical Society of America* 102 (2). 798-805.
- Zhang, W., 2008. Unpublished data.

Chapter 4 – Bubble break-up and the role of frother and salt

Chapter 3 showed the effect of frothers on coalescence prevention, which is considered a major contributor to the production of small bubbles in flotation machines. This Chapter entertains the other possibility, that frothers may influence bubble break-up.

4.1 Introduction

Frothers are surface-active agents (surfactants) widely used in flotation to aid generation of small bubbles (ca. 0.5 – 3 mm) and to help form and stabilize the froth phase. Even though small bubbles are crucial for the flotation performance, little is known about how frothers act in their formation. Analysis of froth formation emphasizes mechanisms that retard coalescence (Pugh, 1996; Harris, 1982), an explanation extended to bubble generation (Metso Minerals CBT, 2002). This in turn has led to apparent quantification by introducing the critical coalescence concentration (*CCC*), which is the frother concentration producing the minimum bubble size in a swarm (Cho and Laskowski, 2002; Grau and Laskowski, 2006). Nettet et al. (2007) substitute *CCC*₉₅, i.e., concentration achieving 95% of bubble size reduction compared to water alone, as the basis of more systematic measurement. The name infers that the function of the frother is to preserve the size of bubble produced (by whatever mechanism) by preventing coalescence. Others have made the same claim (Gomez et al., 2000) and the reference to non-coalescing systems (e.g. Parthasarathy et al., 1991) may also imply this mechanism. Laskowski (2003) states that at frother concentrations lower than *CCC*, the bubble size is

determined by coalescence; while at concentrations higher than *CCC* the bubble size is determined by the generation device and hydrodynamic conditions. He proposed the critical coalescence concentration concept, together with foaming properties, as a way of characterizing flotation frothers.

Studying bubble swarms, as in determining *CCC*, does not permit coalescence prevention to be separated from the other possibility, that frothers may act on break-up, a mechanism that has not received much attention (Finch et al., 2006; Acuna et al., 2007).

It is also known that salt solutions can reduce bubble size in flotation systems (Quinn et al., 2007). Thus, investigation of the mechanism should consider both frothers and salts.

4.2 Coalescence

Coalescence is the process by which two or more bubbles come together to generate a new bubble. The most common coalescence act is probably between two bubbles, which is known as binary coalescence. Coalescence occurs in three steps: collision, film thinning, and film rupture (Oolman and Blanch, 1986; Prince and Blanch, 1990; Machon et al., 1997; Tse et al., 1998). On collision, the opposing bubble surfaces are flattened, leaving a thin film separating them. The initial thickness of this film is typically 10^{-3} to 10^{-4} cm. Collision is controlled by the hydrodynamics of the bulk liquid phase. In the next step, the film must thin until approximately 10^{-6} cm in thickness when it ruptures. The contact time has to exceed the time required for the film to thin to rupture,

otherwise coalescence does not occur. This second step is controlled by the hydrodynamics of the liquid film and forces associated with surface tension gradients or surface visco-elastic effects if surfactants are present (Fruhner et al., 1999). Once the film is sufficiently thin it ruptures due to instability mechanisms, resulting in bubble coalescence. This last step is very fast compared to the other two.

4.3 Break-up

Break-up (breakage) refers to bubbles (or an air stream) breaking into smaller bubbles. The break-up mechanism is modeled considering either collision of bubbles with turbulent eddies or bubbles interacting with wakes in a swarm. The studies based on collision with turbulent eddies derive from the work of Hinze (1955). The eddies considered responsible for break-up are those of comparable size to the bubble. Larger eddies transport groups of bubbles, while eddies much smaller than the bubble do not have enough energy to cause break-up. The studies based on wake interactions are from experimental observations that suggest the wake environment provides the driving force in bubble-bubble interactions, including coalescence and break-up (Stewart, 1995).

Walter and Blanch (1986) observed with high-speed photography that break-up occurred by a dumbbell stretching mechanism, with break-up time of the order of 25 ms. Figure 4.1 is taken from that work identifying one dumbbell dividing (and also showing the difficulty in imaging the event in bubble swarms).

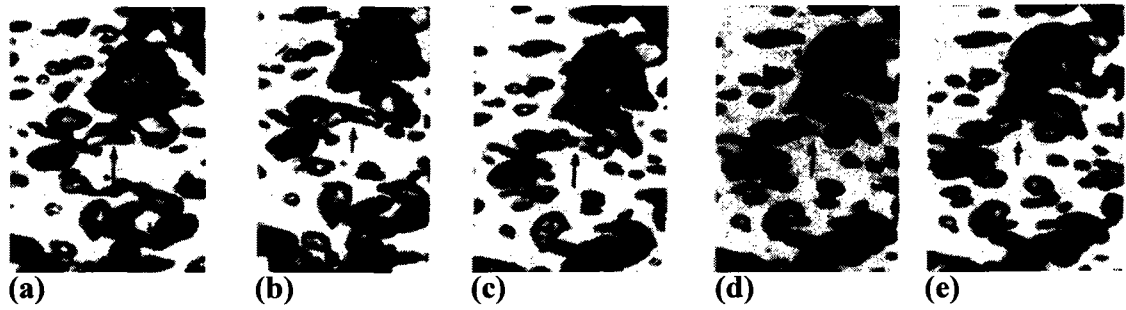


Figure 4.1. Sequence of images of bubble break-up by dumbbell stretching mechanism. (a) $t = 0$ ms, (b) $t = 8$ ms, (c) $t = 20$ ms, (d) $t = 22$ ms, and (e) $t = 25$ ms (Walter and Blanch, 1986. Reprinted with permission from Elsevier).

In the presence of frother, the dumbbell stretching mechanism will cause uneven frother distribution, which generates surface instabilities that may promote or retard break-up (Miller and Neogi, 1985; Dukhin et al., 1998; Finch et al., 2008). The same general argument applies to salts, in this case with water molecules substituting for the frother in terms of surface activity (Finch et al., 2008). This chapter explores frother effects on bubble break-up.

A break-up model must include not only the break-up rate but also the daughter size distribution (Wang et al., 2003). Wang et al. list four characteristics of the daughter bubble size distribution:

1. A local minimum should exist at equal (50:50) break-up fraction because the surface area and therefore surface energy increase is the highest of all possible break-up fractions. (The break-up fraction refers to the volume fraction of the mother bubble that becomes the daughter bubbles.) This local minimum should be

greater than zero because the probability of equal-size break-up, while small, is not zero.

2. The generation of small bubbles requires high energy because of the high capillary (internal) pressure. Therefore, the daughter bubble size distribution should vanish before the break-up fraction approaches zero.
3. The daughter bubble size distribution depends on the mother bubble size and the energy dissipation rate. Because of the restriction in generating small bubbles (high capillary pressures), the equal-size break-up probability increases with decreasing mother bubble size. In the case of energy dissipation rate, the higher the rate the higher the probability of unequal-size break-up.
4. The daughter bubble size distribution should not have any singularity point, i.e., the frequency vs. size plot should be smooth and well defined.

The daughter bubble size distribution is determined by the break-up fraction, so modeling this function is required for the correct representation of the physics of the process. Luo and Svendsen (1996), for instance, generated a break-up model without considering the capillary pressure restriction; consequently, their daughter bubble size distributions do not vanish for break-up fractions approaching zero.

4.4 Experimental

4.4.1 Apparatus

The experimental set-up (Figure 4.2) comprises a 30L acrylic tank where air bubbles are injected through a glass capillary tube of 0.4 mm internal diameter. Gas flow rate is regulated with a mass flow meter controller (Sierra, model 840DL1V1). The aim of the experiments is to study how a mono-size distribution of bubbles, generated at the capillary, changes when exposed to turbulence with and without the presence of frothers or salts. A sleeve is installed to deliver bubbles into the impeller while protecting the capillary from turbulence that tends to alter the bubble size produced. Turbulence is introduced by the use of a three-bladed axial flow impeller (Figure 4.3).

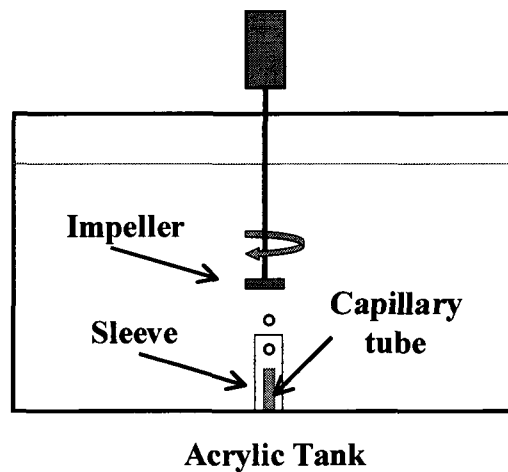


Figure 4.2. Experimental set-up.

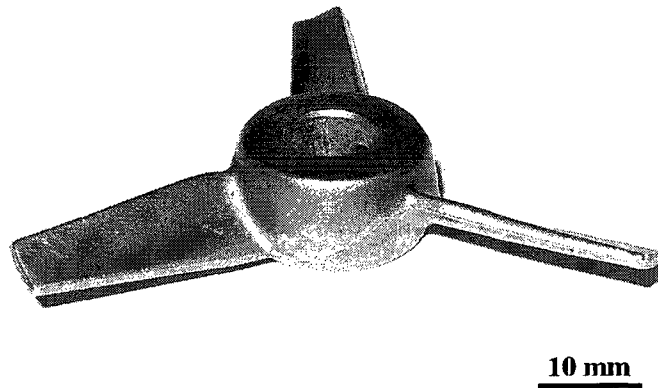


Figure 4.3. Impeller.

Figure 4.4 shows the protective effect of the sleeve. In Figure 4.4 (a) the impeller is off (stationary), so the bubbles are all of the same size. In Figure 4.4 (b) the impeller is on and the bubbles generated at the capillary remain the same size before leaving the sleeve, but the distribution clearly changes in the vicinity of the rotating impeller.

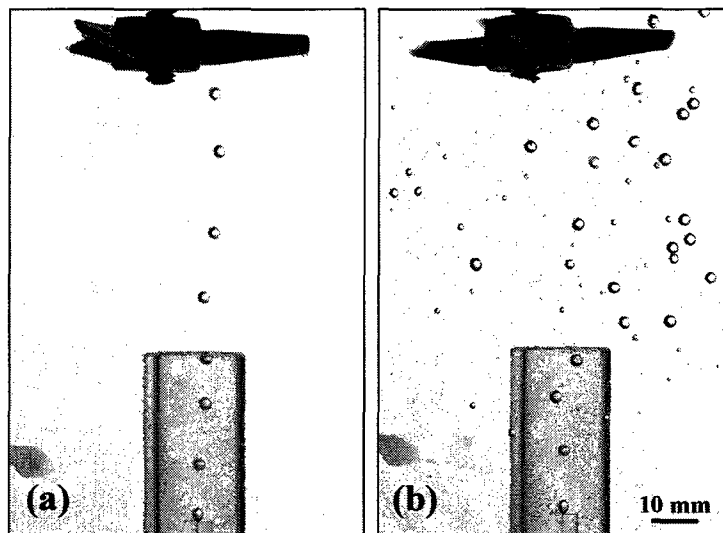


Figure 4.4. Capillary-sleeve system used to generate mono-size distribution of bubbles:
(a) impeller off, (b) impeller on (420 RPM).

4.4.2 Procedure

The gas flow rate delivered to the system was kept constant at 11.8 sccm (standard cubic centimeter per minute), the highest gas flow rate at which coalescence between subsequent bubbles did not occur. This gas flow rate was determined acoustically (see Chapter 3). The addition of frother or salt did not alter the bubbling frequency (determined acoustically) hence they did not alter the bubble size being generated at the capillary, which was 2.5 mm volume equivalent diameter. These are the mother bubbles and constitute a mono-size distribution. Once the bubbles leave the sleeve, they are exposed to the turbulence induced by the impeller; this results in coalescence and break-up events that alter the original mono-size distribution producing a wider distribution. The overall result of the coalescence – break-up events may be inferred from comparing the resulting distribution to the original one: we can conclude that all the bubbles larger than 2.5 mm are associated to coalescence events whereas all the bubbles smaller than 2.5 mm imply break-up events. Repeated coalescence and break-up events are possible but do not change this general conclusion.

Bubble size distributions were measured using image analysis: the acrylic tank was rear illuminated and the region between the sleeve and the impeller was imaged with a digital still camera (Digital SLR Camera Canon EOS30D) of 8.2 mega pixels equipped with a macro lens of 100 mm. Two hundred pictures were taken per test, which allows for about 3,000 bubbles to be sized in order to meet statistic requirements in determining a reliable bubble size distribution (Hernandez-Aguilar et al., 2004; Hernandez-Aguilar et

al., 2005). A special macro (see Appendix 5) was developed to process the images off-line with the software ImageJ, and thus yield bubble size distribution data.

4.4.3 Reagents

Table 4.1 summarizes the reagents used. These represent the four different classes of surfactants (frothers) used in flotation as identified by Moyo et al. (2007): Pentanol, MIBC (methyl isobutyl carbinol), Dowfroth 250 (polyglycol ether), F-150 (polyglycol). In addition, salt (sodium chloride) was tested as high concentrations (for example, above ionic strength of ca. 0.4) decrease bubble size much as frothers do (Quinn et al., 2007).

Table 4.1. Summary of reagents used.

Reagent	Formula	Molecular weight (g/gmol)	Supplier
Pentanol	$\text{CH}_3(\text{CH}_2)_4\text{OH}$	88.15	Fisher
MIBC	$(\text{CH}_3)_2\text{CHCH}_2\text{CH}(\text{OH})\text{CH}_3$	102.18	Dow
Dowfroth 250 ¹	$\text{CH}_3(\text{PO})_4\text{OH}$	264.35	Dow
F-150 ¹	$\text{H}(\text{PO})_7\text{OH}$	425	Flottec
Sodium Chloride	NaCl	58.44	Fisher

¹ PO is propylene oxide (propoxy) [-O-CH₂-CH₂-CH₂-]

Solutions were made using Montréal tap water and the temperature was set at 20 degree Celsius, controlled by mixing warm and cold water (experiments were performed during winter). Between tests, the tank was emptied and carefully cleaned.

The frother concentrations employed cover the range of interest in flotation and were chosen based on the ability of these reagents to prevent coalescence in industrial cells (Nesset et al., 2007), hence the concentrations vary from frother to frother. As a guide to the concentrations used, Table 4.2 shows typical concentrations expressed in terms of the critical coalescence concentration (*CCC*). In the table, the number accompanying *CCC* (e.g. *CCC95*) corresponds to the percentage of bubble size reduction in the flotation machine (Nesset et al., 2007); *CCC95*, thus, corresponds to a concentration achieving 95% of bubble size reduction. For the case of sodium chloride, a concentration of 0.4 mol/L was tested, based on the comparison between MIBC and salts made by Quinn et al. (2007).

Table 4.2. Typical frother concentrations (mmol/L) used in flotation systems expressed on *CCC* scale (adapted from Nesset et al., 2007).

Reagent	<i>CCC50</i>	<i>CCC75</i>	<i>CCC95</i>	<i>CCC99</i>
Pentanol	0.077	0.153	0.331	0.509
MIBC	0.026	0.051	0.111	0.171
Dowfroth 250	0.009	0.018	0.039	0.091
F-150	0.002	0.005	0.010	0.016

4.5 Results

4.5.1 Reliability

Full repeat tests were conducted for F-150 at a concentration of 0.012 mmol/L (5 ppm) and an impeller speed of 420 RPM to establish the precision of the technique (Table 4.3). Figure 4.5 plots the mean values with error bars representing the standard deviation. The pooled relative standard deviation was 0.68%, which shows the technique gives high precision.

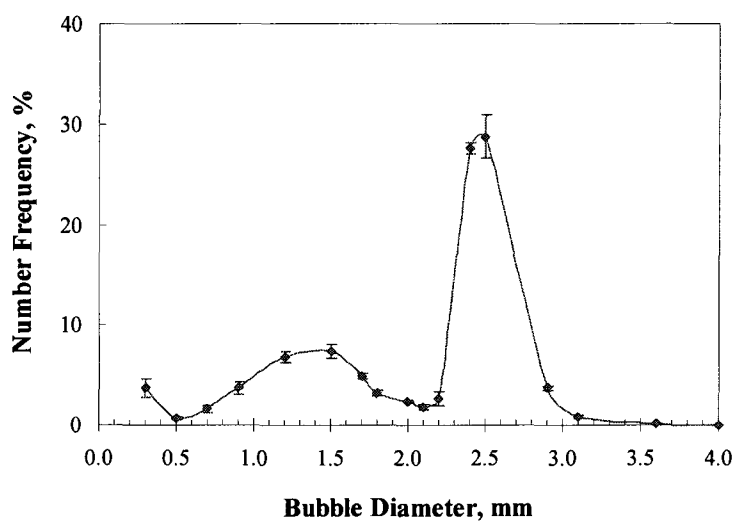


Figure 4.5. Repeat test for F-150: 0.012 mmol/L, 420 RPM.

Table 4.3. Number frequency vs. bubble size: repeat test results for F-150, 0.012 mmol/L, 420 RPM.

Bubble size ¹ (mm)	Number frequency (%)			
	Run 1	Run 2	Run 3	Run 4
0.3	4.3	4.2	4.0	2.4
0.5	0.6	0.6	0.8	0.9
0.7	1.8	1.7	1.1	1.8
0.9	3.5	4.3	2.9	4.2
1.2	7.7	6.4	6.6	6.7
1.5	7.7	6.4	7.3	8.1
1.7	5.1	4.4	5.1	4.9
1.8	3.4	3.0	3.0	3.4
2.0	2.5	2.3	2.5	2.3
2.1	2.0	1.9	2.1	1.5
2.2	3.1	3.2	2.5	1.8
2.4	27.7	28.1	26.8	27.9
2.5	25.7	29.2	30.6	29.6
2.9	4.0	3.7	3.7	3.5
3.1	0.9	0.6	0.8	0.9
3.6	0.1	0.1	0.1	0.1
4.0	0.0	0.0	0.0	0.0

¹ mean bubble size per bin class

4.5.2 Effect of frother type and salt (NaCl) on bubble size distribution

Figure 4.6 shows how frother addition (Dowfroth 250, 0.038 mmol/L) changes the bubble size distribution compared to water alone. The figure includes the line representing the original mono-size distribution (2.5 mm) as a reference. In each bubble size distribution, the sizes larger than 2.5 mm are the result of coalescence events and the sizes smaller than 2.5 mm are due to break-up events. The shaded region in Figure 4.6

corresponds to the difference between coalescence fractions with and without frother, i.e., the reduction of coalescence in the presence of frother.

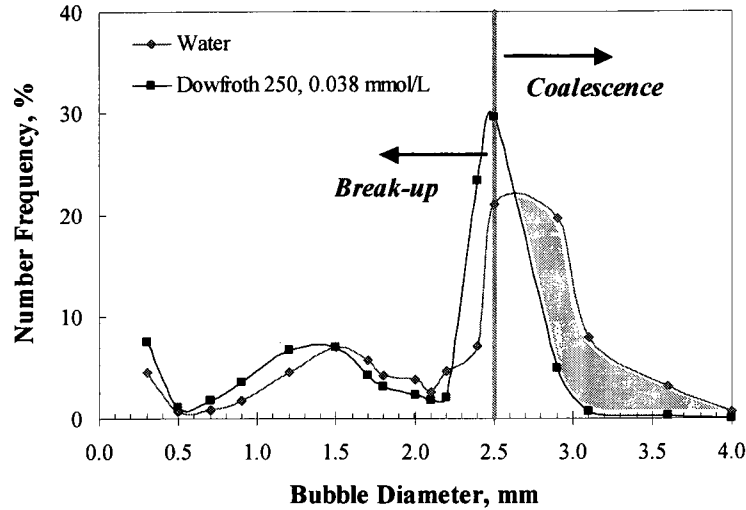


Figure 4.6. Frother effect (Dowfroth 250) on bubble size distribution, 420 RPM.

The action of frother in reducing coalescence is captured in the images in Figures 4.7 and 4.8. Figure 4.7 shows two bubbles coalescing in water; the images in the sequence are 1 ms apart. Note that the bubbles come in contact between the third and fourth frame in the sequence and have coalesced by the fifth frame, giving a coalescence time of one to two milliseconds.

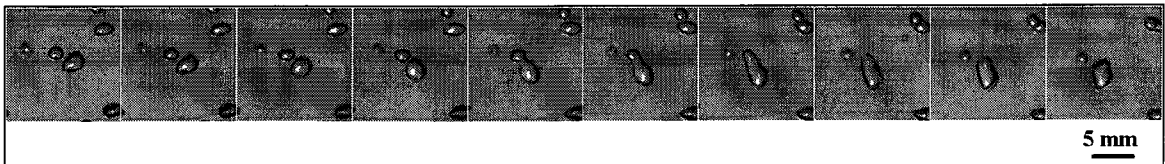


Figure 4.7. Sequence of images (1 ms apart) of bubble coalescence. Water (no-frother), 420 RPM.

Figure 4.8 shows two bubbles interacting in presence of frother. The images in the sequence are 2 ms apart. In this case, bubbles come and stay together for 15 frames (30 ms), between the fifth and nineteenth frames in the sequence, before bouncing apart without coalescence (last frame).

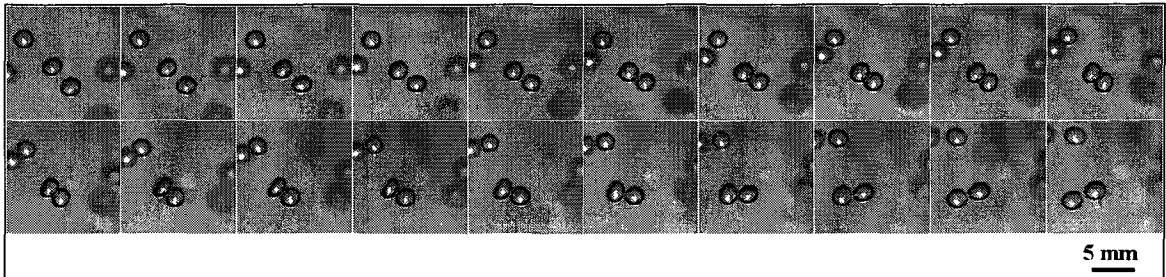


Figure 4.8. Sequence of images (2 ms apart) of bubble coalescence. Dowfroth 250, 0.038 mmol/L, 420 RPM.

From Figure 4.6, in contrast to the clear effect on preventing coalescence, the presence of frother does not seem to hinder bubble break-up, although it does affect the output of the break-up process. Figure 4.6 shows a substantial increment in the fraction of bubbles of 2.4 mm, which increases from 7% to 23% when frother is present. This observation suggests that frother alters the size distribution of daughter bubbles generated by break-up. Note that a bubble of 2.4 mm in diameter has a volume equal to 90% the volume of a 2.5 mm bubble.

The simplest approach to modeling the break-up process is to assume that each bubble breaks only once and that break-up is binary, i.e., only two bubbles are formed per break-up event. In that case, any increment in the fraction of bubbles of 2.4 mm should be accompanied by an increment in the fraction of bubbles of 1.2 mm, which represents the

size of bubbles having 10% of the volume of a 2.5 mm bubble. Inspection of Figure 4.6 does show an increment in the fraction of bubbles of 1.2 mm in the presence of frother (roughly from 5% to 7%). However, this difference is small compared to the 16% increment in the fraction of bubbles of 2.4 mm. This means that either a bubble may break more than once or more than one bubble may be generated per break-up event; whatever the case, the result is the same: a mother bubble generating more than two daughter bubbles, which complicates the analysis.

Figures 4.9 and 4.10 illustrate the events just described, namely highly asymmetric break-up and break-up generating three bubbles (two consecutive break-up events), respectively.

Unlike the difference observed in the sequences of images of coalescence/bouncing between systems with and without frother, the break-up of a bubble in the presence of frother (Figure 4.11) does not show a major difference compared to bubble break-up in water.

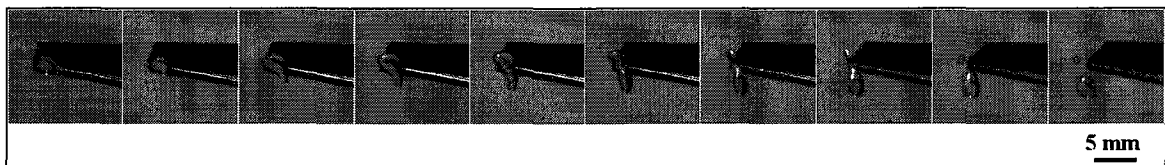


Figure 4.9. Sequence of images (1 ms apart) of bubble break-up in water (no-frother) at 420 RPM showing a break-up event giving one large and one small bubble (frames 9-10).



Figure 4.10. Sequence of images (1 ms apart) of bubble break-up in water (no-frother) at 420 RPM showing 3 daughter bubbles (frame 10) being produced from one mother bubble (frame 1).

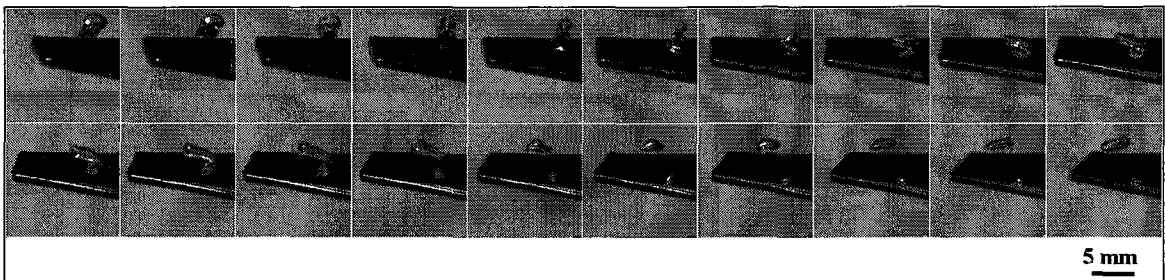


Figure 4.11. Sequence of images (1 ms apart) of bubble break-up. Dowfroth 250, 0.038 mmol/L, 420 RPM.

Figures 4.9 to 4.11 show break-up of bubbles that interact directly with the impeller blade. This is not always the situation; Figure 4.12 shows a bubble breaking-up in the proximity of the impeller blade, but without ever touching it. This is an example of bubble break-up by collision with a turbulent eddy generated by the action of the impeller.

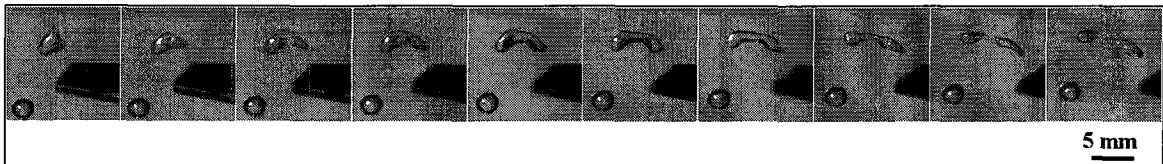


Figure 4.12. Sequence of images (1 ms apart) of bubble break-up in vicinity of blade. Dowfroth 250, 0.038 mmol/L at 420 RPM.

In the break-up sequences shown, bubbles do appear to break by the dumbbell stretching mechanism reported by Prince and Blanch (1986). The break-up time here ranges between 5 and 10 ms, which is shorter than the 25 ms reported by those authors.

Figure 4.13 shows the effect of different frothers (Pentanol, MIBC, and F-150) (concentrations close to the CCC95 (Nesset et al., 2007)). All three frothers hinder coalescence, Pentanol being the weakest one as judged by the increased fraction of bubbles larger than 2.5 mm. Moyo et al. (2007) and Azgomi et al. (2007) previously classified Pentanol as a weak frother compared to the other surfactants tested.

As with Dowfroth 250, these frothers modify the daughter bubble size distribution, favoring the generation of 2.4 mm bubbles.

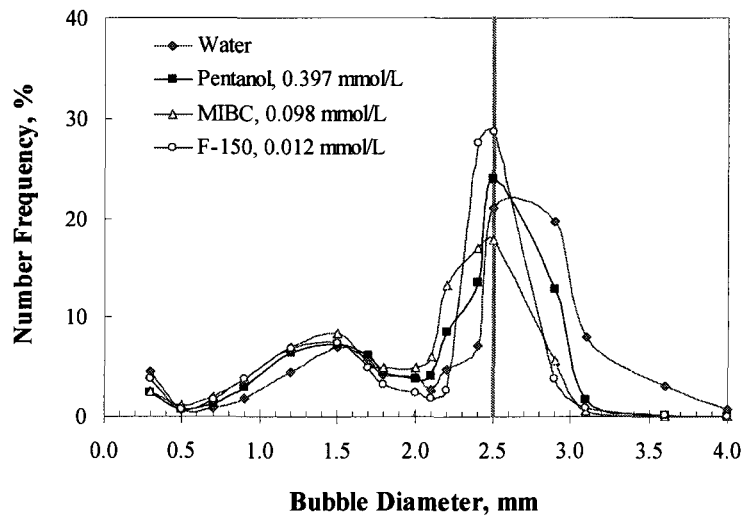


Figure 4.13. Frother effect (Pentanol, MIBC, F-150) on bubble size distribution, 420 RPM.

For all the reagents tested, the output bubble size distribution shows a minimum at 2.0 mm, which corresponds to equal break-up (50:50). This is in accord with the conditions listed by Wang et al. (2003) for daughter bubble size distributions generated by break-up.

The effect of 0.4 mol/L NaCl on bubble size distribution is shown Figure 4.14 together with the results for MIBC and water for comparison. The Figure shows similarity between the bubble size distributions generated with salt and MIBC. This is consistent with the observations of Quinn et al. (2007) who found that salt solutions of ionic strength ca. 0.4, i.e., 0.4 mol/L NaCl, and ca. 0.10 mmol/L MIBC (10 ppm) give similar gas dispersion properties. The similarity implies that whatever the mechanism(s) affecting the coalescence – break-up processes, they should apply not only to surfactants but also to salts, which otherwise give solutions of a very different nature compared to frothers.

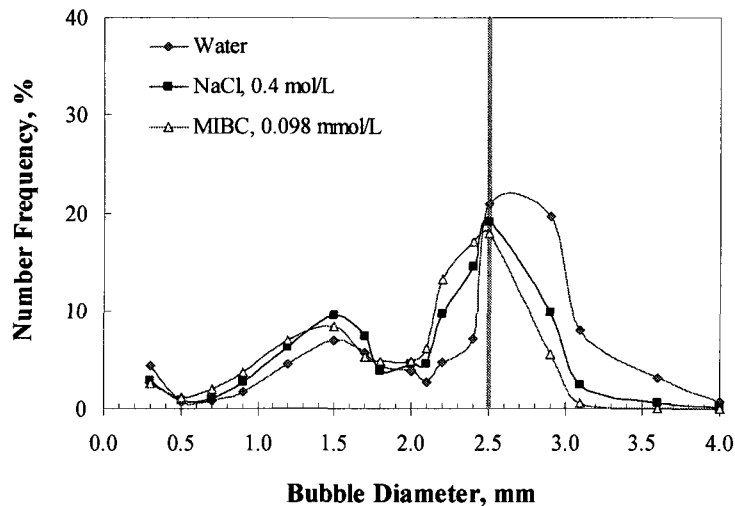


Figure 4.14. Effect of salt (NaCl) on bubble size distribution, 420 RPM.

4.5.3 Effect of frother concentration on bubble size distribution

The effect of frother concentration (Dowfroth 250) on bubble size distribution is shown in Figure 4.15. The concentrations range from CCC55 (0.011 mmol/L) to CCC99.9 (0.095 mmol/L), i.e., from an expected weak effect on bubble size to a strong effect.

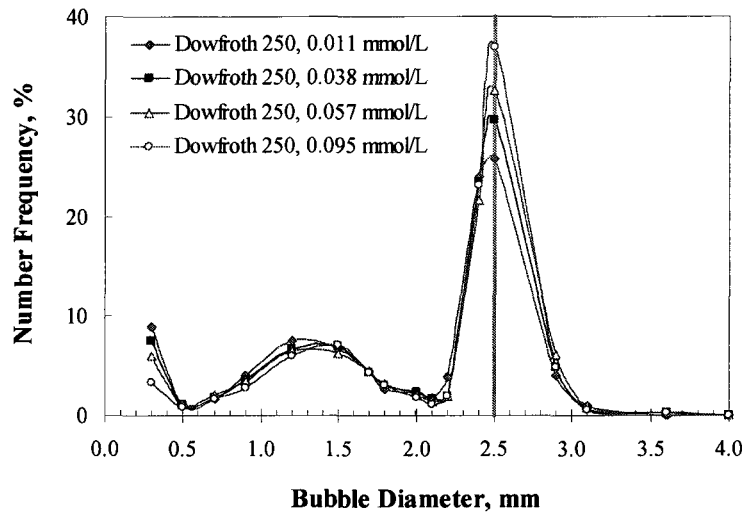


Figure 4.15. Effect of frother (Dowfroth 250) concentration on bubble size distribution, 420 RPM.

No major differences are observed in terms of coalescence prevention (i.e., fraction to right of 2.5 mm) for the concentrations tested; however, as seen from the fraction left at 2.5 mm, which increases with concentration, and that generated at 0.3 mm, which decreases, the fraction of bubbles created by break-up decreases for increasing frother concentration. In terms of volume frequency, the fraction decreases from 47% to 37% over the range of concentration. The reduction in break-up causes the Sauter mean diameter (d_{32}) to increase with frother concentration, from 1.9 mm at the lowest

concentration to 2.1 mm at the highest. This result differs from the observed, and expected, result in studies in flotation machines where bubble size (d_{32}) reduces with increasing frother concentration. Break-up retardation may be associated with the known tendency of surfactant to oppose bubble deformation (in this case oppose dumbbell formation). The bubble rise time in the experiments here may allow more frother adsorption than is typical for bubble generation in a flotation machine thus inducing a retardation effect.

4.5.4 Effect of impeller speed on bubble size distribution

Impeller speed controls both the probability of break-up and coalescence. The overall result will depend on the relative importance of these two events.

Figure 4.16 shows the effect of impeller speed on bubble size distribution in absence of frothers. The impeller speed was varied from 380 RPM (impeller tip speed 1.3 m/s) to 500 RPM (1.7 m/s). The fraction of bubbles generated by coalescence is seen to decrease with increasing impeller speed with a corresponding increase in the fraction generated by break-up (fraction to the left of 2.5 mm), from 42% at 380 RPM (15% by volume) to 60% at 500 RPM (25% by volume). The overall impression, therefore, is that break-up is favored over coalescence as impeller speed is increased.

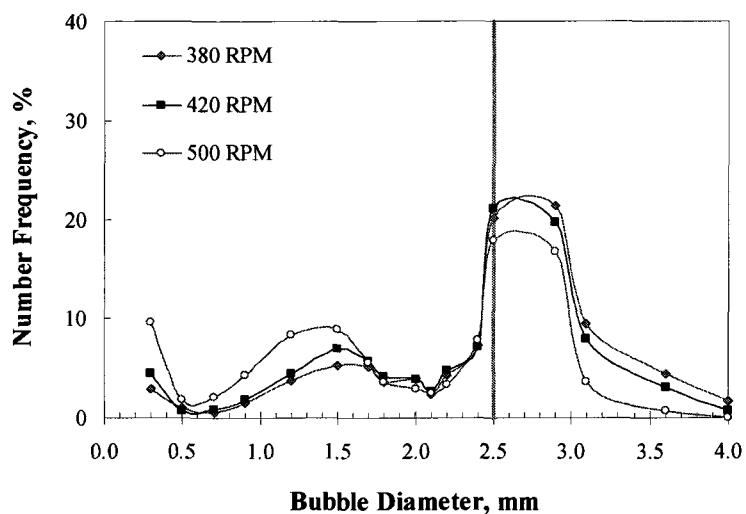


Figure 4.16. Effect of impeller speed on bubble size distributions. Water only.

Figure 4.17 shows the effect of impeller speed on bubble size distribution in presence of frother (F-150). Here the fraction of bubbles generated by coalescence is not significantly affected by the impeller speed. There is a diminishing fraction of bubbles of the original size (2.5 mm) with increasing impeller speed and an increasing fraction of the smallest bubbles (< 0.3 mm), suggesting again that break-up is favored as impeller speed is increased.

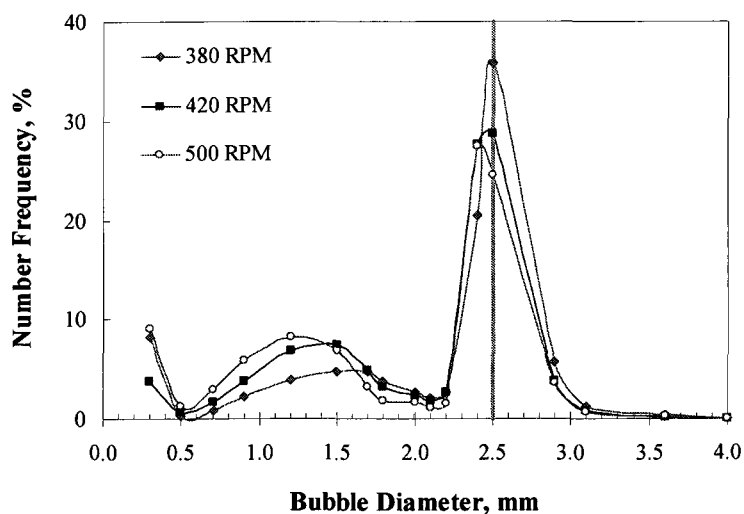


Figure 4.17. Effect of impeller speed on bubble size distributions. F-150, 0.012 mmol/L.

This decrease in bubble size with increasing impeller speed accords with the results of Gorain et al. (1995) and Grau and Laskowski (2006); but apparently not with those of Nasset et al. (2007) who found bubble size was independent of impeller speed. The reconciliation is to consider the energy range (impeller speed) over which the experiments were conducted. At low energy (i.e., low impeller speed), the effect of impeller speed is more obvious (Grau and Laskowski, 2006) than at higher impeller speeds (Grau and Laskowski, 2006; Nasset et al., 2007). The practical range is a tip speed of 5-7 m/s (Nasset et al., 2007), consequently the present results represent low energy. Another difference from practice is that the impeller here is ‘unconstrained’, i.e., there is no stator as in industrial mechanical machines. The stator will intensify the turbulence.

4.6 Discussion

4.6.1 Qualitative Observations

The experiments have shown that the turbulence surrounding the impeller creates an environment favoring both coalescence and break-up. In the absence of frother, coalescence dominates with more than half the volume of output bubble size distribution being larger than the input size (2.5 mm diameter). Nevertheless there is size reduction with a daughter population extending down to < 0.3 mm.

The presence of frother significantly alters the daughter bubble size distribution. The most immediate effect is to block the coalescence events, with sufficient frother effectively eliminating them altogether. This corresponds to the common explanation for the role of frothers (Metso Minerals CBT, 2002; Cho and Laskowski, 2002).

There is also an effect on the break-up process. Compared to water only, the fraction of bubbles of 2.4 mm (i.e., 90% the volume of the mother bubble) increases with a corresponding increase in bubbles less than ca. 1.2 mm (i.e., 10% the volume of the mother bubble). Otherwise, there is broad similarity with the break-up fraction distribution given in water only. Thus overall, frother damps coalescence and modifies breakage to favor $\leq 10\%$ volume fraction break-up.

The set-up was designed to try to access the process(es) occurring in mechanical flotation machines. The connection deserves comment. In this set-up the input (mother)

bubble size is known whereas in reality this is unknown, indeed would be conceptual. One advantage is that a break-up distribution function, analogous to the breakage (or appearance) function in comminution models, can be determined. The distributions presented are in essence just that. By taking a series of input bubble sizes, the break-up function could be determined as a function of input bubble size, which could form the basis for modeling bubble size distribution in mechanical machines.

Apart from inputting a single bubble size, the experiment introduces one other distinction from reality: the bubble is allowed to rise during which time frother adsorbs. Consequently the surface concentration (adsorption density) at break-up is probably higher than in practice. This may have introduced an artifact, namely that with increasing frother dosage the bubble size is expected to decrease whereas here it slightly increased. The dumbbell stretching mechanism may be opposed by high frother adsorption density.

Increasing impeller speed gave what might be considered the expected result, namely bubble size reduced. However, this appears to be dependent on the range over which the energy is expended: at low energies an effect is seen (Grau and Laskowski, 2006) while at high energy it is not (Grau and Laskowski, 2006; Nasset et al., 2007). The latter case appears to correspond more closely to industrial practice.

4.6.2 Quantitative Examination

The role of frother in preventing coalescence is reasonably interpreted by a combination of surface tension gradient driven phenomena (Gibbs elasticity and

Marangoni effect) and viscosity-related effects (Fruhner et al., 1999). These are described in some detail in Chapter 3. Here the break-up mechanism is examined to explore a possible role of frother, and salt.

It is proposed that the change in daughter bubble size distributions generated when frother is present is due to differences in surface tension associated with the dumbbell break-up mechanism. Figure 4.18 shows a stretched bubble before rupture which will generate daughter bubbles 1 and 2. Since stretching is not uniform, the surface surrounding 1 and 2 will have different frother concentration and thus different surface tension. The same argument for a difference in surface tension for sections 1 and 2 applies to salt solutions also.

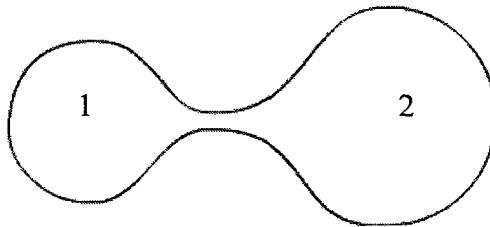


Figure 4.18. Stretched bubble before break-up.

According to the Laplace equation, the pressure inside each bubble (assumed spherical) immediately after break-up is:

$$P_1 = 2 \frac{\sigma_1}{r_1} \quad (\text{Eq. 4.1})$$

$$P_2 = 2 \frac{\sigma_2}{r_2} \quad (\text{Eq. 4.2})$$

where r_1 and r_2 are the radii of bubbles 1 and 2 after break-up, and σ_1 and σ_2 correspond to the surface tension of bubbles 1 and 2.

Equations 4.1 and 4.2 represent the pressure inside each end of the stretched bubble just prior to break-up. Generating a pressure difference inside a bubble costs energy, and the higher the pressure difference the higher the energy needed to generate that difference. From geometry, when a bubble breaks into two daughter bubbles the total bubble surface area increases. Unless the original bubble breaks into two equal size bubbles (break-up fraction equal to 50%), the increase in surface area contributed by both daughter bubbles is not the same and depends on the relative size of the daughter bubbles.

Figure 4.19 represents an original (mother) bubble divided by a plane into two regions (two spherical caps) that will generate the two daughter bubbles after break-up. It will be assumed that the break-up occurred by the dumbbell mechanism (Figure 4.18), and that equations 4.1 and 4.2 represent the pressures inside bubble 1 and 2 in Figure 4.19.

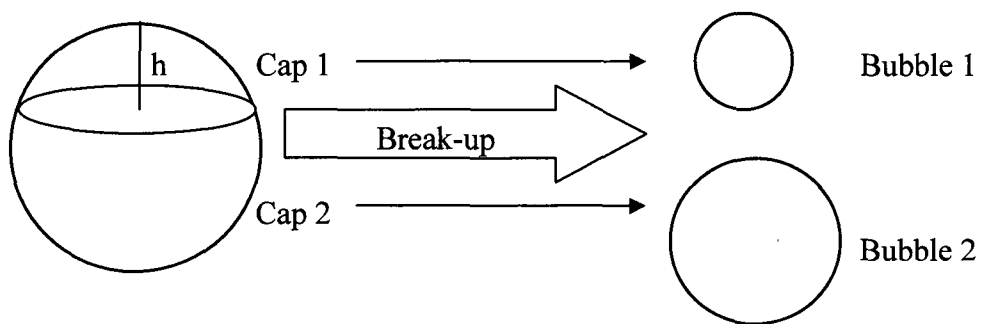


Figure 4.19. Schematic of bubble break-up.

If the original bubble has a radius equal to r_0 , the area corresponding to spherical caps 1 and 2 are:

$$A_{Cap1} = 2\pi h r_0 \quad (\text{Eq. 4.3})$$

$$A_{Cap2} = 2\pi(2r_0 - h)r_0 \quad (\text{Eq. 4.4})$$

The volumes associated to caps 1 and 2 correspond to the volumes of the daughter bubbles 1 and 2, and may be expressed as:

$$V_1 = \pi h^2 \left(r_0 - \frac{1}{3}h \right) \quad (\text{Eq. 4.5})$$

$$V_2 = \pi(2r_0 - h)^2 \left(r_0 - \frac{1}{3}(2r_0 - h) \right) \quad (\text{Eq. 4.6})$$

The bubbles generated after break-up (bubbles 1 and 2 in Figure 4.19) have volumes of:

$$V_1 = \frac{4}{3}\pi r_1^3 \quad (\text{Eq. 4.7})$$

$$V_2 = \frac{4}{3}\pi r_2^3 \quad (\text{Eq. 4.8})$$

where r_1 and r_2 are the radii of bubble 1 and 2, respectively. These radii may be calculated by equating to equations 4.5 and 4.6:

$$r_1 = \left(\frac{3}{4}h^2 \left(r_0 - \frac{1}{3}h \right) \right)^{\frac{1}{3}} \quad (\text{Eq. 4.9})$$

$$r_2 = \left(\frac{3}{4}(2r_0 - h)^2 \left(r_0 - \frac{1}{3}(2r_0 - h) \right) \right)^{\frac{1}{3}} \quad (\text{Eq. 4.10})$$

The area ratios between the newly generated bubbles and the original bubble caps are:

$$\frac{A_1}{A_{Cap1}} = \frac{2r_1^2}{hr_0} \quad (\text{Eq. 4.11})$$

$$\frac{A_2}{A_{Cap2}} = \frac{2r_2^2}{r_0(2r_0 - h)} \quad (\text{Eq. 4.12})$$

Equations 4.11 and 4.12 represent the relative change in area with respect to the original bubble caps. Figure 4.20 shows the difference between the area ratios versus break-up fraction, for the case relevant to the situation here, namely $r_0 = 1.25$ mm. In the analysis, bubble 2 is always the larger of the two. The results show that the relative change in area is greater for the large daughter bubble for all break-up fractions.

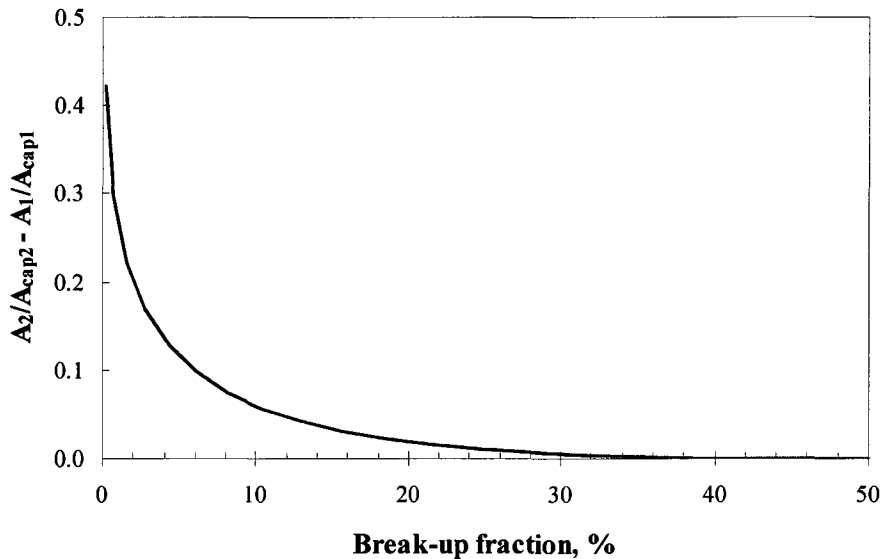


Figure 4.20. Difference between relative change in area for two daughter bubbles generated from a 2.5 mm diameter mother bubble. Bubble 2 is the larger of the two bubbles.

Since the break-up process occurs over a very short period of time, < 10 ms, it is unlikely that the new area generated will be replenished with frother, thus the two ends of the dumbbell, and the daughter bubbles immediately after break-up, have different surface concentration of frother and different surface tensions. For the analysis, therefore, adsorption of fresh frother molecules on the dumbbell will be neglected and the dumbbell will be assumed to share the same frother load as the mother bubble. Based on this, it is possible to evaluate the difference in pressure inside the daughter bubbles immediately after break-up, for both cases with and without frother or salt.

The general expression for the difference in pressure is:

$$\Delta P = 2 \left(\frac{\sigma_1}{r_1} - \frac{\sigma_2}{r_2} \right) \quad (\text{Eq. 4.13})$$

If the surface tension is assumed to be linearly proportional to the surface loading (adsorption density) Γ ($\text{mol}\cdot\text{m}^{-2}$) (Comley et al., 2002), the surface tension may be written as:

$$\sigma = \sigma_0 - k_y \Gamma \quad (\text{Eq. 4.14})$$

where σ_0 corresponds to the surface tension of (uncontaminated) water and k_y ($\text{mN}\cdot\text{m}\cdot\text{mol}^{-1}$) is the change in surface tension with loading. Equation 4.13 may be re-written as:

$$\Delta P = 2 \left(\frac{\sigma_0 - k_y \Gamma_1}{r_1} - \frac{\sigma_0 - k_y \Gamma_2}{r_2} \right) \quad (\text{Eq. 4.15})$$

But, following the assumption made, Γ_1 and Γ_2 may be expressed as:

$$\Gamma_1 = \frac{A_{cap1}}{A_1} \Gamma^* \quad (\text{Eq. 4.16})$$

$$\Gamma_2 = \frac{A_{cap2}}{A_2} \Gamma^* \quad (\text{Eq. 4.17})$$

where Γ^* represents the surface loading of the mother bubble, immediately prior to break-up.

Combining equations 4.15, 4.16, and 4.17 yields:

$$\Delta P = 2 \left(\frac{\sigma_0}{r_1} - \frac{\sigma_0}{r_2} \right) - 2k_y \Gamma^* \left(\frac{A_{cap1}}{r_1 A_1} - \frac{A_{cap2}}{r_2 A_2} \right) \quad (\text{Eq. 4.18})$$

The first term on the right hand side of equation 4.18 corresponds to the difference in capillary pressure between two bubbles generated by break-up in water only:

$$\Delta P_{water} = 2 \left(\frac{\sigma_0}{r_1} - \frac{\sigma_0}{r_2} \right) \quad (\text{Eq. 4.19})$$

hence, the difference in capillary pressure between two bubbles generated by break-up in the presence of frothers is:

$$\Delta P_{frother} = \Delta P_{water} - 2k_y \Gamma^* \left(\frac{A_{cap1}}{r_1 A_1} - \frac{A_{cap2}}{r_2 A_2} \right) \quad (\text{Eq. 4.20})$$

The second term on the right hand side of equation 4.20 is always positive (k_y and Γ^* are both positive and Figure 4.21 shows values for the parenthesis are always positive), thus it follows that for any break-up fraction different from 0% (no break-up) and 50% (equal

size break-up), ΔP is greater for water alone than for frother solutions meaning that less energy is needed to break bubbles in the presence of frothers.

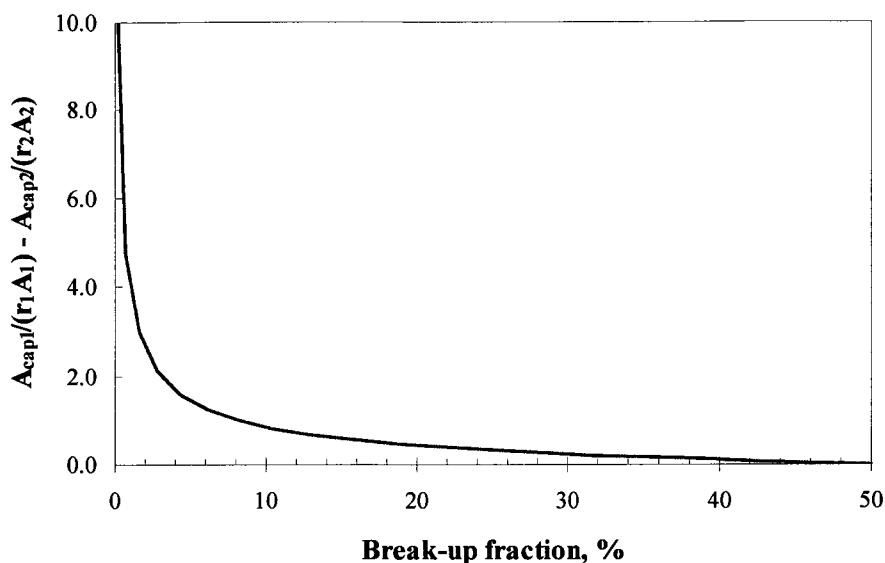


Figure 4.21. Evaluation of parenthesis in Equation 4.20.

This translates to the fact that it requires less energy to break bubbles in the presence of frothers. While this is not a new argument, Figure 4.21 does introduce a new component. The decrease in energy needed to break bubbles is accentuated towards highly asymmetric break-up, i.e., small break-up fractions ($< 10\%$). This is in accord with the increase in the number of bubbles of 90% and 10% (or less) of the original (mother) bubble volume generated in the presence of frothers compared to water only observed in this study.

The focus has been on frothers but the analysis for salts is analogous, with water molecules substituting for the frother in terms of surface activity. In this case, the

maximum surface tension value is that of the electrolyte solution at equilibrium, whereas σ_0 represents the minimum value σ_1 and σ_2 can take.

4.7 Conclusions

An experimental set-up delivering a single size bubble (2.5 mm diameter) into an impeller is used for a basic study of the coalescence/break-up events in the mechanical production of small bubbles. It is the first such study aimed at a basic understanding of fine bubble production in mechanical flotation machines. The approach permits coalescence and break-up events to be distinguished.

The observations confirm the common explanation that frothers and salt (NaCl) prevent coalescence. In the current set-up they are also shown to influence break-up. The evidence points to a predominance of break-up events favoring an asymmetric 90:10 volume division or higher in the presence of frothers and salt (NaCl); i.e., for the starting bubble size of 2.5 mm diameter, the output size is dominated by 2.4 mm diameter bubbles.

An analysis of the break-up event is presented based on the dumbbell model. It is determined that less energy is needed in the presence of frother to generate strongly asymmetric break-up which corresponds to the 90:10 division observed.

References

- Acuna, C. Nasset, J. E., Finch J.A. 2007. Impact of Frother on Bubble Production and Behaviour in the Pulp Zone. In Proceedings of the Sixth International Copper-Cobre Conference, Aug. 25-30, Toronto, Ont. Canada, Volume II Mineral Processing (Eds. R del Villar, J. E. Nasset, C. O. Gomez and A. W. Stradling) MetSoc CIM. 197-210.
- Azgomi, F., Gomez, C.O., Finch, J.A., 2007. Characterizing frothers using gas hold-up. Canadian Metallurgical Quarterly 46 (3). 237-242.
- Cho, Y.S., Laskowski, J.S., 2002. Effect of flotation frothers on bubble size and foam stability. International Journal of Mineral Processing 64. 69-80.
- Comley, B.A., Harris, P.J., Bradshaw, D.J., Harris, M.C., 2002. Frother characterisation using dynamic surface tension measurements. International Journal of Mineral Processing 64. 81-100.
- Dukhin, S.S., Miller, R., Loglio, G., 1998. Physico-chemical hydrodynamics of rising bubble. Studies in Interface Science Vol. 6: Drops and Bubbles in Interfacial Research. D. Möbius and R. Miller Editors, Elsevier Science.
- Finch, J.A., Gélinas, S., Moyo, P., 2006. Frother-related research at McGill University. Minerals Engineering 19. 726-733.
- Finch, J.A., Nasset, J.E., Acuña, C., 2008. Role of frother on bubble production and behaviour in flotation. Minerals Engineering. Article in Press.
- Fruhner, H., Wantke, K.-D., Lunkenheimer, K., 1999. Relationship between surface dilational properties and foam stability. Colloids and Surfaces A: Physicochemical and Engineering Aspects 162. 193-202.

- Gomez, C.O., Escudero, R., Finch, J.A., 2000. Determining equivalent pore diameter for rigid porous spargers. *Canadian Journal of Chemical Engineering* 78. 785-792.
- Gorain, B.K., Franzidis, J.-P., Manlapig, E.V., 1995. Studies on impeller type, impeller speed and air flow rate in an industrial scale flotation cell – Part 1: Effect on bubble size distribution. *Minerals Engineering* 8 (6). 615-635.
- Grau, R.A., Laskowski, J.S., 2006. Role of frothers in bubble generation and coalescence in a mechanical flotation cell. *The Canadian Journal of Chemical Engineering* 84. 170-182.
- Harris, P.J., 1982. Principles of flotation. Chapter 13: Frothing phenomena and frothers. King, R.P., ed. *South African Institute of Mining and Metallurgy Monograph Series No. 3*.
- Hernandez-Aguilar, J.R., Coleman, R.G., Gomez, C.O., Finch, J.A., 2004. A comparison between capillary and imaging techniques for sizing bubbles in flotation systems. *Minerals Engineering* 17 (1), 53-61.
- Hernandez-Aguilar J.R., Finch J. A., 2005. An experiment to validate bubble sizing techniques using bi-modal populations of known proportions. In: Graeme J. Jameson (Ed.), *Centenary of Flotation Symposium, 6-9 June 2005, Brisbane, Queensland, Australia*, pp. 465-472.
- Hinze, J.O., 1955. Fundamentals of the hydrodynamic mechanism of splitting in dispersion processes. *AIChE Journal*. 1 (3). 289-295.
- Laskowski, J.S., 2003. Fundamental properties of flotation frothers. *Proceedings of the 22nd International Mineral Processing Congress*. Cape Town, South Africa. 788-797.
- Luo, H., Svendsen H.F., 1996. Theoretical model for drop and bubble breakup in turbulent dispersions. *AIChE Journal* 42 (5). 1225-1233.

- Machon, V., Pacek, A.W., Nienow A.W., 1997. Bubble sizes in electrolyte and alcohol solutions in a turbulent stirred vessel. *Trans IChemE* 75 (A). 339-348.
- Metso Minerals CBT (Computer Based Training), 2002. Mill Operator Training Package. Flotation Module. Formerly Brenda Process Technology CBT (Computer Based Training) (1996). Mill Operator Training Package. Flotation Module.
- Miller, C.A., Neogi, P., 1985. Interfacial phenomena: equilibrium and dynamic effects. In: *Surfactant Science Series*, vol. 17, Chapter VI: Transport Effects on Interfacial Phenomena. 240-298.
- Moyo, P., Gomez, C.O., Finch, J.A., 2007. Characterizing frothers using water carrying rate. *Canadian Metallurgical Quarterly* 46. 215-220.
- Nesset, J.E., Finch, J.A., Gomez, C.O., 2007. Operating variables affecting the bubble size in forced-air mechanical flotation machines. In proceedings of Ninth Mill Operators' Conference, Freemantle, WA, Australia. 55-65.
- Oolman, T.O., Blanch, H.W., 1986. Bubble coalescence in stagnant liquids. *Chemical Engineering Communications* 43. 237-261.
- Parthasarathy, R., Jameson, G.J., Ahmed, N., 1991. Bubble breakup in stirred vessels. Predicting the Sauter mean diameter. *Chemical Engineering Research and Design* 69. 295-301.
- Prince, M.J., Blanch, H.W., 1990. Bubble coalescence and break-up in air-sparged bubble columns. *AIChE Journal* 36 (10). 1485-1499.
- Pugh, R.J., 1996. Foaming, foam films, antifoaming and defoaming. *Advances in Colloid and Interface Science* 64. 67-102.

- Quinn, J.J., Kracht, W., Gomez, C.O., Gagnon, C., Finch, J.A., 2007. Comparing the effect of salts and frother (MIBC) on gas dispersion and froth properties. *Minerals Engineering* 20. 1296-1302.
- Stewart C.W., 1995. Bubble interaction in low-viscosity liquids. *Int. J. Multiphase Flow* 21, No. 6, 1037-1046.
- Tse, K.L., Martin, T., McFarlane, C.M., Nienow, A.W., 1998. Visualisation of bubble coalescence in a coalescence cell, a stirred tank and a bubble column. *Chemical Engineering Science* 53 (23). 4031-4036.
- Walter J.F., Blanch H.W., 1986. Bubble break-up in gas-liquid bioreactors: break-up in turbulent flows. *The Chemical Engineering Journal* 32. B7-B17.
- Wang, T., Wang, J., Jin, J., 2003. A novel theoretical breakup kernel function of bubble/droplet in a turbulent flow. *Chemical Engineering Science* 58. 4629-4637.

Chapter 5 – Bubble rise velocity and shape

Chapter 3 employed a capillary-generated bubble to examine coalescence. In the course of those experiments, phenomena associated with the bubble in the few milliseconds after release were recorded. Subsequent analysis showed frothers effect on shape (aspect ratio) and local velocity that appeared to be related. This possibility stimulated the work that forms Chapter 5. The findings are related to coalescence and break-up events as they point to the time-dependence of frother (and salt)-accumulation on a bubble surface.

5.1 Introduction

Frothers are surface-active agents (surfactants) widely used in flotation to aid generation of small bubbles and to help form and stabilize the froth phase. They also influence how bubbles move in a liquid (Frumkin and Levich, 1947; Dukhin et al., 1998). Clift et al. (2005), summarizing data spanning 70 years, show a decrease in terminal rise velocity of single air bubbles over the size (diameter) range ca. 1 to 10 mm in water in the presence of so-called ‘surface-active contaminants’. Other authors have found that bubbles move at different terminal velocities depending on frother type (Zhou et al., 1992; Sam et al., 1996; Zhang et al., 1996). Azgomi et al. (2007) observed that, for a given gas rate, different frothers may generate the same gas holdup but with different bubble size, which suggests that bubble swarm velocity is affected by the presence of frothers. Zhou et al. (1993) made a similar claim. Acuna and Finch (2008) generating a

2D swarm confirmed this frother type effect. The time history or local velocity profiles and bubble shape also depend on frother type and concentration (Sam et al., 1996; Krzan et al., 2004). These prior studies tracked bubble rise for at least one second. This chapter shows the effect that common frothers (Pentanol, MIBC (methyl isobutyl carbinol), Dowfroth 250 (polyglycol ether), F-150 (polyglycol)) and salt (sodium chloride) have on bubble shape and rise velocity over the first ca. 0.4 seconds. Salt is included as high concentrations (> 0.4 ionic strength) also reduce bubble size (Quinn et al., 2007).

5.2 Bubble shape and rise velocity

Bubble motion may be classified into three regimes depending on rise velocity (Kulkarni and Joshi, 2000). The bubble Reynolds (Re) and Eötvös (Eo) numbers are used in the characterization, calculated from (Clift et al., 2005):

$$Eo = \frac{g(\rho_l - \rho_{air})d_{eq}^2}{\sigma} \quad (\text{Eq. 5.1})$$

$$Re = \frac{\rho_l d_{eq} v}{\mu} \quad (\text{Eq. 5.2})$$

where g is the acceleration of gravity, ρ_l and ρ_{air} are the liquid and air density respectively, d_{eq} is the bubble equivalent spherical diameter, σ the surface tension, μ the liquid viscosity, and v the bubble rise velocity. The range of Eötvös number for bubbles in this study is $0.78 < Eo < 0.87$, and the range in Reynolds number is $210 < Re < 900$.

According to Tomiyama et al. (2002) the role of surfactants on bubble dynamics in the three regimes can be summarized as follows:

1. Viscous force dominant regime (small spherical bubble, $Eo < 0.25$): Accumulation of surfactants on bubble surface, together with the bubble motion, induces surface tension gradient effects that make the surface immobile and the bubble rise as a rigid sphere. The surface goes from free-slip to no-slip condition, resulting in an increase in viscous drag and decrease in terminal velocity.
2. Surface tension force dominant regime (intermediate size bubble, $0.25 < Eo < 40$): Surfactants reduce the shape oscillation, making bubbles more spherical. The terminal velocity becomes close to that of bubbles in clean systems with small initial shape deformation. Terminal velocity gradually decreases with increasing bubble size in this regime (the authors give a range of bubble sizes (1.3 mm – 6 mm) based on a previous study (Peebles and Garber, 1953)). Most bubbles in flotation practice fall into categories 1 and 2.
3. Inertial force dominant regime (large bubble, $Eo > 40$): High inertia reduces the impact of surfactant in bubble motion and shape. The drag due to inertia is much higher than the viscous drag induced by surface tension gradient effects.

At Reynolds numbers higher than 200 ($Re > 200$), bubble buoyancy is complicated by bubble shape variation and bubble path instability (Dukhin et al., 1998). In a qualitative approach, it is suggested (Dukhin et al., 1998; Linton and Sutherland, 1957; Frumkin and Levich, 1947) that surfactants are swept to the rear of a rising bubble, generating a region of low surface concentration at the leading surface of the bubble and a region of large concentration at the rear pole of the bubble. The low concentration

(leading) region remains mobile, whereas the high concentration (rear) region is characterized by retarded surface mobility (rear stagnant cap).

Acuna (2007) studied the effect of surfactants (frothers) on single bubbles of ca. 3.5 mm diameter generated at a capillary tip over the first 50 ms or so. Bubbles blown in tap water and in surfactant solution (0.1 mmol/L polyglycol, F-150) behaved identically in terms of aspect ratio and local velocity over the first 10 ms following bubble detachment. After this the bubble in surfactant solution became more spherical than its water only cousin and slowed down significantly. The observation reveals that frother requires time to adsorb sufficiently to produce effects on bubble behavior. Although over much shorter time periods, this work is in agreement with others (Sam et al., 1996; Zhang et al., 2001; Krzan et al., 2004, 2007).

Krzan et al. (2004, 2007) studied local (instantaneous) velocities and shape variations of bubbles rising in presence of surfactants. They confirmed the previous findings of Sam et al. (1996) and Zhang et al. (2001, 2003) that after initial acceleration, bubbles either attained a constant velocity (terminal velocity) at high concentrations of surfactant, or passed through a maximum in the local velocity followed by a deceleration prior to reaching terminal velocity for low concentrations of surfactant. The maximum in local velocity indicates that the dynamic steady state structure of the adsorption layer on the rising bubble is not yet established. Bubble shape also stabilized once terminal velocity was reached.

Differences in local rise velocity are not restricted to surfactant systems. Wu and Gharib (2002) produced spherical and ellipsoidal bubbles of equivalent volume in purified water and found that the spherical bubbles moved significantly slower than their ellipsoidal counterparts.

Figure 5.1 is taken from Wu and Gharib (2002), and shows the correlation that exists between bubble rise velocity and bubble shape: spherical bubbles rose more slowly than ellipsoidal bubbles (note the latter reaches the top of the frame sooner than the spherical bubble).

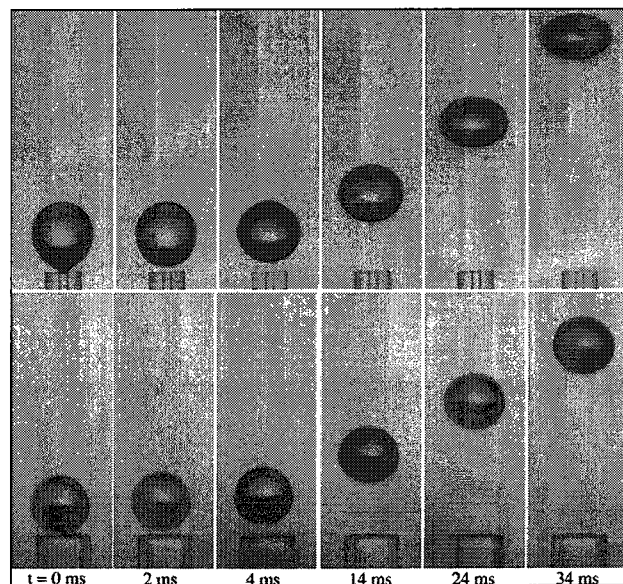


Figure 5.1. Bubbles of equivalent volume rising in water. The size of each image is 0.32 cm \times 0.88 cm. (Wu and Gharib, 2002. Reprinted with permission from the American Institute of Physics).

De Vries et al. (2002) studied the influence of bubble shape oscillations on local velocities of bubbles in the absence of surfactants. They found that shape oscillations

correlated with an oscillating bubble rise velocity and deduced that the oscillations in velocity were caused by variations in the added-mass term, which corresponds to an inertia effect originating as the rising bubble has to push water out of the way. The virtual or added-mass term is taken into account to calculate the exact rate of exchange of momentum of objects (bubbles) accelerating, rotating or oscillating in fluids, which depends on the shape of the bubbles (Kendoush, 2007).

From numerical analysis, Dijkhuizen et al. (2005) predicted oscillations in both shape and velocity of bubbles of 3 mm and larger in initially quiescent pure water. They considered the drag and virtual mass forces in their calculations.

The works of Wu and Gharib (2002), De Vries et al. (2002), and Dijkhuizen et al. (2005) therefore suggest it is bubble shape that controls velocity. The action of surfactant is then seen as one of modulating shape, making a bubble more spherical (due to surface tension gradient effects) that cause the bubble to slow down as opposed to the more direct effect of increasing drag due to surface tension gradient effects.

In this study, bubble shape and rise velocity over the first ca. 400 ms from release is examined in the presence of frothers and (separately) salt.

5.3 Experimental

5.3.1 Apparatus

The experimental set-up (Figure 5.2) comprises a 30L acrylic tank where air bubbles are injected through a glass capillary tube of 0.2 mm internal diameter. Gas flow rate is regulated by controlling the pressure in the line with a pressure regulator to generate a bubble growth rate of ca. 6.2 cc/min to produce bubbles of ca. 2.4 mm diameter (i.e., a growing time of ca. 70 ms). The tank is rear illuminated and bubbles are imaged with a high-speed camera (TroubleShooter HR) at a rate of 1,000 frames per second and a resolution of 1280 x 512 pixels.

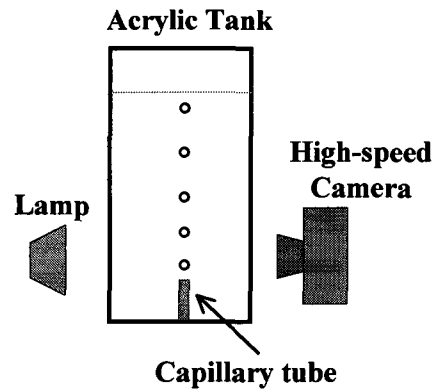


Figure 5.2. Experimental set-up.

5.3.2 Reagents

Table 5.1 summarizes the reagents used. These represent the four classes of frothers from ‘weakest’ to ‘strongest’ as identified by Moyo et al. (2007): Pentanol, MIBC (methyl isobutyl carbinol), Dowfroth 250 (polyglycol ether), F-150 (polyglycol), and a member of the class of salts (sodium chloride) that at high concentration have the same effect on producing fine bubbles as frothers (Quinn et al., 2007). The HLB number (hydrophile-lipophile balance) is included as a scale of solubility of surfactant in water (Rao, 2004): the higher the HLB number the more water soluble (i.e., hydrophilic) is the reagent.

Table 5.1. Summary of reagents used.

Reagent	Formula	Molecular weight (g/gmol)	HLB number	Supplier
Pentanol	$\text{CH}_3(\text{CH}_2)_4\text{OH}$	88.15	6.5	Fisher
MIBC	$(\text{CH}_3)_2\text{CHCH}_2\text{CH}(\text{OH})\text{CH}_3$	102.18	6.1	Dow
Dowfroth 250 ¹	$\text{CH}_3(\text{PO})_4\text{OH}$	264.35	7.8	Dow
F-150 ¹	$\text{H}(\text{PO})_7\text{OH}$	425	8.5	Flottec
Sodium Chloride	NaCl	58.44	--	Fisher

¹ PO is propylene oxide (propoxy) [-O-CH₂-CH₂-CH₂-]

Solutions were made using Montréal tap water and the temperature was set at 20 degree Celsius, controlled by mixing warm and cold water (experiments were performed during winter). Between tests, the tank was emptied and carefully cleaned.

The frother concentrations employed cover the range of interest in flotation and were chosen based on the ability of these reagents to prevent coalescence in industrial cells (Nesset et al., 2007), hence the concentrations vary from frother to frother. As a guide to the concentrations used, Table 5.2 shows concentrations corresponding to a scale based on the critical coalescence concentration (*CCC*). In the table, the number accompanying *CCC* (e.g. *CCC95*) corresponds to the percentage of bubble size reduction compared to water alone (Nesset et al., 2007); *CCC95*, thus, corresponds to a concentration achieving 95% of bubble size reduction. For the case of sodium chloride, concentrations up to 1 mol/L were tested, based on the comparison between MIBC and salts made by Quinn et al. (2007).

Table 5.2. Typical frother concentrations (mmol/L) used in flotation systems expressed on *CCC* scale (adapted from Nesset et al., 2007).

Reagent	<i>CCC50</i>	<i>CCC75</i>	<i>CCC95</i>	<i>CCC99</i>
Pentanol	0.077	0.153	0.331	0.509
MIBC	0.026	0.051	0.111	0.171
Dowfroth 250	0.009	0.018	0.039	0.091
F-150	0.002	0.005	0.010	0.016

5.3.3 The Technique

Bubble shape and velocity were recorded with the high-speed camera over a distance of 85 mm from the capillary tip (equivalent to 35 times the bubble diameter). Each video was processed off-line with ImageJ to yield bubble position, and dimensions

(i.e., maximum and minimum diameter) vs. time. The position (x, y) was determined from the center point of the bubble, and the maximum and minimum diameters were determined by the best-fitted ellipse to the 2D-bubble image. The best-fitted ellipse is determined directly by ImageJ, which also determines the angle between the maximum diameter and the y -axis (vertical axis). This allows not only calculation of the aspect ratio but whether the maximum or minimum diameter corresponds to the direction of movement of the bubble (d_v). The aspect ratio (A_R) is defined as the ratio between the diameters d_h and d_v , the diameters perpendicular and parallel to the direction of movement of the bubble respectively (Figure 5.3):

$$A_R = \frac{d_h}{d_v} \quad (\text{Eq. 5.2})$$

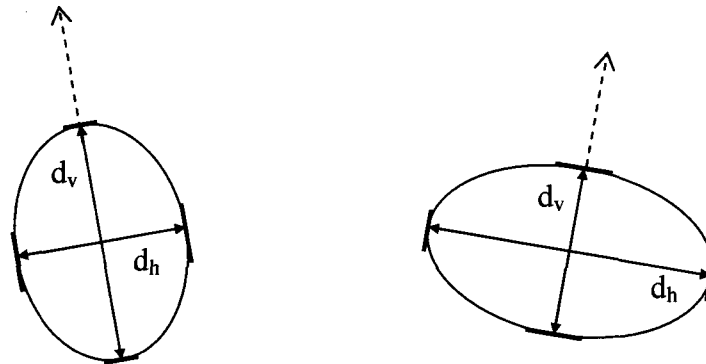


Figure 5.3. Diameters d_h and d_v used to calculate the aspect ratio where dashed arrow indicates direction of movement.

The rise velocity (v) is calculated from the vertical position (y) of the bubble over two consecutive frames ($i, i+1$) as:

$$v = \frac{y_{i+1} - y_i}{\Delta t} \quad (\text{Eq. 5.3})$$

where Δt is the time interval between the two frames (1 ms).

The equivalent diameter (d_{eq}) is calculated assuming axial symmetry over the direction of movement:

$$d_{eq} = (d_v d_h^2)^{1/3} \quad (\text{Eq. 5.4})$$

For the purpose of this chapter, bubbles will be described as ‘spherical’ if the aspect ratio lies within 15% of unity ($A_R < 1.15$); otherwise, the bubble will be described as ‘ellipsoidal’. Other bubble geometries, presented by Clift et al. (2005), are spherical-cap and ellipsoidal-cap, but these correspond to large bubbles (>10 mm) that tend to adopt flat or indented bases; these geometries were not observed in this study.

5.4 Results

The measurements, repeated 5 times for each condition (5 bubbles were recorded), were consistent; for instance, for Dowfroth 250 (0.095 mmol/L), the pooled standard deviation for the aspect ratio, equivalent diameter, and velocity were 0.009, 0.01 mm, and 0.59 cm/s respectively.

5.4.1 Effect of frother type and salt

Figure 5.4 shows images of bubbles in tap water, Pentanol (0.40 mmol/L), and F-150 (0.012 mmol/L). It is clear that F-150 has a dramatic effect on shape stabilization, whereas Pentanol has virtually no effect and is comparable to tap water. Note that for the region close to the capillary (the first 3 bubbles) the bubble motion for the three conditions look similar, differences appearing after this, as Acuna (2007) noted.

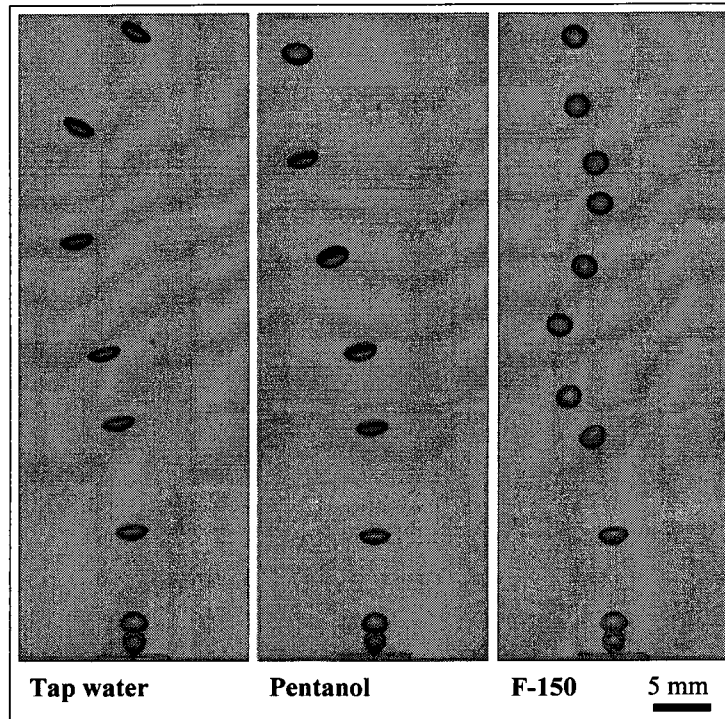


Figure 5.4. Example of recorded images (taken from video each 30 ms). Tap water (no frother), Pentanol (0.40 mmol/L), and F-150 (0.012 mmol/L).

Figure 5.5 shows the results of velocity and aspect ratio for a bubble in tap water (without frother). The velocity increases rapidly over the first ca. 40 ms, after which it continues to slowly increase (until ca. 150 ms), when it decreases from 38 cm/s to 26 cm/s followed by an increase again in what seems to be an oscillating pattern. The reported bubble rise velocity for bubbles of 2.4 mm diameter in clean water is 28 cm/s (Clift et al., 2005). Note that the aspect ratio varies in accord with the velocity. The bubble leaves the capillary as a spherical bubble, but after ca. 10 ms it becomes ellipsoidal and retains that general shape ($A_R > 1.15$) for all other times, reaching a peak aspect ratio of 2.6.

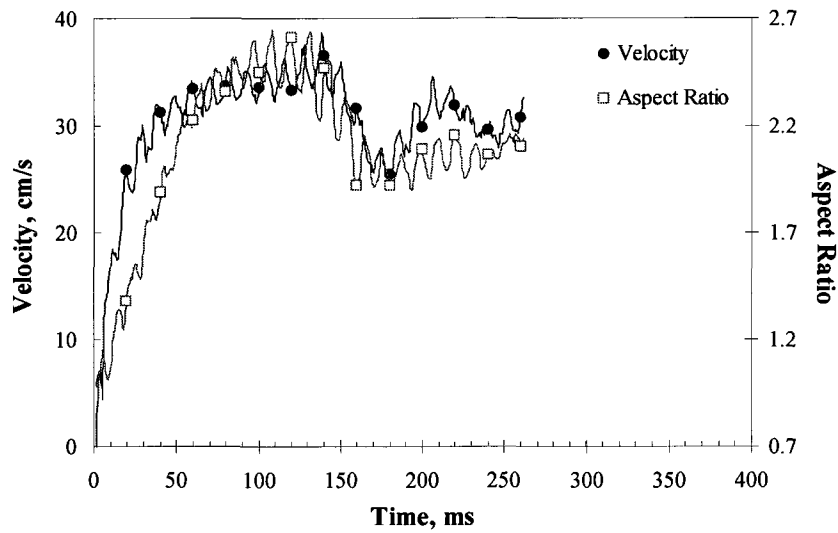


Figure 5.5. Velocity and aspect ratio. Tap water. (Note symbols are used to identify the curves and have no other significance.)

The high frequency oscillation observed in aspect ratio and velocity over the whole period correspond to high frequency oscillations in d_v (diameter in the vertical direction).

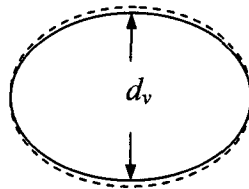


Figure 5.6. Sketch of high frequency oscillations of vertical diameter d_v .

Tap water will contain impurities but they evidently are not sufficient to stabilize the bubble shape. Figure 5.7, on the other hand, presents the significant impact that deliberately added surfactant (Dowfroth 250, 0.095 mmol/L) has on velocity and shape.

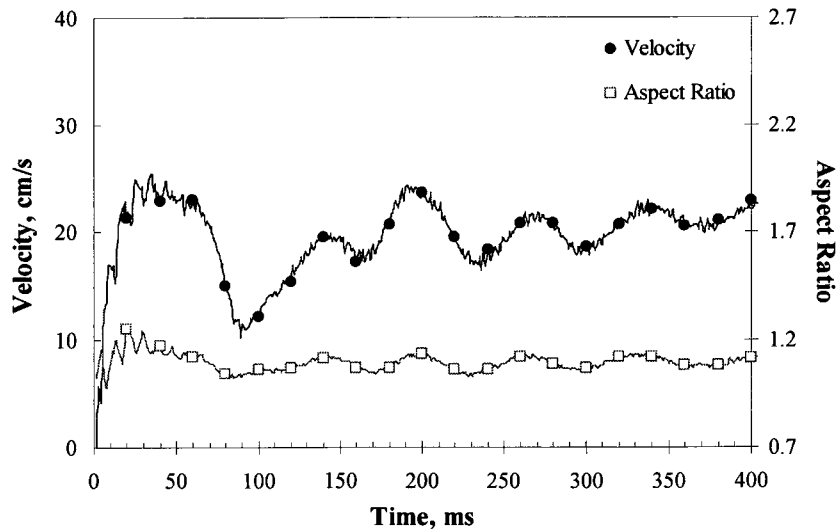


Figure 5.7. Velocity and aspect ratio. Dowfroth 250, 0.095 mmol/L.

In this case, after detaching from the capillary as a spherical bubble ($A_R \sim 1$), it changes shape to ellipsoidal between ca. 10 – 40 ms, after which its spherical shape is reestablished, varying around a mean $A_R \sim 1.1$. The high frequency oscillations associated to rapid changes in d_v detected in water only are damped in the presence of frother. This further confirms that the presence of frother stabilizes the bubble shape. In terms of velocity, after accelerating for the first ca. 30 ms, the bubble reaches a maximum velocity of 25 cm/s, much lower than the maximum velocity in tap water (38 cm/s) (this lower velocity means it stays in the frame for 400 ms rather than ca. 250 ms as in the water-only case). This is followed by deceleration to a minimum velocity of 10 cm/s prior to starting to oscillate about a mean of ca. 20 cm/s. For a 2.4 mm diameter bubble in ‘contaminated’ water, Clift et al. (2005) give a velocity of ca. 17 cm/s. Again, observe how the aspect ratio oscillates in accord with the velocity.

Figure 5.8 shows results for F-150 (0.012 mmol/L): again, after an initial period (ca. 75 ms) the presence of frother stabilizes a spherical bubble shape with an aspect ratio varying in accord with velocity.

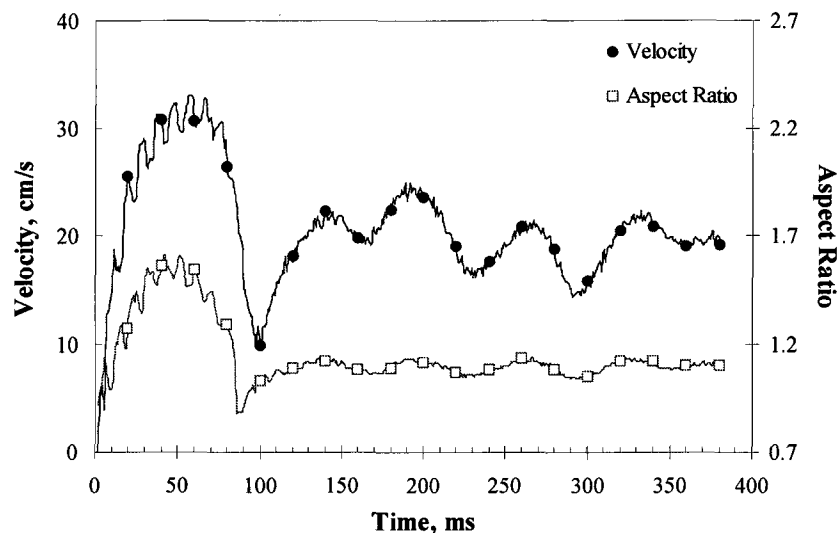


Figure 5.8. Velocity and aspect ratio. F-150, 0.012 mmol/L.

Figure 5.7 and Figure 5.8 show how frother (Dowfroth 250, F-150) influences bubble shape and velocity; however not all frothers have the same magnitude of effect. Figure 5.9 shows the results for Pentanol (0.40 mmol/L). Compared to water alone the presence of this frother did not restore the original spherical shape (although did still dampen the high frequency oscillations) or reduce velocity significantly. The correlation between shape (aspect ratio) and velocity nevertheless remains.

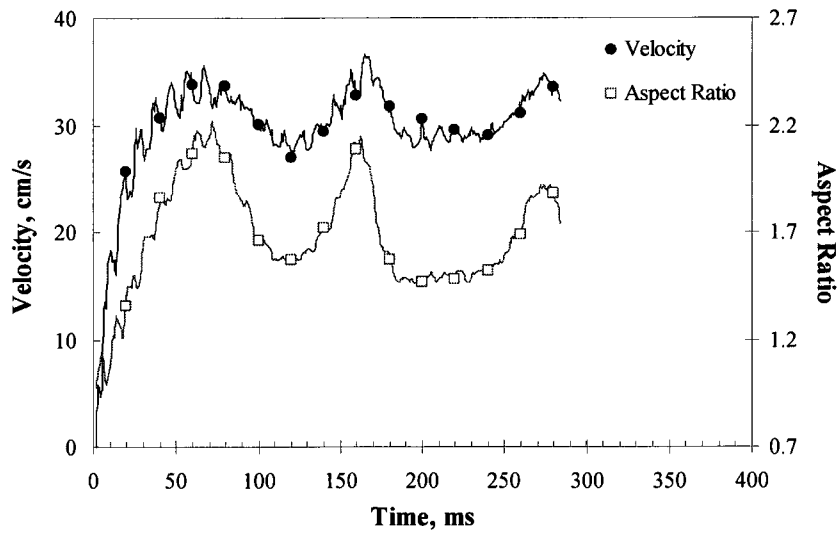


Figure 5.9. Velocity and aspect ratio. Pentanol, 0.40 mmol/L.

The work of Quinn et al. (2007) showed that 0.098 mmol/L MIBC gave the same bubble size (and gas holdup) as 0.4 mol/L NaCl. Results for these two conditions are shown in Figure 5.10 and Figure 5.11 respectively.

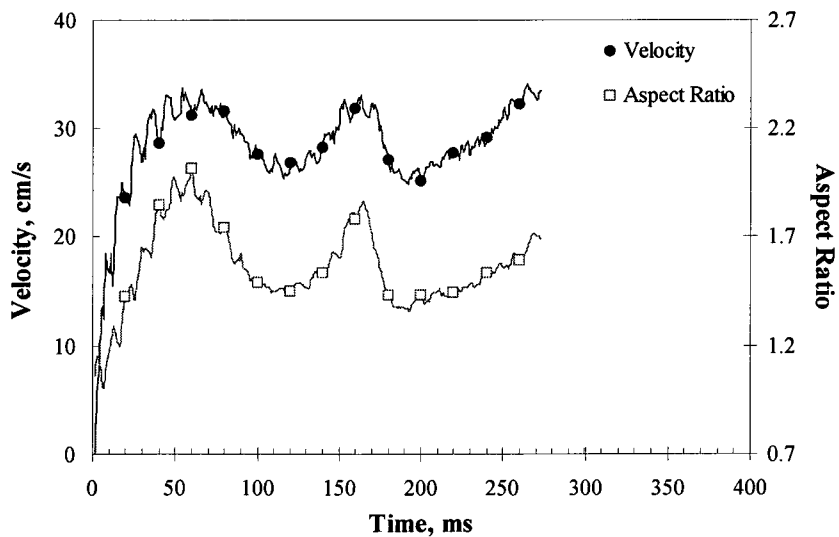


Figure 5.10. Velocity and aspect ratio. MIBC, 0.098 mmol/L.

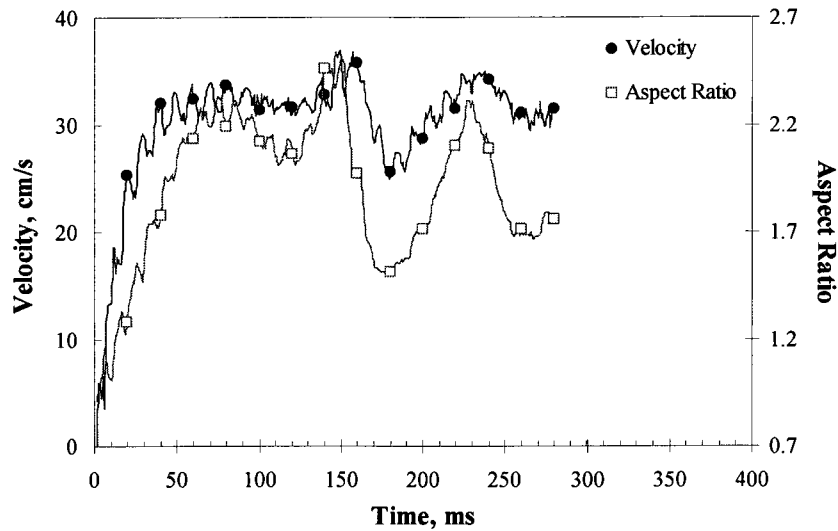


Figure 5.11. Velocity and aspect ratio. NaCl, 0.4 mol/L.

Even though frother (MIBC) and sodium chloride behave differently with regard to the bubble surface (frother positively adsorbs, salt negatively adsorbs), they give similar results, for example the bubble accelerating over the first 50 ms to reach a similar mean velocity and showing oscillations in shape and velocity of similar frequency. Their effect is comparable to Pentanol and less than for F-150 and Dowfroth 250.

The images in Figure 5.4 suggested similar behavior regardless of conditions over the first few milliseconds. This is explored in Figure 5.12 and Figure 5.13, which show the velocity and aspect ratio for tap water and Dowfroth 250 (the two extremes) over the first 20 ms. No difference is observed in the velocity or aspect ratio profile over the first ca. 15 ms. The finding conforms with the observation of Acuna (2007).

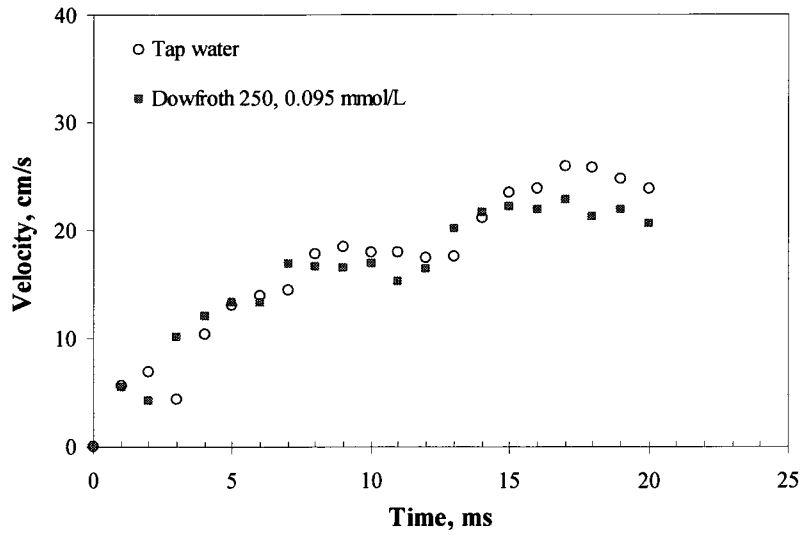


Figure 5.12. Velocity over first 20 ms. Tap water; Dowfroth 250, 0.095 mmol/L.

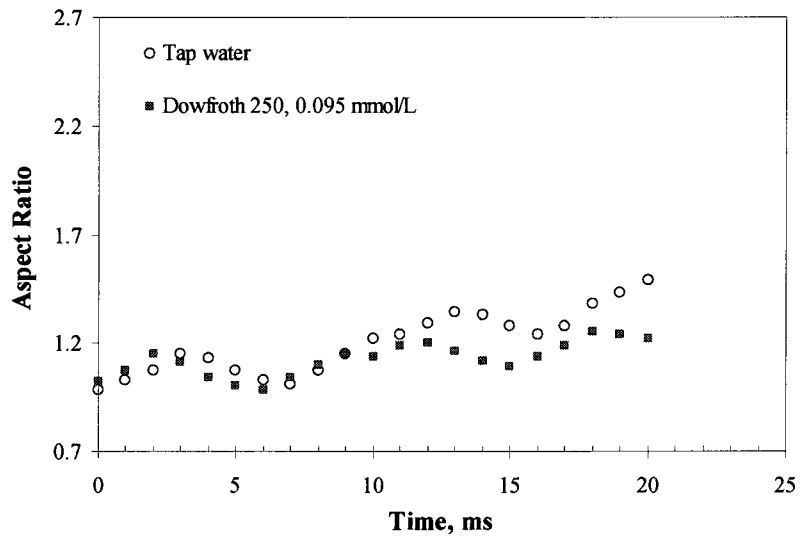


Figure 5.13. Aspect ratio over first 20 ms. Tap water; Dowfroth 250, 0.095 mmol/L.

5.4.2 Effect of frother concentration

Figure 5.14 visualizes the effect on bubble rise velocity as frother concentration increases. Note with increasing frother concentration that the bubbles become more spherical and slow down (more bubbles in the frame).

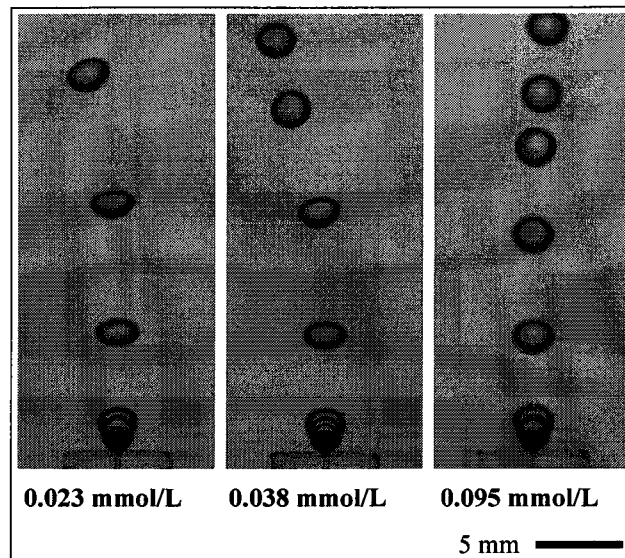


Figure 5.14. Images showing impact of frother concentration (taken from video each 25 ms). Dowfroth 250.

Figure 5.15 (Dowfroth 250) and Figure 5.16 (F-150) show how the acceleration period and maximum velocity decrease as concentration is increased. Subsequently, the oscillations appear to be similar in frequency and amplitude.

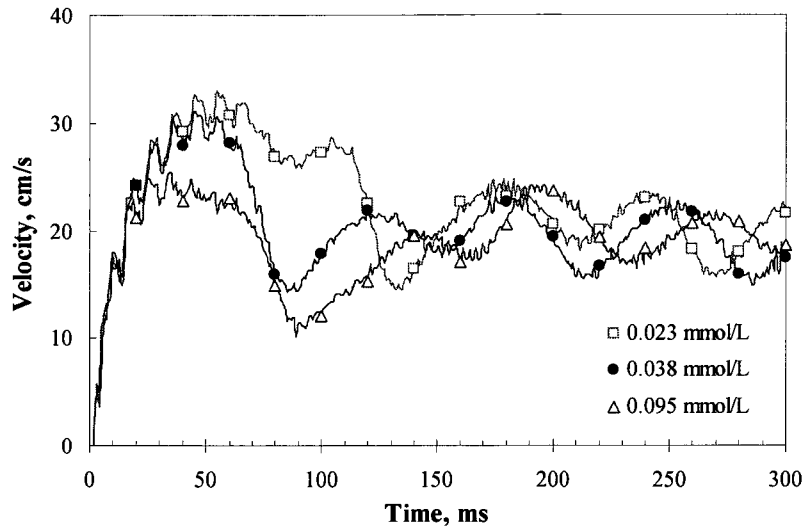


Figure 5.15. Velocity profile as a function of frother concentration. Dowfroth 250: 0.023, 0.038, and 0.095 mmol/L.

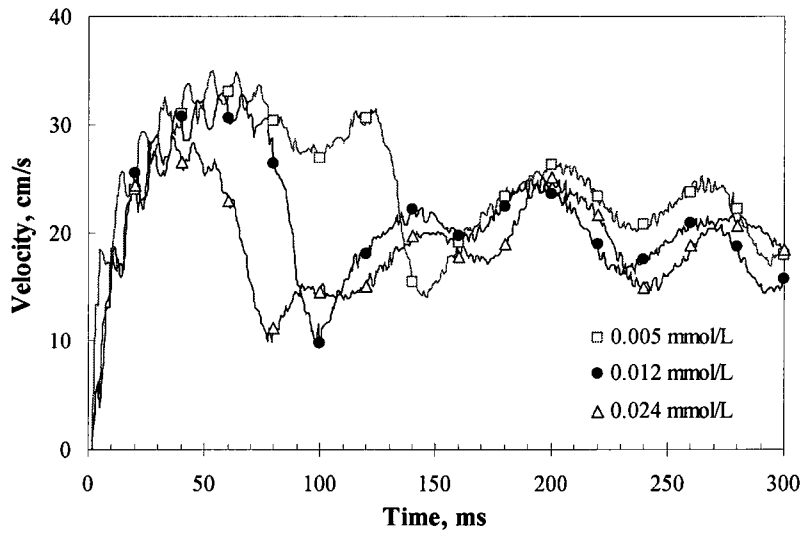


Figure 5.16. Velocity profile as a function of frother concentration. F-150: 0.005, 0.012, and 0.024 mmol/L.

Note that bubbles reach a different maximum velocity that depends on concentration. The time at which bubbles reach this maximum also depends on frother

concentration. Bubbles seem to behave alike again after ca. 150 ms simply being offset in time.

This shift in the first peak (maximum velocity) to shorter time is not so evident for the other reagents tested, namely MIBC, Pentanol, and sodium chloride. The results for MIBC are shown in Figure 5.17 as an example. This is evidence of a weaker effect of these reagents on bubble shape stabilization. The response in velocity continues to have its counterpart in shape.

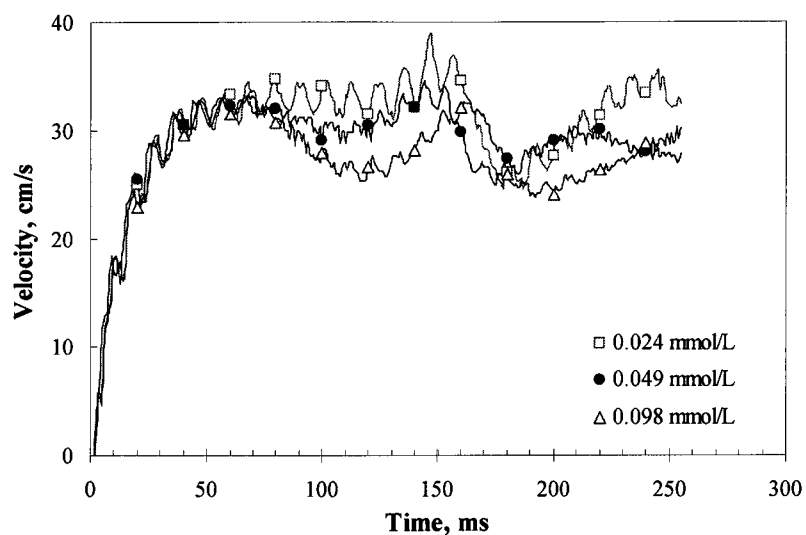


Figure 5.17. Velocity profiles as a function of frother concentration. MIBC: 0.024, 0.049, and 0.098 mmol/L.

5.4.3 Bubble rise velocity versus aspect ratio

The results indicate bubble shape varies in time in like manner as velocity. The literature (Wu and Gharib, 2002; De Vries et al., 2002; Dijkhuizen et al., 2005) suggests

that there is a relationship between bubble shape and velocity regardless of the presence of surfactant. To explore, data were processed to yield the average velocity corresponding to each aspect ratio, the standard deviation also being computed. Only data collected after the first deceleration period (i.e., following the initial maximum velocity) are considered, i.e., conditions where frother concentration on the bubble surface is approaching dynamic equilibrium with the bulk.

Figure 5.18 shows the relationship between velocity and aspect ratio for Dowfroth 250. Note that all the concentrations follow the same trend.

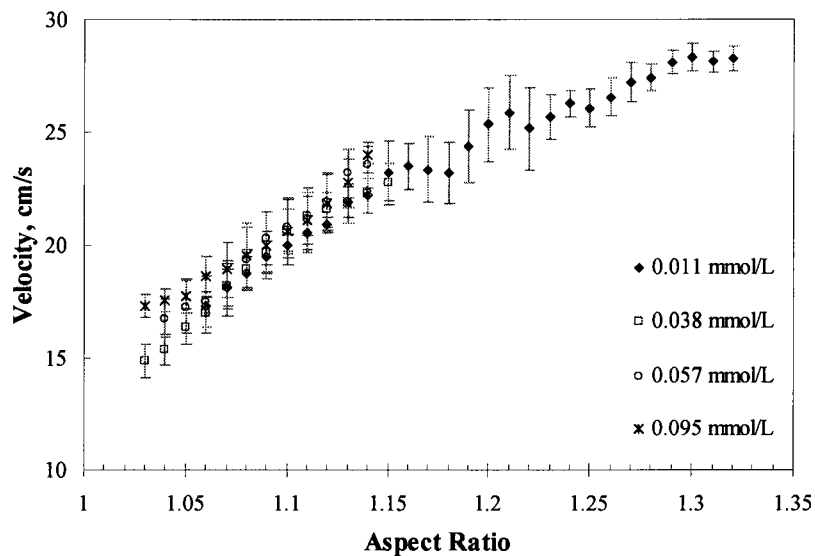


Figure 5.18. Velocity vs. aspect ratio. Dowfroth 250: 0.011, 0.038, 0.057, and 0.095 mmol/L

Figure 5.19 shows the data for MIBC; in this case, unlike Dowfroth 250, the highest concentration (0.196 mmol/L) exhibits a slightly different behavior than the

others. However, the aspect ratio (bubble shape) – velocity relationship still holds with perhaps a secondary effect of frother concentration entering.

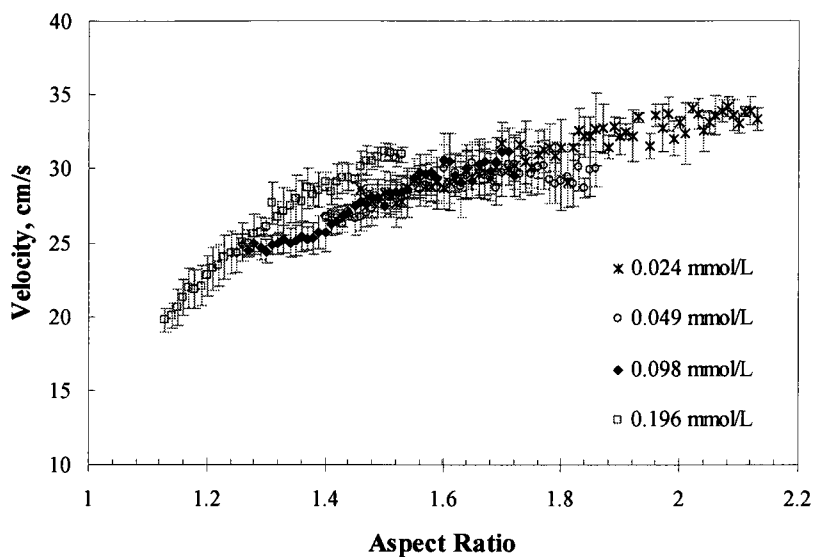


Figure 5.19. Velocity vs. aspect ratio. MIBC: 0.024, 0.049, 0.098, 0.196 mmol/L.

As a summary, Figure 5.20 shows the velocity versus aspect ratio for the maximum concentration tested for each reagent. The Figure confirms the strong relationship between shape and bubble velocity, an increasing aspect ratio (bubbles more ellipsoidal) resulting in an increasing velocity. This supports the dependence recently reported in the literature.

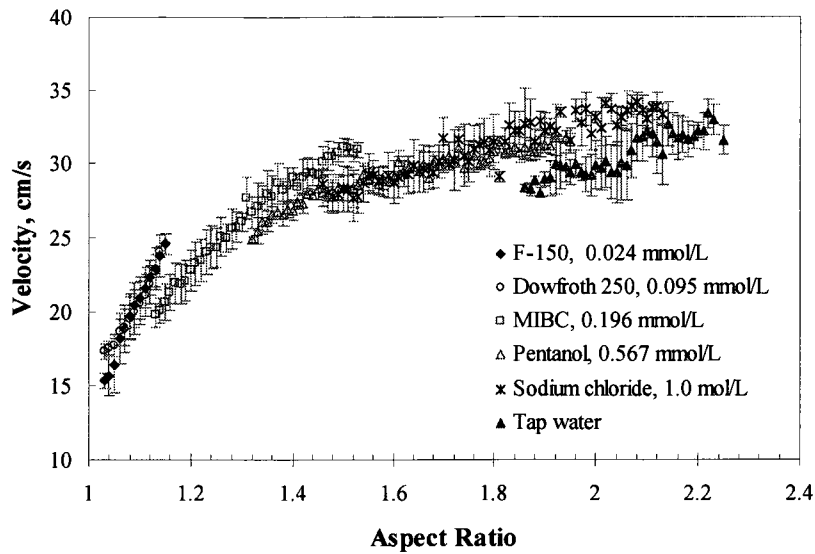


Figure 5.20. Velocity vs. aspect ratio. F-150, 0.024 mmol/L; Dowfroth 250, 0.095 mmol/L; MIBC, 0.196 mmol/L; Pentanol, 0.567 mmol/L; sodium chloride 1.0 mol/L; and tap water.

5.5 Discussion

The experiments have shown that the presence of surfactant (frother) stabilizes bubble shape, in particular eliminating the high frequency shape (aspect ratio) oscillation shown in water only. In the case of F-150 and Dowfroth 250 the shape was even maintained near spherical (aspect ratio 1.1). Bubble shape stabilization may be explained in terms of surface tension gradient driven phenomena (Gibbs elasticity and Marangoni effect). The bubble is not stabilized instantaneously but after ca. 15 ms. The bubbles show a maximum in velocity followed by a deceleration associated with frother adsorption on the rising bubble in accord with previous observations (Sam et al., 1996; Zhang et al., 2001; Krzan et al., 2004, 2007). The rise velocity in Pentanol, MIBC, and sodium chloride does not decrease as much as for the case of Dowfroth 250 or F-150. This may

be due to the time range tested (< 400 ms); for longer times the velocity in MIBC, for example, is expected to decrease further (Sam et al., 1996).

With increasing frother concentration the maximum velocity decreases as does the time at which it is reached. The deceleration after the maximum velocity is associated to bubble shape stabilization, which appears to be the factor affecting bubble velocity. De Vries et al. (2002) argued that bubble shape oscillations influenced bubble velocity as a consequence of variations in the added mass which changes with bubble shape. The results here show that for all conditions, there is a correlation between bubble shape (aspect ratio, A_R) and velocity: the more spherical the bubble the lower its velocity. This behavior is typical of bubbles in the surface tension force dominant regime (Tomiya et al., 2002). For the concentrations tested, Dowfroth 250 and F-150 are strong bubble shape stabilizers; indeed both make bubbles spherical according to the criterion used ($A_R < 1.15$) within 100 ms and produce the lowest rising velocities within the time frame measured. A lesser effect on bubble shape is observed for MIBC; even for the maximum concentration tested (0.196 mmol/L) bubbles do not become spherical and the rising velocities are higher than those observed for Dowfroth 250 and F-150. Finally, Pentanol, and sodium chloride are the weakest in terms of bubble shape stabilization and the aspect ratios for these reagents are comparable to those in tap water. Consequently, Pentanol and sodium chloride give the highest velocities. The order of effect on shape and velocity mirror those for coalescence prevention for these same reagents (Chapter 3).

The Eötvös number for bubbles in this study fall within the range corresponding to the surface tension dominant regime (Tomiya et al. 2002), hence, the current

findings apply to bubbles in this regime. According to Tomiyama et al., the effect that frothers have is to make bubbles more spherical which reduces their velocity. Figure 5.20 confirms this primary effect of shape on velocity; however, given there is some difference between frother types (and salt) it appears system chemistry plays at least a secondary role to shape. The findings support that an important role of surfactant (and salt) in bubble velocity is through control of bubble shape. In the case of smaller Eötvös number (i.e., in the viscous force dominant regime), bubbles present a more spherical shape regardless the presence of surfactant; hence the effect of system chemistry is expected to become more relevant.

5.6 Conclusions

New findings are presented on the effect of frother (and salt) on bubble shape and velocity immediately after creation at an orifice (time < 400 ms). The results show no effect for the first ca. 15 ms after bubble detachment for any reagent tested. Bubbles reach different maximum velocities at different times depending on frother type and concentration. The maximum velocity is followed by a deceleration period and then oscillation about a mean velocity.

The oscillation in velocity is matched by oscillation in shape (aspect ratio). A relationship between bubble shape and local velocity is observed: the more spherical the bubble, the slower it rises in agreement with Wu and Gharib (2002) who showed this in the absence of surfactants. Dowfroth 250 and F-150 have a strong effect on stabilizing a spherical shape, and consequently they produce the lowest velocities. The other reagents

tested, MIBC, Pentanol, and salt (NaCl), are less able to produce a spherical shape and consequently velocity is higher. Nevertheless the correlation between shape and velocity is maintained.

For the tested conditions (i.e., bubbles in the surface tension dominant regime) the findings support the recent argument that surfactants, to which can now be added salt, affect bubble rise velocity primarily through control of bubble shape, with a secondary effect of system chemistry.

References

- Acuna, C., 2007. Measurement techniques to characterize bubble motion in swarms. McGill University, Montréal, QC, Canada. PhD Thesis.
- Acuna, C., Finch, J.A., 2008. Motion of individual bubbles rising in a swarm. Submitted to IMPC 2008, Beijing, China.
- Azgoni, F., Gomez, C.O., Finch, J.A., 2007. Characterizing frothers using gas hold-up. Canadian Metallurgical Quarterly 46 (3). 237-242.
- Clift, R., Grace, J.R., Weber, M.E., 2005. Bubbles, Drops, and Particles. Academic Press, New York, 2nd edition.
- De Vries, J., Luther, S., Lohse, D., 2002. Induced bubble shape oscillations and their impact on the rise velocity. The European Physical Journal B 29. 503-509.
- Dijkhuizen, W., van den Hengel, E.I.V., Deen, N.G., van Sint Annaland, M., Kuipers, J.A.M., 2005. Numerical investigation of closures for interface forces acting on

- single air-bubbles in water using Volume of Fluid and Front Tracking models. *Chemical Engineering Science* 60. 6169-6175.
- Dukhin, S.S., Miller, R., Loglio, G., 1998. Physico-chemical hydrodynamics of rising bubble. *Studies in Interface Science Vol. 6: Drops and Bubbles in Interfacial Research*. D. Möbius and R. Miller Editors, Elsevier Science.
- Frumkin, A., Levich, V.G., 1947. On surfactants and interfacial motion. *Zh. Fizicheskoi Khimii* 21. 1183-1204.
- Kendoush, A.A., 2007. The virtual mass of an oblate-ellipsoidal bubble. *Physics Letters A* 366. 253-255.
- Krzan, M., Lunkenheimer, K., Malysa, K., 2004. On the influence of the surfactant's polar group on the local and terminal velocities of bubbles. *Colloids and Surfaces A: Physicochemical and Engineering Aspects* 250. 431-441.
- Krzan, M., Zawala, J., Malysa, K., 2007. Development of steady state adsorption distribution over interface of a bubble rising in solutions of *n*-alkanols (C₅, C₈) and *n*-alkyltrimethylammonium bromides (C₈, C₁₂, C₁₆). *Colloids and Surfaces A: Physicochemical and Engineering Aspects* 298. 42-51.
- Kulkarni, A.A., Joshi, J.B., 2005. Bubble formation and bubble rise velocity in gas-liquid systems: a review. *Industrial & Chemical Engineering Research* 44. 5873-5931.
- Linton, M., Sutherland, K.L. 1957. Dynamic surface forces, drop circulation and liquid-liquid mass transfer. *Second International Congress on Surface Activity*, 1. Butterworth, London. 494-501.
- Moyo, P., Gomez, C.O., Finch, J.A., 2007. Characterizing frothers using water carrying rate. *Canadian Metallurgical Quarterly* 46. 215-220.

- Nesset, J.E., Finch, J.A., Gomez, C.O., 2007. Operating variables affecting the bubble size in forced-air mechanical flotation machines. In proceedings of Ninth Mill Operators' Conference, Freemantle, WA, Australia. 55-65.
- Peebles, F.N., Garber, H.J., 1953. Studies on the motion of gas bubbles in liquids. *Chemical Engineering Progress* 49 (2). 88-97.
- Quinn, J.J., Kracht, W., Gomez, C.O., Gagnon, C., Finch, J.A., 2007. Comparing the effect of salts and frother (MIBC) on gas dispersion and froth properties. *Minerals Engineering* 20. 1296-1302.
- Rao, S.R., 2004. *Surface Chemistry of Froth Flotation, Second Edition, Vol 2. Reagents and Mechanisms. Revised Edition. First Edition by Jan Leja. Kluwer Academic/Plenum Publishers.*
- Sam, A., Gomez, C.O., Finch, J.A., 1996. Axial velocity profiles of single bubbles in water/frother solutions. *International Journal of Mineral Processing* 47. 177-196.
- Tomiyama, A. Celata G.P., Hosokawa, S., Yoshida, S., 2002. Terminal velocity of single bubbles in surface tension force dominant regime. *International Journal of Multiphase Flow* 28. 1497-1519.
- Wu, M., Gharib, M, 2002. Experimental studies on the shape and path of small air bubbles rising in clean water. *Physics of Fluids* 14 (7). L49-L52.
- Zhang, Y., Gomez, C.O., Finch, J.A., 1996. Terminal velocity of bubbles: approach and preliminary investigations. In *Proceedings of the International Symposium of Column Flotation, COLUMN'96, Aug. 26-28, Montréal, Québec, Canada.* Eds. C.O. Gomez, J.A. Finch. 63-69.

- Zhang, Y., McLaughlin, J.B., Finch, J.A., 2001. Bubble velocity profile and model of surfactant mass transfer to bubble surface. *Chemical Engineering Science* 56. 6605-6616.
- Zhang, Y., Sam, A., Finch, J.A., 2003. Temperature effect on single bubble velocity profile in water and surfactant solution. *Colloids and Surfaces A: Physicochemical and Engineering Aspects* 223. 45-54.
- Zhou, Z.A., Egiebor, N.O., Plitt, L.R., 1992. Frother effect on single bubble motion in a water column. *Canadian Metallurgical Quarterly* 31 (1). 11-16.
- Zhou, Z.A., Egiebor, N.O., Plitt, L.R., 1993. Frother effects on bubble motion in a swarm. *Canadian Metallurgical Quarterly* 32 (2). 89-96.

Chapter 6 – Unifying discussion

6.1 Introduction

The previous Chapters showed diverse aspects of frothers in bubble coalescence, break-up, bubble shape and local rise velocity. The discussion and conclusions in each Chapter apply for the specific conditions studied with little cross-reference between Chapters. This chapter provides some unification.

6.2 Summary of frother effects

Chapter 3 presents results of coalescence prevention for different frothers at the generation stage. Increasing frother concentration proved to protect bubbles against coalescence. The concentrations tested cover a range much wider than the range of concentrations usually found in flotation systems. In Chapter 4, coalescence is almost completely suppressed in presence of frothers at concentrations typical of flotation systems; frothers were also observed to promote strongly asymmetrical break-up (90:10 in volume) attributed to the uneven frother distribution over the bubble surface immediately prior to break-up. Chapter 5 shows no effect of frother over the first ca. 15 ms after bubble detachment from a capillary tube, effects due to system chemistry appearing after this initial time. The concentrations tested in Chapter 5 also cover the typical flotation range.

6.3 Commentary

Results from Chapter 5 indicate reaching steady state in the presence of frother is not instantaneous. The adsorption rate is increased with increasing frother concentration because it promotes frother diffusion (mass transfer) to the bubble surface, and thus dynamic equilibrium reached earlier.

Newly formed bubbles, however, are not free of frother. At the moment an air surface is introduced into a frother solution it will have a surface concentration reflective of the bulk concentration (consider frother molecules as points in a 3D array (bulk concentration), on introducing a plane (air surface) some frother molecules will be on that plane). As a first-order approximation, the bubble may be considered to ‘sweep’ the frother molecules that are in the liquid region displaced by the bubble during the growing process (Figure 6.1).

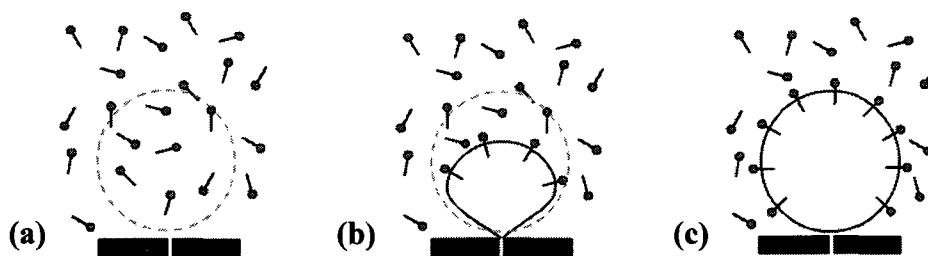


Figure 6.1. Schematic of initial frother surface concentration at bubble surface. (a) before bubble starts growing (dashed circle shows region that will be occupied by bubble), (b) during bubble growth, (c) bubble immediately after detachment.

If all the frother molecules ‘swept’ by the bubble while growing are considered captured and neglecting diffusion from the bulk solution, the initial frother load (surface concentration or adsorption density) may be estimated from the bubble volume and the bulk frother concentration. For instance, bubbles of 2.5 mm diameter in an MIBC solution of 0.098 mmol/L would have an initial frother load of $4.08\text{e-}15 \text{ mol/cm}^2$, which is four orders of magnitude lower than the Gibbs equilibrium loading ($1.10\text{e-}11 \text{ mol/cm}^2$) (Wang, 2006). (The Gibbs equilibrium loading (Γ_m) is calculated from the Langmuir isotherm:

$$\Gamma_m = \Gamma_s \frac{bc}{1+bc} \quad (\text{Eq. 6.1})$$

where the Γ_s is saturation loading ($5.00\text{e-}10 \text{ mol/cm}^2$) (Comley et al., 2002), c is the bulk frother concentration, and b is the Langmuir equilibrium constant (0.230 L/mmol) (Wang, 2006.) Hence, regardless of the fact that no difference in properties is observed during the first ca. 15 ms after bubble release from the capillary, it is evident that the surface frother concentration at bubble detachment is different from zero. With a non-zero surface concentration, phenomena associated with the presence of frother are initiated. This conclusion is supported by the results in Chapter 3, where this initial surface frother concentration is sufficient to prevent coalescence at the generation point. These results may be presented as evidence that coalescence prevention is a more sensitive way of detecting presence of contaminants compared to bubble velocity as proposed by Zawala et al. (2007).

Increasing the frother concentration (in the bulk solution) increases the bubble surface load at detachment. This is why in Chapter 3 increasing bulk concentration was

able to counter the increasingly intense coalescence conditions as flow rate was increased. When the bubble surface is stretched as bubbles are forced together, the higher frother load helps create sufficient surface concentration gradients and visco-elastic effects to oppose coalescence. The concentrations are taken well above those encountered in flotation practice suggesting the coalescence conditions are more intense in the current experiments. Note that in Chapter 3 the new bubble is pushed against the prior one before the latter starts accelerating to leave the region close to the capillary. Estimating the energy involved in the coalescence event may permit an estimate of the apparent energies involved in bubble production in flotation systems.

Chapter 4 emphasizes that even low frother concentrations can prevent coalescence. This may be due to the time that elapses between bubble generation and interaction with the impeller, which allows additional frother to adsorb. Alternatively, the energy involved in the impeller-induced coalescence events is more reflective of the energy in actual practice (which in mechanical flotation machines is likewise impeller driven); bubbles move and interact because of the turbulence generated by the action of the impeller and from observation, these interactions are weak compared to those in Chapter 3. Again, this simplified experiment may allow the energy involved to be estimated.

In Chapter 3 sodium chloride (NaCl) does not present the same behavior as frother (MIBC) as reported in the literature (Quinn et al., 2007), yet in Chapter 4 it does. The difference may be due to the already mentioned different intensity of the bubble-bubble interactions in each set-up.

In Chapter 3, further frother adsorption is said to take place during film stretching; however, in Chapter 4 adsorption of new frother molecules onto the surface of the stretching bubble is neglected in the analysis. Since in Chapter 3 the frother surface concentration is far from equilibrium, frother molecules in the liquid film trapped between touching bubbles will have the possibility to adsorb onto the bubble surfaces, affecting the region of 'organized' water and the viscous component in the total stress theory. The adsorption of new frother molecules is expected to have only a marginal effect on surface tension, otherwise the elastic component would be compromised. In Chapter 4 the frother surface concentration on the stretching bubble (dumbbell) is closer to equilibrium than in Chapter 3, hence the driving force for further frother adsorption is lessened. Even though some new frother molecules may adsorb onto the dumbbell, they again can be considered to have a minimal effect, so both ends of the dumbbell will have different surface tension when break-up is asymmetrical.

References

- Comley, B.A., Harris, P.J., Bradshaw, D.J., Harris, M.C., 2002. Frother characterisation using dynamic surface tension measurements. *International Journal of Mineral Processing* 64. 81-100.
- Quinn, J.J., Kracht, W., Gomez, C.O., Gagnon, C., Finch, J.A., 2007. Comparing the effect of salts and frother (MIBC) on gas dispersion and froth properties. *Minerals Engineering* 20. 1296-1302.
- Wang, L., 2006. Surface forces in foam films. Virginia Polytechnic Institute and State University. Ph.D. Thesis.
- Zawala, J., Swiech, K., Malysa, K., 2007. A simple physicochemical method for detection of organic contaminations in water. *Colloids and Surfaces A: Physicochemical and Engineering Aspects* 302. 293-300.

Chapter 7 – Conclusions, contributions, and future work

7.1 Conclusions

This thesis addressed the effect of frothers and salt on bubble coalescence, break-up and initial rise velocity. The following conclusions can be drawn from the study:

1. The characteristic sound trace found when bubbles coalesce at a capillary tip allowed development of a novel technique to study bubble coalescence without incurring the high costs and disk space requirements of high-speed imaging. The technique uses a hydrophone to record sounds, which are shown to be related to coalescence events. Signal recognition is straightforward and the technique has a resolution high enough to discriminate events that occur within 1 to 2 milliseconds.
2. The gas flow rate marking the boundary between coalescence and non-coalescence was determined as a function of reagent concentration. The results show that common flotation frothers and *n*-alcohols (C₄-C₈) prevent coalescence and that the effectiveness increases with increasing concentration and chain length.
3. The total stress model, which considers elastic and viscous components and represents the internal forces that appear as a reaction to film stretching, is used to

describe the process. The elastic component of the total stress increases in magnitude with increasing surfactant surface activity, which generally correlates with increasing chain length. On the other hand, the viscous component becomes less important for increasing chain length because of the lower diffusion-adsorption rates. The relative importance of both effects appears evident in the similar results of coalescence prevention for Heptanol and Octanol, where it can be argued the increase in elasticity due to the higher surface activity of Octanol is counterbalanced by the reduction in its diffusion-adsorption rate (viscous component) due to the larger size of the Octanol molecule.

4. Results for sodium chloride do not show such a well-defined boundary between coalescence and non-coalescence as the surfactants. The total stress generated in presence of sodium chloride is expected to be lower than with surfactants; the elastic component is insignificant because of the small surface gradients generated, and the viscous component is not as effective because of the different nature of the electrolyte molecules compared to frothers.
5. An experimental set-up delivering a single size bubble (2.5 mm diameter) into an impeller is used for a basic study of the coalescence/break-up events in the mechanical production of small bubbles. It is the first such study aimed at a basic understanding of fine bubble production in mechanical flotation machines. The approach permits coalescence and break-up events to be distinguished.

6. The observations confirm the common explanation that frothers and salt (NaCl) prevent coalescence. In the current set-up they are also shown to influence break-up. The evidence points to a predominance of break-up events favoring a 90:10 volume division (or higher) in the presence of frothers and salt (NaCl); i.e., for the starting bubble size of 2.5 mm diameter, the output size is dominated by 2.4 mm diameter bubbles.

7. An analysis of the break-up event is presented based on the dumbbell model. It is determined that less energy is needed in the presence of frother to generate strongly asymmetric break-up which corresponds to the 90:10 division observed.

8. New findings are presented on the effect of frother (and salt) on bubble shape and velocity immediately after creation at an orifice (time < 400 ms). The results show no effect for the first ca. 15 ms after bubble detachment for any reagent tested. Bubbles reach different maximum velocities at different times depending on frother type and concentration. The maximum velocity is followed by a deceleration period and then oscillation about a mean velocity.

9. The oscillation in velocity is matched by oscillation in shape (aspect ratio). A relationship between bubble shape and local velocity is observed: the more spherical the bubble, the slower it rises in agreement with Wu and Gharib (2002) who showed this in the absence of surfactants. Dowfroth 250 and F-150 have a strong effect on stabilizing a spherical shape, and consequently they produce the lowest velocities. The other reagents tested, MIBC, Pentanol, and salt (NaCl), are

less able to produce a spherical shape and consequently velocity is higher. Nevertheless the correlation between shape and velocity is maintained.

10. For the tested conditions (i.e., bubbles in the surface tension dominant regime) the findings support the recent argument that surfactants, to which can now be added salt, affect bubble rise velocity primarily through control of bubble shape, with a secondary effect of system chemistry.

7.2 Contributions to original knowledge

- Development of a technique based on sound bubbles emit to study bubble coalescence at the generation point (capillary tube).
- Provided experimental evidence to support that frothers prevent bubble coalescence over time intervals so short (ca. 1-2 ms) that other surfactant-related properties are not detectable
- Development of a technique, based on image analysis, able to discriminate between bubble coalescence and break-up in a turbulent field.
- Demonstrated experimentally that frothers (and salt) affect the output distribution of bubbles after break-up, favoring the generation of strongly asymmetrical daughter bubbles.
- Provided a theoretical framework to explain the effect of frothers (and salt) on bubble break-up.
- Provided experimental evidence of the relationship between bubble shape and rise velocity in the presence of frothers (and salt).

7.3 Suggestions for future work

The sound technique to study bubble coalescence opens an entirely new way to approach the problem. A role of solid particles in bubble formation is often speculated. The presence of solids makes it difficult, if not impossible, to use image analysis but sound could provide a method of attack.

Another possibility is to use the sound technique as an indirect method to measure frother concentration. Frother concentration may be inferred from the maximum gas flow rate prior to coalescence.

There is no model to predict bubble size generated in flotation machines. This is necessary to complete CFD simulations that currently input a bubble size. Chapter 4 speculated that measuring the daughter bubble size as a function of mother bubble size may open an opportunity. To avoid frother adsorption due to bubble rise (in the current experiment) the distance between bubble input and impeller should be shortened. To approach the industrial situation an impeller-stator assembly should be substituted for the unconstrained impeller used here.

The bubble shape-velocity relationship should be re-visited for the data far from the generation point (capillary) where the possibility of frothers affecting bubble shape and bubble shape affecting velocity is generally disregarded. Conversely, experiments should be performed on bubbles of identical shape (spherical is the obvious one) in the presence of surfactants (frothers) to determine if the secondary role of system chemistry

ascribed here becomes apparent under these conditions. The large difference in gas holdup observed by Azgomi et al. (2007) between F-150 and Pentanol at concentration where both reagents likely give equal sized (ca. 1 mm diameter) spherical bubbles suggests a chemistry effect persists.

References

- Acuna, C. Nasset, J. E., Finch J.A. 2007. Impact of Frother on Bubble Production and Behaviour in the Pulp Zone. In Proceedings of the Sixth International Copper-Cobre Conference, Aug. 25-30, Toronto, Ont. Canada, Volume II Mineral Processing (Eds. R del Villar, J. E. Nasset, C. O. Gomez and A. W. Stradling) MetSoc CIM. 197-210.
- Acuna, C., 2007. Measurement techniques to characterize bubble motion in swarms. McGill University, Montréal, QC, Canada. PhD Thesis.
- Acuna, C., Finch, J.A., 2008. Motion of individual bubbles rising in a swarm. Submitted to IMPC 2008, Beijing, China.
- Adamson, A.W., 1990. Physical chemistry of surfaces, 5th Edition. John Wiley & Sons, Inc. New York.
- Ata, S., Jameson, G.J., 2007. Behaviour of particles during coalescence of bubbles. In proceedings of Flotation 07. Cape Town, South Africa, November 6-9. MEI Conferences. CD ROM.
- Azgomi, F., Gomez, C.O., Finch, J.A., 2007. Characterizing frothers using gas hold-up. Canadian Metallurgical Quarterly 46 (3). 237-242.
- Boyd, J.W.R., Varley, J., 2001. The uses of passive measurement of acoustic emissions from chemical engineering processes. Chemical Engineering Science 56. 1749-1767.
- Cho, Y.S., Laskowski, J.S., 2002. Effect of flotation frothers on bubble size and foam stability. International Journal of Mineral Processing 64. 69-80.
- Clift, R., Grace, J.R., Weber, M.E., 2005. Bubbles, Drops, and Particles. Academic Press, New York, 2nd edition.

- Comley, B.A., Harris, P.J., Bradshaw, D.J., Harris, M.C., 2002. Frother characterisation using dynamic surface tension measurements. *International Journal of Mineral Processing* 64. 81-100.
- Dai, Z., Fornasiero, D, Ralston, J., 2000. Particle-bubble collision models – a review. *Advances in Colloid and Interface Science* 85. 231-256.
- Dawson, P., 2002. The physics of the oscillating bubble made simple. *European Journal of Radiology* 41. 176-178.
- De Vries, J., Luther, S., Lohse, D., 2002. Induced bubble shape oscillations and their impact on the rise velocity. *The European Physical Journal B* 29. 503-509.
- Dickinson, E., 1999. Adsorbed protein layers at fluid interfaces: interactions, structure and surface rheology. *Colloids and Surfaces B: Biointerfaces* 15. 161-176.
- Dijkhuizen, W., van den Hengel, E.I.V., Deen, N.G., van Sint Annaland, M., Kuipers, J.A.M., 2005. Numerical investigation of closures for interface forces acting on single air-bubbles in water using Volume of Fluid and Front Tracking models. *Chemical Engineering Science* 60. 6169-6175.
- Drogaris, G., Weiland, P., 1983. Coalescence behaviour of gas bubbles in aqueous solutions of *n*-alcohols and fatty acids. *Chemical Engineering Science* 38 (9). 1501-1506.
- Dukhin, S.S., Miller, R., Loglio, G., 1998. Physico-chemical hydrodynamics of rising bubble. *Studies in Interface Science Vol. 6: Drops and Bubbles in Interfacial Research*. D. Möbius and R. Miller Editors, Elsevier Science.
- Finch, J.A., Doby, G.S., 1990. *Column flotation*. Pergamon Press: Elmsford, New York.
- Finch, J.A., Gélinas, S., Moyo, P., 2006. Frother-related research at McGill University. *Minerals Engineering* 19. 726-733.

- Finch, J.A., Nasset, J.E., Acuña, C., 2008. Role of frother on bubble production and behaviour in flotation. *Minerals Engineering*. Article in Press.
- Fruhner, H., Wantke, K.-D., 1996. A new oscillating bubble technique for measuring surface dilational properties. *Colloids and Surfaces A: Physicochemical and Engineering Aspects* 114. 53-59.
- Fruhner, H., Wantke, K.-D., Lunkenheimer, K., 1999. Relationship between surface dilational properties and foam stability. *Colloids and Surfaces A: Physicochemical and Engineering Aspects* 162. 193-202.
- Frumkin, A., Levich, V.G., 1947. On surfactants and interfacial motion. *Zh. Fizicheskoi Khimii* 21. 1183-1204.
- Gomez, C.O., Escudero, R., Finch, J.A., 2000. Determining equivalent pore diameter for rigid porous spargers. *Canadian Journal of Chemical Engineering* 78. 785-792.
- Gomez, C.O., Finch, J.A., 2002. Gas dispersion measurements in flotation machines. *CIM Bulletin* 95 (1066). 73-78.
- Gomez, C.O., Finch, J.A., 2007. Gas dispersion measurements in flotation cells. *International Journal of Mineral Processing* 84 (1-4). 51-58.
- Gorain, B.K., Franzidis, J.P., Manlapig, E.V., 1997. Studies on impeller type, impeller speed and air flow rate in an industrial scale flotation cell, Part 4: Effect of bubble surface area flux on flotation performance. *Minerals Engineering* 10 (4). 367-379.
- Gorain, B.K., Franzidis, J.-P., Manlapig, E.V., 1995. Studies on impeller type, impeller speed and air flow rate in an industrial scale flotation cell – Part 1: Effect on bubble size distribution. *Minerals Engineering* 8 (6). 615-635.
- Gorain, B.K., Napier-Munn, T.J., Franzidis, J.P., Manlapig, E.V., 1998. Studies on impeller type, impeller speed and air flow rate in an industrial scale flotation cell,

- Part 5: Validation of k-Sb relationship and effect of froth depth. *Minerals Engineering* 11 (7). 615-626.
- Grau, R.A., Laskowski, J.S., 2006. Role of frothers in bubble generation and coalescence in a mechanical flotation cell. *The Canadian Journal of Chemical Engineering* 84. 170-182.
- Grau, R.A., Laskowski, J.S., Heiskanen, K., 2005. Effect of frothers on bubble size. *International Journal of Mineral Processing* 76. 225-233.
- Harris, P.J., 1982. Principles of flotation. Chapter 13: Frothing phenomena and frothers. King, R.P., ed. *South African Institute of Mining and Metallurgy Monograph Series No. 3*.
- Hernandez, H., Gomez, C.O., Finch, J.A., 2003. Gas dispersion and de-inking in a flotation column. *Mineral Engineering* 16 (6). 739-744.
- Hernandez-Aguilar J.R., Finch J. A., 2005. An experiment to validate bubble sizing techniques using bi-modal populations of known proportions. In: Graeme J. Jameson (Ed.), *Centenary of Flotation Symposium, 6-9 June 2005, Brisbane, Queensland, Australia*, pp. 465-472.
- Hernandez-Aguilar, J.R., Coleman, R.G., Gomez, C.O., Finch, J.A., 2004. A comparison between capillary and imaging techniques for sizing bubbles in flotation systems. *Minerals Engineering* 17 (1), 53-61.
- Hinze, J.O., 1955. Fundamentals of the hydrodynamic mechanism of splitting in dispersion processes. *AIChE Journal*. 1 (3). 289-295.
- Hofmeier, U., Yaminsky, V.V., Christenson, H.K., 1995. Observations of solute effects on bubble formation. *Journal of Colloid and Interface Science* 174. 199-210.

- Horozov, T.S., Kralchevsky, P.A., Danov, K.D., Ivanov, I.B., 1997. Interfacial rheology and kinetics of adsorption from surfactant solution. *Journal of Dispersion Science and Technology* 18 (6-7), 593-607.
- Keitel, G., Onken, U., 1982. Inhibition of bubble coalescence by solutes in air/water dispersions. *Chemical Engineering Science* 37 (11). 1635-1638.
- Kendoush, A.A., 2007. The virtual mass of an oblate-ellipsoidal bubble. *Physics Letters A* 366. 253-255.
- Kim, J.W., Lee, W.K., 1988. Coalescence behavior of two bubbles growing side-by-side. *Journal of Colloid and Interface Science* 123 (1), 303-305.
- Krzan, M., Lunkenheimer, K., Malysa, K., 2004. On the influence of the surfactant's polar group on the local and terminal velocities of bubbles. *Colloids and Surfaces A: Physicochemical and Engineering Aspects* 250. 431-441.
- Krzan, M., Zawala, J., Malysa, K., 2007. Development of steady state adsorption distribution over interface of a bubble risitn in solutions of *n*-alkanols (C₅, C₈) and *n*-alkyltrimethylammonium bromides (C₈, C₁₂, C₁₆). *Colloids and Surfaces A: Physicochemical and Engineering Aspects* 298. 42-51.
- Kulkarni, A.A., Joshi, J.B., 2005. Bubble formation and bubble rise velocity in gas-liquid systems: a review. *Industrial & Chemical Engineering Research* 44. 5873-5931.
- Laskowski, J.S., 2003. Fundamental properties of flotation frothers. *Proceedings of the 22nd International Mineral Processing Congress*. Cape Town, South Africa. 788-797.
- Leighton, T.G., Walton, A., 1987. An experimental study of the sound emitted from gas bubbles in a liquid. *Eur. J. Phys.* 8. 98-104.
- Leighton, T.G., 1994. *The acoustic bubble*. New York: Academic Press.

- Leighton, T.G., 2004. From seas to surgeries, from babbling brooks to baby scans: the acoustics of gas bubbles in liquids. *International Journal of Modern Physics B* 18 (25). 3267-3314.
- Linton, M., Sutherland, K.L. 1957. Dynamic surface forces, drop circulation and liquid-liquid mass transfer. *Second International Congress on Surface Activity*, 1. Butterworth, London. 494-501.
- Lucassen, J., Van Den Tempel, M. 1972. Dynamic measurements of dilational properties of a liquid interface. *Chemical Engineering Science* 27. 1283-1291.
- Luo, H., Svendsen H.F., 1996. Theoretical model for drop and bubble breakup in turbulent dispersions. *AIChE Journal* 42 (5). 1225-1233.
- Machon, V., Pacek, A.W., Nienow A.W., 1997. Bubble sizes in electrolyte and alcohol solutions in a turbulent stirred vessel. *Trans IChemE* 75 (A). 339-348.
- Marrucci, G., 1969. A theory of coalescence. *Chemical Engineering Science* 24, 975-985.
- Metso Minerals CBT (Computer Based Training), 2002. Mill Operator Training Package. Flotaion Module. Formerly Brenda Process Technology CBT (Computer Based Training) (1996). Mill Operator Training Package. Flotation Module.
- Miller, C.A., Neogi, P., 1985. Interfacial phenomena: equilibrium and dynamic effects. In: *Surfactant Science Series*, vol. 17, Chapter VI: Transport Effects on Interfacial Phenomena. 240-298.
- Minnaert, M., 1933. On musical air-bubbles and the sounds of running water. *Philosophical Magazine* 16, 235-248.
- Monroy, F., Giermanska Kahn, J., Langevin, D., 1998. Dilational viscoelasticity of surfactant monolayers. *Colloids and Surfaces A: Physicochemical and Engineering Aspects* 143, 251-260.

- Moyo, P., Gomez, C.O., Finch, J.A., 2007. Characterizing frothers using water carrying rate. *Canadian Metallurgical Quarterly* 46. 215-220.
- Nesset, J.E., Finch, J.A., Gomez, C.O., 2007. Operating variables affecting the bubble size in forced-air mechanical flotation machines. In proceedings of Ninth Mill Operators' Conference, Freemantle, WA, Australia. 55-65.
- Oolman, T.O., Blanch, H.W., 1986. Bubble coalescence in stagnant liquids. *Chemical Engineering Communications* 43. 237-261.
- Parthasarathy, R., Jameson, G.J., Ahmed, N., 1991. Bubble breakup in stirred vessels. Predicting the Sauter mean diameter. *Chemical Engineering Research and Design* 69. 295-301.
- Peebles, F.N., Garber, H.J., 1953. Studies on the motion of gas bubbles in liquids. *Chemical Engineering Progress* 49 (2). 88-97.
- Prince, M.J., Blanch, H.W., 1990. Bubble coalescence and break-up in air-sparged bubble columns. *AIChE Journal* 36 (10). 1485-1499.
- Pugh, R.J., 1996. Foaming, foam films, antifoaming and defoaming. *Advances in Colloid and Interface Science* 64. 67-102.
- Quinn, J.J., Kracht, W., Gomez, C.O., Gagnon, C., Finch, J.A., 2007. Comparing the effect of salts and frother (MIBC) on gas dispersion and froth properties. *Minerals Engineering* 20. 1296-1302.
- Rao, S.R., 2004. *Surface Chemistry of Froth Flotation, Second Edition, Vol 2. Reagents and Mechanisms. Revised Edition. First Edition by Jan Leja. Kluwer Academic/Plenum Publishers.*
- Rusanov, A.I., Krotov, V.V., 2003. Gibbs elasticity of free thin liquid films. *Doklady Physical Chemistry* 393 (4-6). 350-352.

- Sam, A., Gomez, C.O., Finch, J.A., 1996. Axial velocity profiles of single bubbles in water/frother solutions. *International Journal of Mineral Processing* 47. 177-196.
- Schott, H. 1995. Hydrophilic-lipophilic balance, solubility parameter, and oil-water partition coefficient as universal parameters of nonionic surfactants. *Journal of Pharmaceutical Sciences* 84 (10). 1215-1222.
- Schwarz, S., Alexander, D., 2006. Gas dispersion measurements in industrial flotation cells. *Minerals Engineering* 19 (6-8). 554-560.
- Stewart C.W., 1995. Bubble interaction in low-viscosity liquids. *Int. J. Multiphase Flow* 21, No. 6, 1037-1046.
- Strasberg, 1956. Gas bubbles as sources of sound in liquids. *The Journal of the Acoustical Society of America* 28 (1). 20-26.
- Sweet, C., Van Hoogstraten, J., Harris, M., Laskowski, J.S., 1997. The effect of frothers on bubble size and frothability of aqueous solutions. In proceedings of Second UBC-McGill Bi-annual International Symposium of Fundamentals of Mineral Processing. Finch, J.A., Rao, S.R., Holubec, I., eds. Sudbury, Ontario. 235-245.
- Tao, D., 2004. Role of bubble size in flotation of coarse and fine particles – A review. *Separation Science and Technology* 39 (4). 741-760.
- Tomiyama, A. Celata G.P., Hosokawa, S., Yoshida, S., 2002. Terminal velocity of single bubbles in surface tension force dominant regime. *International Journal of Multiphase Flow* 28. 1497-1519.
- Tse, K.L., Martin, T., McFarlane, C.M., Nienow, A.W., 1998. Visualisation of bubble coalescence in a coalescence cell, a stirred tank and a bubble column. *Chemical Engineering Science* 53 (23). 4031-4036.

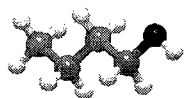
- Tuckermann, R., 2007. Surface tension of aqueous solutions of water-soluble organic and inorganic compounds. *Atmospheric Environment* 41. 6265-6275.
- Vandevaille, N., Lentz, J.F., Dorbolo, S., Brisbois, F., 2001. Avalanches of popping bubbles in collapsing foams. *Physical Review Letters* 86 (1). 179-182.
- Walter J.F., Blanch H.W., 1986. Bubble break-up in gas-liquid bioreactors: break-up in turbulent flows. *The Chemical Engineering Journal* 32. B7-B17.
- Wang, L., 2006. Surface forces in foam films. Virginia Polytechnic Institute and State University. Ph.D. Thesis.
- Wang, L., Yoon, R-H., 2006. Role of hydrophobic force in the thinning of foam films containing a nonionic surfactant. *Colloids and Surfaces A: Physicochemical and Engineering Aspects* 282-283. 84-91.
- Wang, T., Wang, J., Jin, J., 2003. A novel theoretical breakup kernel function of bubble/droplet in a turbulent flow. *Chemical Engineering Science* 58. 4629-4637.
- Weissenborn, P.K., Pugh, R.J., 1996. Surface tension of aqueous solutions of electrolytes: relationship with ion hydration, oxygen solubility, and bubble coalescence. *Journal of colloid and interface science* 184. 550-563.
- Wu, M., Gharib, M, 2002. Experimental studies on the shape and path of small air bubbles rising in clean water. *Physics of Fluids* 14 (7). L49-L52.
- Ye, Z., Feuillade, C., 1997. Sound scattering by an air bubble near a plane sea surface. *The Journal of the Acoustical Society of America* 102 (2). 798-805.
- Zawala, J., Swiech, K., Malysa, K., 2007. A simple physicochemical method for detection of organic contaminations in water. *Colloids and Surfaces A: Physicochemical and Engineering Aspects* 302. 293-300.

- Zhang, Y., Gomez, C.O., Finch, J.A., 1996. Terminal velocity of bubbles: approach and preliminary investigations. In Proceedings of the International Symposium of Column Flotation, COLUMN'96, Aug. 26-28, Montréal, Québec, Canada. Eds. C.O. Gomez, J.A. Finch. 63-69.
- Zhang, Y., McLaughlin, J.B., Finch, J.A., 2001. Bubble velocity profile and model of surfactant mass transfer to bubble surface. Chemical Engineering Science 56. 6605-6616.
- Zhang, Y., Sam, A., Finch, J.A., 2003. Temperature effect on single bubble velocity profile in water and surfactant solution. Colloids and Surfaces A: Physicochemical and Engineering Aspects 223. 45-54.
- Zhang, W., 2008. Unpublished data.
- Zhou, Z.A., Egiebor, N.O., Plitt, L.R., 1992. Frother effect on single bubble motion in a water column. Canadian Metallurgical Quarterly 31 (1). 11-16.
- Zhou, Z.A., Egiebor, N.O., Plitt, L.R., 1993. Frother effects on bubble motion in a swarm. Canadian Metallurgical Quarterly 32 (2). 89-96.

Appendixes

Appendix 1 – Reagent structure*

Butanol ($\text{CH}_3(\text{CH}_2)_3\text{OH}$)



Pentanol ($\text{CH}_3(\text{CH}_2)_4\text{OH}$)



Hexanol ($\text{CH}_3(\text{CH}_2)_5\text{OH}$)



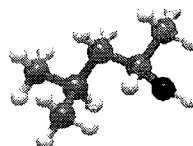
Heptanol ($\text{CH}_3(\text{CH}_2)_6\text{OH}$)



Octanol ($\text{CH}_3(\text{CH}_2)_7\text{OH}$)



MIBC ($((\text{CH}_3)_2\text{CHCH}_2\text{CH}(\text{OH})\text{CH}_3)$)



Dowfroth 250 ($\text{CH}_3(\text{PO})_4\text{OH}$)**:



F-150 ($\text{H}(\text{PO})_7\text{OH}$)**:



* Carbon atoms are represented in grey, oxygen atoms in black, and hydrogen atoms in white.

** PO is propylene oxide (propoxy) [$-\text{O}-\text{CH}_2-\text{CH}_2-\text{CH}_2-$]

Appendix 2 – High speed camera specifications

Model:	TroubleShooter HR.
Sensor:	CMOS array up to 1280 x 1024 pixels, 8 bit resolution (monochrome).
Shutter speed:	1x, 2x, 3x, 4x, 5x, 10x and 20x the recording rate.
Recording rate (fps):	16,000; 8,000; 4,000; 2,000; 1,000; 500; 250; 125.
Playback rates:	1 to 1,000 frames per second forward and reverse.
Display:	Built-in 5" LCD color digital display.
I/O Connectors:	USB 2.0 port, compact flash memory.
Mounts:	Standard C-mount lens mount, 1/4-20 tripod mount.
Power supply:	Four (4) D-cell batteries or 110/220 VAC adapter.
Size & weight:	6" W x 5" H x 4" D, 2.2 lbs. without batteries.

Table A2.1. Recording rate (fps) and image size configurations.

Frames per second	Sensor	Standard Memory- 1gb	
		Total frames	Record time (sec)
125	1280 x 1024	1,022	8.2
250	1280 x 1024	1,022	4.1
500	1280 x 1024	1,022	2.0
1000	1280 x 512	2,044	2.0
2000	1280 x 256	4,088	2.0
4000	1280 x 128	8,176	2.0
8000	1280 x 64	16,352	2.0
16000	1280 x 32	32,704	2.0
125	640 x 480	4,368	34.9
250	640 x 480	4,368	17.5
500	640 x 480	4,368	8.7
1000	640 x 480	4,368	4.4
125	320 x 240	17,472	139.8
250	320 x 240	17,472	69.9
500	320 x 240	17,472	34.9
1000	320 x 240	17,472	17.5
2000	320 x 240	17,472	8.7

Appendix 3 – Experimental results of coalescence inhibition

Table A3.1. Gas flow meter calibration.

Set point	Reading, %	Vol, cm3	Time, min	Q, sccm
5.1	4.71	63	9.5	6.2
5.5	5.05	53	6.0	8.2
5.8	5.37	64	6.0	9.9
6.1	5.67	62	5.0	11.6
6.4	5.98	56	4.0	13.0
6.7	6.28	63	4.0	14.7
7.0	6.59	69	4.0	16.1

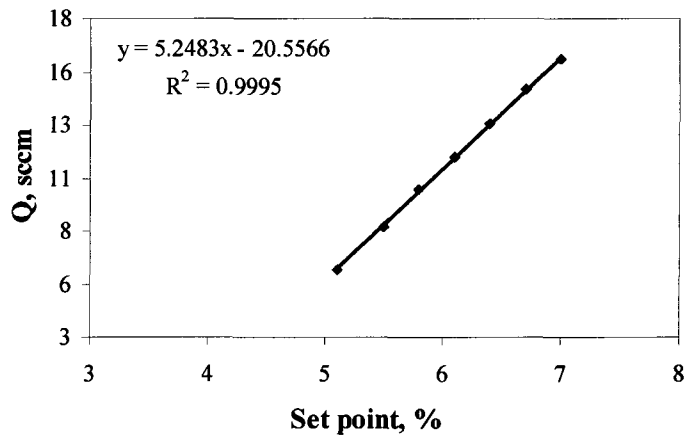


Figure A3.1. Gas flow meter calibration curve.

Table A3.2. Boundary between coalescence and no-coalescence region for 1-butanol.

Concentration, ppm	Concentration, mmol/L	Gas flow rate set point	Gas flow rate, sccm
0	0	5.1	6.2
2.5	0.034	5.1	6.2
5	0.068	5.1	6.2
7.5	0.101	5.1	6.2
10	0.135	5.1	6.2
15	0.202	5.1	6.2
20	0.270	5.6	8.8
25	0.337	5.8	9.9
30	0.405	5.8	9.9
35	0.472	5.8	9.9
40	0.540	5.9	10.4
45	0.607	5.9	10.4
50	0.675	5.9	10.4
60	0.810	6	10.9
70	0.944	6.2	12.0
80	1.079	6.3	12.5
90	1.214	6.6	14.1
100	1.349	6.6	14.1
110	1.484	6.7	14.6
125	1.687	6.7	14.6

Table A3.3. Boundary between coalescence and no-coalescence region for 1-pentanol (run 1).

Concentration, ppm	Concentration, mmol/L	Gas flow rate set point	Gas flow rate, sccm
0	0	5.1	6.2
2.5	0.028	5.1	6.2
5	0.057	5.1	6.2
7.5	0.085	5.4	7.8
10	0.113	5.5	8.3
12.5	0.142	5.7	9.4
15	0.170	5.8	9.9
20	0.227	5.9	10.4
25	0.284	5.9	10.4
30	0.340	5.9	10.4
35	0.397	6.1	11.5
40	0.454	6.3	12.5
45	0.511	6.5	13.6
50	0.567	6.6	14.1
55	0.624	6.7	14.6
60	0.681	6.7	14.6
65	0.737	6.7	14.6
70	0.794	6.7	14.6

Table A3.4. Boundary between coalescence and no-coalescence region for 1-pentanol (run 2).

Concentration, ppm	Concentration, mmol/L	Gas flow rate set point	Gas flow rate, sccm
0	0	5.2	6.7
2.5	0.028	5.2	6.7
5	0.057	5.2	6.7
7.5	0.085	5.4	7.8
10	0.113	5.5	8.3
12.5	0.142	5.7	9.4
15	0.170	5.8	9.9
20	0.227	6	10.9
25	0.284	6	10.9
30	0.340	6	10.9
35	0.397	6.2	12.0
40	0.454	6.4	13.0
45	0.511	6.6	14.1
50	0.567	6.7	14.6
55	0.624	6.7	14.6
60	0.681	6.8	15.1
65	0.737	6.8	15.1
70	0.794	6.8	15.1

Table A3.5. Boundary between coalescence and no-coalescence region for 1-pentanol (run 3).

Concentration, ppm	Concentration, mmol/L	Gas flow rate set point	Gas flow rate, sccm
0	0	5.1	6.2
2.5	0.028	5.1	6.2
5	0.057	5.2	6.7
7.5	0.085	5.3	7.3
10	0.113	5.6	8.8
12.5	0.142	5.7	9.4
15	0.170	5.7	9.4
20	0.227	5.8	9.9
25	0.284	5.8	9.9
30	0.340	6	10.9
35	0.397	6.2	12.0
40	0.454	6.5	13.6
45	0.511	6.6	14.1
50	0.567	6.6	14.1
55	0.624	6.6	14.1
60	0.681	6.6	14.1
65	0.737	6.6	14.1
70	0.794	6.7	14.6

Table A3.6. Boundary between coalescence and no-coalescence region for 1-hexanol.

Concentration, ppm	Concentration, mmol/L	Gas flow rate set point	Gas flow rate, sccm
0	0	5.1	6.2
1	0.010	5.1	6.2
2.5	0.025	5.1	6.2
5	0.049	5.3	7.3
7.5	0.073	5.4	7.8
10	0.098	5.7	9.4
15	0.147	5.9	10.4
20	0.196	6.1	11.5
25	0.245	6.3	12.5
30	0.294	6.6	14.1
35	0.343	6.7	14.6
40	0.392	6.7	14.6
45	0.440	6.7	14.6
50	0.489	6.7	14.6

Table A3.7. Boundary between coalescence and no-coalescence region for 1-heptanol.

Concentration, ppm	Concentration, mmol/L	Gas flow rate set point	Gas flow rate, sccm
0	0	5.2	6.7
2.5	0.022	5.3	7.3
5	0.043	5.4	7.8
10	0.086	5.8	9.9
15	0.129	6	10.9
20	0.172	6.5	13.6
25	0.215	6.7	14.6
30	0.258	6.7	14.6
35	0.301	6.7	14.6
40	0.344	6.8	15.1
45	0.387	6.8	15.1
50	0.430	6.9	15.7
55	0.473	7	16.2
60	0.516	7	16.2

Table A3.8. Boundary between coalescence and no-coalescence region for 1-octanol.

Concentration, ppm	Concentration, mmol/L	Gas flow rate set point	Gas flow rate, sccm
0	0	5.1	6.2
2.5	0.019	5.1	6.2
5	0.038	5.4	7.8
10	0.077	5.8	9.9
15	0.115	6	10.9
20	0.154	6.4	13.0
25	0.192	6.7	14.6
30	0.230	6.7	14.6
35	0.269	6.8	15.1
40	0.307	6.8	15.1
45	0.346	6.8	15.1
50	0.384	6.9	15.7
55	0.422	7	16.2
60	0.461	7.1	16.7
65	0.499	7.2	17.2
70	0.538	7.2	17.2

Table A3.9. Boundary between coalescence and no-coalescence region for F-150.

Concentration, ppm	Concentration, mmol/L	Gas flow rate set point	Gas flow rate, sccm
0	0	5.2	6.7
0.25	0.001	5.2	6.7
1	0.002	5.2	6.7
2	0.005	5.2	6.7
3	0.007	5.2	6.7
4	0.009	5.2	6.7
5	0.012	5.2	6.7
7.5	0.018	5.2	6.7
10	0.024	5.4	7.8
12.5	0.029	5.5	8.3
15	0.035	5.5	8.3
20	0.047	5.7	9.4
25	0.059	5.9	10.4
30	0.071	5.9	10.4
35	0.082	6.1	11.5
40	0.094	6.2	12.0
45	0.106	6.4	13.0
50	0.118	6.6	14.1
55	0.129	6.7	14.6
60	0.141	6.8	15.1
65	0.153	6.9	15.7
70	0.165	7	16.2
75	0.177	7	16.2
80	0.188	7	16.2
90	0.212	7	16.2

Table A3.10. Boundary between coalescence and no-coalescence region for MIBC.

Concentration, ppm	Concentration, mmol/L	Gas flow rate set point	Gas flow rate, sccm
0	0	5.2	6.7
1	0.010	5.2	6.7
2.5	0.025	5.2	6.7
5	0.049	5.6	8.8
7.5	0.073	5.8	9.9
10	0.098	6	10.9
15	0.147	6.1	11.5
20	0.196	6.4	13.0
25	0.245	6.6	14.1
30	0.294	6.9	15.7
35	0.343	6.9	15.7
40	0.392	6.9	15.7
45	0.440	6.9	15.7

Table A3.11. Boundary between coalescence and no-coalescence region for Dowfroth 250.

Concentration, ppm	Concentration, mmol/L	Gas flow rate set point	Gas flow rate, sccm
0	0	5.3	7.3
1	0.004	5.3	7.3
2.5	0.010	5.2	6.7
5	0.019	5.2	6.7
7.5	0.028	5.3	7.3
10	0.038	5.4	7.8
12.5	0.047	5.5	8.3
15	0.057	5.7	9.4
20	0.076	5.9	10.4
25	0.095	6	10.9
30	0.114	6.1	11.5
35	0.132	6.2	12.0
40	0.151	6.4	13.0
45	0.170	6.6	14.1
50	0.189	6.9	15.7
55	0.208	6.9	15.7
60	0.227	7	16.2
70	0.265	7	16.2
80	0.303	7	16.2

Appendix 4 – Experimental results of bubble coalescence and break-up

Table A4.1. Bubble size distribution. Water: 380, 420, and 500 RPM.

Bubble size, mm	Number Frequency, %		
	Water		
	380 RPM	420 RPM	500 RPM
0.3	3.0	4.5	9.6
0.5	0.9	0.7	1.8
0.7	0.5	0.9	2.0
0.9	1.6	1.8	4.4
1.2	3.7	4.5	8.3
1.5	5.3	7.0	9.0
1.7	5.2	5.7	5.5
1.8	3.7	4.2	3.7
2.0	3.9	3.8	2.9
2.1	2.4	2.7	2.5
2.2	4.4	4.7	3.4
2.4	7.3	7.1	7.8
2.5	20.1	21.0	17.8
2.9	21.4	19.7	16.7
3.1	9.5	7.9	3.6
3.6	4.4	3.1	0.8
4.0	1.7	0.7	0.1
4.3	0.5	0.1	0.1
4.5	0.4	0.0	0.0
4.8	0.2	0.0	0.0

Table A4.2. Bubble size distribution. F-150: 380, 420, and 500 RPM.

Bubble size, mm	Number Frequency, %		
	F-150, 0.012 mmol/L		
	380 RPM	420 RPM	500 RPM
0.3	8.2	3.7	9.1
0.5	0.3	0.7	1.2
0.7	0.9	1.6	3.0
0.9	2.3	3.7	5.9
1.2	3.9	6.9	8.2
1.5	4.8	7.4	6.9
1.7	4.8	4.9	3.1
1.8	3.8	3.2	1.8
2.0	2.7	2.4	1.6
2.1	2.1	1.9	1.1
2.2	2.7	2.6	1.5
2.4	20.4	27.6	27.5
2.5	35.8	28.8	24.5
2.9	5.7	3.7	3.7
3.1	1.2	0.8	0.7
3.6	0.5	0.1	0.2
4.0	0.0	0.0	0.0
4.3	0.0	0.0	0.0
4.5	0.0	0.0	0.0
4.8	0.0	0.0	0.0

Table A4.3. Bubble size distribution. Dowfroth 250.

Bubble size, mm	Number Frequency, %			
	Dowfroth 250			
	0.011 mmol/L	0.038 mmol/L	0.057 mmol/L	0.095 mmol/L
0.3	9.0	7.5	6.0	3.4
0.5	1.2	1.1	1.1	0.9
0.7	1.7	1.8	2.1	1.7
0.9	4.1	3.6	3.5	2.7
1.2	7.6	6.7	6.5	6.0
1.5	6.7	6.9	6.2	7.1
1.7	4.5	4.3	4.4	4.4
1.8	2.6	3.1	3.1	3.0
2.0	2.2	2.3	2.1	1.9
2.1	1.9	1.7	1.4	1.2
2.2	3.9	2.0	2.0	1.9
2.4	24.0	23.4	21.7	23.1
2.5	25.7	29.7	32.6	37.0
2.9	4.0	4.9	6.1	4.9
3.1	0.9	0.7	0.9	0.6
3.6	0.0	0.2	0.2	0.2
4.0	0.0	0.0	0.0	0.0
4.3	0.0	0.0	0.0	0.0
4.5	0.0	0.0	0.0	0.0
4.8	0.0	0.0	0.0	0.0

Table A4.4. Bubble size distribution. Pentanol, MIBC, F-150, NaCl.

Bubble size, mm	Number Frequency, %			
	Pentanol, 0.397 mmol/L	MIBC, 0.098 mmol/L	F-150, 0.012 mmol/L	NaCl, 0.4M
0.3	2.4	2.5	3.7	2.8
0.5	0.7	1.1	0.7	0.9
0.7	1.3	2.0	1.6	1.0
0.9	2.9	3.7	3.7	2.7
1.2	6.4	6.9	6.9	6.3
1.5	7.3	8.4	7.4	9.6
1.7	6.1	5.3	4.9	7.4
1.8	4.5	4.8	3.2	3.9
2.0	3.8	4.9	2.4	4.5
2.1	4.0	6.0	1.9	4.6
2.2	8.6	13.2	2.6	9.6
2.4	13.6	17.1	27.6	14.6
2.5	23.9	17.9	28.8	19.0
2.9	12.9	5.5	3.7	9.8
3.1	1.6	0.6	0.8	2.5
3.6	0.2	0.0	0.1	0.6
4.0	0.0	0.0	0.0	0.1
4.3	0.0	0.0	0.0	0.1
4.5	0.0	0.0	0.0	0.0
4.8	0.0	0.0	0.0	0.0

Appendix 5 – Macro code for ImageJ

The following code allows processing bubble size for multiple tests with ImageJ:

```
macro "Multi Bubble Size Analyzer" {
  Dir_r = getDirectory("Choose Source Directory ");
  listfolder = getFileList(Dir_r);
  Dir_w = Dir_r;
  //Prompt for Information
  Dialog.create("Parameters for multiple tests");
  Dialog.addNumber("Pixels per mm.", 50.0, 2, 10, "");
  Dialog.addNumber("Min. Circularity", 0.65, 2, 10, "");
  Dialog.addNumber("Min. Object diameter", 5, 0, 10, "pixels");
  Dialog.addNumber("Files to skip", 0, 0, 10, "");
  Dialog.addString("File Extension", "JPG");
  Dialog.addMessage("\n");
  Dialog.addCheckbox("Substract Background", false);
  Dialog.addCheckbox("Save Results in same folder", true);
  Dialog.show();

  Cal = Dialog.getNumber();
  Circ = Dialog.getNumber();
  min_diam = Dialog.getNumber();
  s = Dialog.getNumber();
  extension = Dialog.getString();
  BG = Dialog.getCheckbox();
  Keep_folder = Dialog.getCheckbox();

  if (Keep_folder == false) {
    Dir_w = getDirectory("Choose Destination for Results ");
  }
}
```

```

if (s != (round(s)) || (s < 0)) {
    exit("Files to skip must be a positive integer");
}

min_area = (min_diam/Cal)*(min_diam/Cal)/4*3.1416;
run("Clear Results");

j = 0;

for (f=0; f<listfolder.length; f++) {
    //Get Subfolder Name
    n = lengthOf(listfolder[f]);
    subfolder = substring(listfolder[f], 0, n-1);
    Sub_dir = Dir_r + subfolder + "\\";
    list = getFileList(Sub_dir);
    if (s >= list.length) {
        exit("Too many files to skip")
    }

    for (i=s; i<list.length; i++) {
        if (endsWith(list[i], extension) == 1) {
            open(Sub_dir + list[i]);
            run("Out");
            run("Out");
            run("Out");
            run("8-bit");
            if (BG == true) {
                run("Subtract Background...", "rolling=50 white");
            }
            //run("Threshold...");

```

```

setAutoThreshold();
if (j==0){
run("Set Scale...", "distance=" + Cal + " known=1 pixel=1 unit=mm global");
j = 1;
}

run("Set Measurements...", "area perimeter circularity feret's display
redirect=None decimal=3");
run("Analyze Particles...", "size=" + min_area + "-Infinity circularity=" + Circ +
"-1.00 show=Nothing display exclude include");

close();
}
}
//instructions to generate only one big txt-file per test
saveAs("Measurements", Dir_w + subfolder + ".txt");
run("Clear Results");
}
}

```